

POLITECNIC OF TURIN

Department of Mechanical and Aerospace Engineering  
MSc in Mechanical Engineering

Master Thesis

# Modal Study of a Vertical Axis Test Bench.

Comparison between analytic and experimental results.



**Advisor**

prof. Giancarlo GENTA

**Candidate**

Michele Giovanni MASSAFRA  
ID: 235427

Academic advisor in  
UNICAMP - Universidade Estadual de Campinas - Brasil  
prof. Katia LUCCHESI CAVALCA DEDINI

ACADEMIC YEAR 2019-2020



*Alla mia famiglia*

*†A mia nonna Lina*

*†All' ing. Vincenzo  
Mignogna*

# Summary

The aim of this work is the modal behaviour study for a test bench for rotational vertical axes.

In the first part of the dissertation, the vibration and modal analysis knowledge are presented. The importance of modal analysis in the design process, therefore, the way how this study stage complete the final product performance, in terms of safety and comfort, are discussed.

A description of the software used for the analytic study, and a critical comparison between the most common programs actually used in academic and industrial field, is presented.

The fourth chapter exposes the theoretical steps, discussed in the first chapters, for setting up an analytic modal analysis, and the way how they are applied in all the sub assembly, and global assembly test bench. The results from the analytic modal analysis executed with commercial CAD/CAE softwares are exposed, and compared between the models.

The experimental setting up, and result obtained from structure impulse excitation study are successively exposed. The DAQ process, following the SISO theory, are presented.

In the end a comparison between the analytic and experimental studies is discussed, and possible future works are suggested.

# Acknowledgements

A thanks to all the people form Faculdade de Engenharia Mecânica LAMAR laboratory, in the persons of Prof. Dr. Gregory Bregion Daniel, Prof. Dr. Helio Fiori di Castro and Prof. Dr. Tiago Henrique Machado, for receive and integrate me in their laboratory.

A special thanks to Eng. Felipe Wenzel da S. Tuckmantel for its help and support in all the stages of this work, sharing information and knowledge.

# Contents

List of Figures	VI
List of Tables	IX
Latins Characters	XI
Greek Characters	XI
Superscripts	XI
Shortcuts	XI
Acronyms	XII
<b>1 Introduction</b>	<b>1</b>
1.1 Modal analysis	1
1.1.1 Modal analysis in design process	1
1.2 Vibration theory for multi-dof systems	2
1.2.1 Basics of vibration problem	2
1.2.2 Free response solution for a conservative system	3
1.2.3 State space theory	4
1.2.4 Non-conservative system solution through state space theory	5
1.2.5 Theory of experimental modal analysis for frequency response	6
<b>2 FEM Theory for CAE Studies</b>	<b>8</b>
2.1 Introduction	8
2.2 Analytic modal study: steps procedure	8
2.3 Geometry definition	10
2.4 Material definition	11
2.5 Constrains, loads and boundary conditions definitions	11
2.6 Basic theory for finite elements	12
2.7 Mesh generation	14
2.7.1 Possible mesh generation failures	14
2.8 A posteriori adaptive FE error estimation technique	14

<b>3</b>	<b>PTC Creo® review</b>	<b>16</b>
3.1	Introduction . . . . .	16
3.1.1	PTC Creo® environment . . . . .	16
3.2	PTC Creo Parametric® . . . . .	17
3.2.1	Sketch tab . . . . .	18
3.2.2	Model tab . . . . .	19
3.2.3	Assembly procedure . . . . .	19
3.2.4	Drawing model . . . . .	20
3.3	PTC Creo Simulate® . . . . .	20
3.3.1	Simulate environment . . . . .	20
3.3.2	Description of the simulation setup process . . . . .	22
3.3.3	The analysis . . . . .	24
3.3.4	Result visualiser tool . . . . .	27
<b>4</b>	<b>Analytic modal analysis results</b>	<b>28</b>
4.1	Introduction . . . . .	28
4.2	External simplified structure . . . . .	30
4.2.1	First analysis for simplified external structure: coarse mesh . . . . .	31
4.2.2	Second analysis for simplified external structure: medium mesh . . . . .	33
4.2.3	Third analysis for simplified external structure: fine mesh . . . . .	36
4.2.4	External simplified vibration modes: rigid link contact . . . . .	37
4.2.5	Fourth analysis for simplified external structure: Ansys AIM 18® . . . . .	38
4.2.6	External simplified vibration modes: Ansys AIM 18® results . . . . .	40
4.2.7	Fifth analysis for simplified external structure: medium mesh . . . . .	41
4.2.8	Sixth analysis for simplified external structure: fine triangular and theraedral mesh . . . . .	43
4.2.9	Seventh analysis for simplified external structure: fine mixed mesh . . . . .	45
4.2.10	External simplified vibration modes: rigid link contact . . . . .	46
4.3	Full external structure . . . . .	47
4.3.1	First analysis for complete external structure: coarse mesh . . . . .	49
4.3.2	Second analysis for complete external structure: medium mesh . . . . .	51
4.3.3	Third analysis for complete external structure: fine mesh . . . . .	53
4.3.4	Complete external vibration modes . . . . .	55
4.4	Internal structure . . . . .	57
4.4.1	First analysis for internal structure: coarse mesh . . . . .	59
4.4.2	Second analysis for internal structure: medium mesh . . . . .	60
4.4.3	Third analysis for internal structure: fine mesh . . . . .	62
4.4.4	Internal structure vibration modes . . . . .	63
4.5	Superior shaft . . . . .	65
4.5.1	First analysis for superior shaft: coarse mesh . . . . .	66
4.5.2	Second analysis for superior shaft: medium mesh . . . . .	68
4.5.3	Superior shaft vibration modes . . . . .	70
4.6	Inferior shaft . . . . .	70
4.6.1	Analysis for inferior shaft . . . . .	71
4.7	Shafts assembly . . . . .	73
4.7.1	First analysis for shafts assembly: coarse mesh . . . . .	75

4.7.2	Second analysis for shafts assembly: medium mesh . . . . .	77
4.7.3	Shafts assembly vibration modes . . . . .	79
4.8	Test bench structure . . . . .	79
4.8.1	First analysis for test bench: coarse mesh . . . . .	82
4.8.2	Second analysis for test bench: medium mesh . . . . .	84
4.8.3	Third analysis for test bench: fine mesh . . . . .	87
4.8.4	Test bench vibration modes . . . . .	88
4.8.5	Conclusion . . . . .	97
<b>5</b>	<b>Experimental analysis</b>	<b>99</b>
5.1	Introduction . . . . .	99
5.2	DAQ system . . . . .	100
5.3	DAQ process . . . . .	101
5.3.1	Possible error source . . . . .	101
5.4	Data analyses procedure . . . . .	102
5.5	Results . . . . .	105
5.5.1	External structure . . . . .	105
5.5.2	Internal structure . . . . .	106
5.5.3	Conclusion . . . . .	106
<b>6</b>	<b>Conclusion</b>	<b>107</b>
6.1	Comparison between the analytic and experimental results . . . . .	107
6.2	Prospective for future works . . . . .	108
<b>Appendices</b>		
<b>A</b>	<b>DAQ hardware properties</b>	<b>I</b>
<b>B</b>	<b>Matlab codes</b>	<b>III</b>
<b>C</b>	<b>FRF for internal and external beams</b>	<b>VIII</b>
<b>Bibliography</b>		<b>x</b>

# List of Figures

1.1	Fatigue phenomena in rotating systems . . . . .	2
1.2	Flutter phenomena in Tacoma Bridge disaster . . . . .	2
2.1	Beam element for detail levels example . . . . .	10
2.2	Example of two beams junction for FEM generation . . . . .	12
2.3	Example of finite elements . . . . .	13
3.1	PTC Creo Parametric® user interface . . . . .	17
3.2	PTC Creo Parametric® first dialog windows . . . . .	18
3.3	PTC Creo Parametric® sketch features . . . . .	18
3.4	Assembly dialog window for components assembly . . . . .	20
3.5	Model Tree for PTC Creo Simulate® . . . . .	21
3.6	Rapid menu - Home tab . . . . .	21
3.7	Simulation tools for Refine Mode tab . . . . .	22
3.8	Setup options for Structure study . . . . .	22
3.9	PTC Creo Simulate® material library . . . . .	23
3.10	Analysis dialog windows . . . . .	25
3.11	Modal analysis definition . . . . .	25
3.12	PTC Creo Result® user interface . . . . .	27
4.1	Test bench for vertical shafts 3D CAD model . . . . .	28
4.2	Simplified external structure CAD model . . . . .	30
4.3	External simplified structure, boundary condition . . . . .	31
4.4	Redefinition of contact between external simplified structure parts . . . . .	32
4.5	Coarse mixed mesh, simplified external structure . . . . .	33
4.6	Medium mixed mesh, simplified external structure . . . . .	35
4.7	Fine mixed mesh, simplified external structure . . . . .	36
4.8	External simplified structure vibration modes: rigid link contact . . . . .	38
4.9	Very fine mesh, simplified external structure: Ansys AIM 18® . . . . .	39
4.10	External simplified structure vibration modes: Ansys AIM 18®, bounded contact . . . . .	40
4.11	Medium triangular and thetragonal mesh, simplified external structure . . . . .	42
4.12	Fine triangular and thetragonal mesh, simplified external structure . . . . .	44
4.13	External simplified structure vibration modes: bounded contact . . . . .	47
4.14	Full external structure CAD model . . . . .	48

4.15	Complete external structure boundary condition . . . . .	49
4.16	Complete external structure bounded contact . . . . .	49
4.17	Coarse mesh, complete external structure . . . . .	50
4.18	Medium mesh, complete external structure . . . . .	52
4.19	Fine mesh, complete external structure . . . . .	54
4.20	Complete external structure, beams vibration modes . . . . .	56
4.21	Complete external structure, internal structures vibration modes . . . . .	57
4.22	Internal structure CAD model . . . . .	57
4.23	Internal structure boundary condition . . . . .	58
4.24	Internal structure bounded contact . . . . .	58
4.25	Coarse mesh, internal structure . . . . .	59
4.26	Medium mesh, internal structure . . . . .	61
4.27	Fine mesh, internal structure . . . . .	63
4.28	Internal structure, vibration modes . . . . .	64
4.29	Superior shaft CAD model . . . . .	65
4.30	Superior shaft boundary condition . . . . .	66
4.31	Coarse mesh, superior shaft . . . . .	67
4.32	Medium mesh, superior shaft . . . . .	68
4.33	Superior shaft, vibration modes . . . . .	70
4.34	Superior shaft CAD model . . . . .	71
4.35	Inferior shaft boundary condition . . . . .	72
4.36	Coarse mesh, inferior shaft . . . . .	72
4.37	Shafts assembly CAD model . . . . .	74
4.38	Shafts assembly boundary condition . . . . .	75
4.39	Shafts assembly bounded contact . . . . .	75
4.40	Coarse mesh, shafts assembly . . . . .	75
4.41	Medium mesh, shafts assembly . . . . .	78
4.42	Shafts assembly, vibration modes . . . . .	79
4.43	Shafts supports parts detail . . . . .	80
4.44	Test bench structure CAD model . . . . .	80
4.45	Test bench boundary condition constrains . . . . .	82
4.46	Test bench contact conditions between parts . . . . .	82
4.47	Coarse mesh, test bench structure . . . . .	83
4.48	Medium mesh, test bench structure . . . . .	85
4.49	Fine mesh, test bench structure . . . . .	87
4.50	Comparison between models, 1 <sup>st</sup> external structure mode . . . . .	89
4.51	Comparison between models, 2 <sup>nd</sup> external structure mode . . . . .	90
4.52	Comparison between models, 3 <sup>rd</sup> external structure mode . . . . .	91
4.53	Comparison between models, 4 <sup>th</sup> external structure mode . . . . .	91
4.54	Comparison between models, 5 <sup>th</sup> external structure mode . . . . .	92
4.55	Comparison between models, 6 <sup>th</sup> external structure mode . . . . .	92
4.56	Comparison between models, 7 <sup>th</sup> external structure mode . . . . .	93
4.57	Comparison between models, 1 <sup>nd</sup> internal structure mode . . . . .	93
4.58	Comparison between models, 2 <sup>nd</sup> internal structure mode . . . . .	94
4.59	Comparison between models, 3 <sup>rd</sup> internal structure mode . . . . .	94
4.60	Comparison between models, shafts assembly mode . . . . .	95

4.61	Additional shafts assembly modes in test bench model . . . . .	96
4.62	Shafts supports vibrations modes . . . . .	96
4.63	Magnetic exciter support vibration modes . . . . .	97
5.1	Test bench structure . . . . .	99
5.2	DAQ system hardware . . . . .	100
5.3	DAQ system hardware . . . . .	102
5.4	Time domain signals . . . . .	103
5.5	Hanning window spectrum in time and frequency domains . . . . .	104
5.6	FRF for a single signal . . . . .	104
5.7	Averaged FRF signal . . . . .	105

# List of Tables

3.1	PTC Creo Simulate <sup>®</sup> analysis types . . . . .	24
4.1	List of materials for simplified external structure . . . . .	30
4.2	Structural steel properties from PTC Creo Simulate <sup>®</sup> . . . . .	31
4.3	Simplified external structure, coarse mesh, FE size . . . . .	32
4.4	Natural frequencies and RMS errors, external simplified structure: coarse mesh	34
4.5	Simplified external structure, medium mesh, FE size . . . . .	34
4.6	Natural frequencies and RMS errors, external simplified structure: medium mesh . . . . .	35
4.7	Simplified external structure, fine mesh, FE size . . . . .	36
4.8	Natural frequencies and RMS errors, external simplified structure: fine mesh	37
4.9	Natural frequencies, external simplified structure: Ansys AIM 18 <sup>®</sup> . . . . .	40
4.10	Simplified external structure, medium mesh, triangular and thetragonal FEs size . . . . .	41
4.11	Multi-Pass Adaptive steps, simplified external structure, medium mesh . . . . .	42
4.12	Natural frequencies and RMS errors, external simplified structure: medium triangular and thertaedrical mesh . . . . .	43
4.13	Simplified external structure, fine mesh, triangular and thetragonal FEs size	43
4.14	Multi-Pass Adaptive steps, simplified external structure, fine mesh . . . . .	44
4.15	Natural frequencies and RMS errors, external simplified structure: fine triangular and thertaedrical mesh . . . . .	45
4.16	Natural frequencies and RMS errors, external simplified structure, based on section 4.2.3 . . . . .	46
4.17	Bill of materials for full external structure . . . . .	48
4.18	Complete external structure, coarse mesh, FE size . . . . .	50
4.19	Multi-Pass Adaptive steps, complete external structure, coarse mesh . . . . .	51
4.20	Natural frequencies and RMS errors, complete external structure: coarse mesh	51
4.21	Complete external structure, medium mesh, FE size . . . . .	52
4.22	Multi-Pass Adaptive steps, complete external structure, medium mesh . . . . .	53
4.23	Natural frequencies and RMS errors, complete external structure: medium mesh . . . . .	53
4.24	Complete external structure, fine mesh, FE size . . . . .	54
4.25	Multi-Pass Adaptive steps, complete external structure, fine mesh . . . . .	55
4.26	Natural frequencies and RMS errors, complete external structure: fine mesh	55
4.27	Bill of materials for internal structure . . . . .	58

4.28	Internal structure, coarse mesh, FE size . . . . .	59
4.29	Multi-Pass Adaptive steps, internal structure, coarse mesh . . . . .	60
4.30	Natural frequencies and RMS errors, internal structure: coarse mesh . . . . .	60
4.31	Internal structure, medium mesh, FE size . . . . .	61
4.32	Multi-Pass Adaptive steps, internal structure, medium mesh . . . . .	62
4.33	Natural frequencies and RMS errors, internal structure: medium mesh . . . . .	62
4.34	Internal structure, fine mesh, FE size . . . . .	63
4.35	Multi-Pass Adaptive steps, internal structure, fine mesh . . . . .	64
4.36	Natural frequencies and RMS errors, internal structure: fine mesh . . . . .	64
4.37	Superior shaft volume division . . . . .	65
4.38	Superior shaft, coarse mesh, FE size . . . . .	66
4.39	Multi-Pass Adaptive steps, superior shaft, coarse mesh . . . . .	67
4.40	Natural frequencies and RMS errors, superior shaft: coarse mesh . . . . .	68
4.41	Superior shaft, medium mesh, FE size . . . . .	68
4.42	Multi-Pass Adaptive steps, superior shaft, medium mesh . . . . .	69
4.43	Natural frequencies and RMS errors, superior shaft: coarse mesh . . . . .	69
4.44	Inferior shaft volume division . . . . .	71
4.45	Inferior shaft, FE size . . . . .	72
4.46	Natural frequencies, inferior shaft . . . . .	73
4.47	List of materials for shafts assembly . . . . .	74
4.48	Material properties for modal analyses simulations . . . . .	75
4.49	Shafts assembly, coarse mesh, FE size . . . . .	76
4.50	Multi-Pass Adaptive steps, shafts assembly, coarse mesh . . . . .	76
4.51	Natural frequencies and RMS errors, shafts assembly: coarse mesh . . . . .	77
4.52	Shafts assembly, medium mesh, FE size . . . . .	77
4.53	Multi-Pass Adaptive steps, shafts assembly, medium mesh . . . . .	78
4.54	Natural frequencies and RMS errors, shafts assembly: medium mesh . . . . .	79
4.55	Table of test bench model parts . . . . .	81
4.56	Material properties for test bench modal analyses . . . . .	81
4.57	Test bench structure, coarse mesh, FE size . . . . .	83
4.58	Multi-Pass Adaptive steps, test bench structure, coarse mesh . . . . .	84
4.59	Natural frequencies and RMS errors, test bench structure: coarse mesh . . . . .	84
4.60	Test bench structure, medium mesh, FE size . . . . .	85
4.61	Multi-Pass Adaptive steps, test bench structure, medium mesh . . . . .	86
4.62	Natural frequencies and RMS errors, test bench structure: medium mesh . . . . .	86
4.63	Test bench structure, fine mesh, FE size . . . . .	87
4.64	Multi-Pass Adaptive steps, test bench structure, fine mesh . . . . .	88
4.65	Natural frequencies and RMS errors, test bench structure: fine mesh . . . . .	89

## Latins Characters

$M$ : Mass matrix  
 $C$ : Damping matrix  
 $K$ : Stiffness matrix  
 $\mathbf{x}$ : displacement vector in absolute coordinate  
 $\mathbf{f}$ : external force vector  
 $I$ : Identity matrix  
 $\mathbf{y}$ : displacement vector in state space coordinate  
 $j$ : imaginary number  
 $a$ : constant factor  
 $t$ : time  
 $A$ : matrix of constants therms  
 $B$ : matrix of constants therms  
 $E$ : elasticity (or Young's) modulus

## Greek Characters

$\omega$ : frequency  
 $\theta$ : angular displacement  
 $\phi$ : phase shift  
 $\beta$ : constant coefficient  
 $\gamma$ : constant coefficient  
 $\xi$ : damping coefficient  
 $\alpha(\omega)$ : receptance matrix  
 $\rho$ : density  
 $\nu$ : Poisson coefficient  
 $\sigma$ : maximum strength  
 $\eta$ : error index

## Superscripts

$^{\circ}$ : degree  
 $^{\circledR}$ : registered trademark  
 $^{\copyright}$ : Copyright

## Shortcuts

3D: three dimensions or three dimensional space  
2D: two dimensional space

## **Acronyms**

FRF: Frequency Response Function

CAE: Computer Aid Engineering

FEM: Finite Elements Method

dof: Degree of Freedom

CAD: Computer Aid Design

RMS: Root Mead Square

DAQ: Data Acquisition

SISO: Single input-Single Output

# Chapter 1

## Introduction

### 1.1 Modal analysis

The modal analysis concerns the dynamic study of a system in the vibration field. The focus of such kind of study is investigating the system modes and its response function for the applied problem. It means that knowing the geometrical and physical system properties (mass, stiffness and damping coefficients), the initial conditions (displacement and velocities) and eventual input forces, it is possible to get the system response function for each frequency solving the so called eigenvalue problem.

Often in real applications the system properties, stiffness and damping coefficients, are unknown. The classical eigenvalues and eigenvectors approach solution for natural frequencies and modes, as well as FRFs, is no more useful. Different approaches are required for solving such kind of realistic problems. Several are the mathematical approaches [3] for experimental tests, as well CAE software for analytic studies, which involves sophisticated solving procedures throughout FEM analyses.

#### 1.1.1 Modal analysis in design process

A modal analysis study could be a decisive step in the design process for systems in which their operations conditions include rotational parts, such as rotors or rotating shafts [9], structure subjected to periodic or random excitation, such as civil engineering problems, acoustic field [8].

The primary modal analysis aim is the system modal properties, therefore modes and natural frequencies. Supposing that we know the external frequency excitation field for our system, to analyse system natural frequencies permit to avoid the system to work in its natural frequencies.

A further modal analysis step can be detect loading conditions [6, 7]. Being the system excited with inconstant forces, ideally both in the frequency and time domain, cyclical loads are applied too. Analysing the stress applied during the system working life can avoid catastrophic failure due to induction of fatigue phenomena, or permanent damages.

The latter example, as shown in Figure 1.1, is what concern rotor-dynamics, or in general systems with rotational parts, therefore systems in which elements like bearings and shafts are involved with.

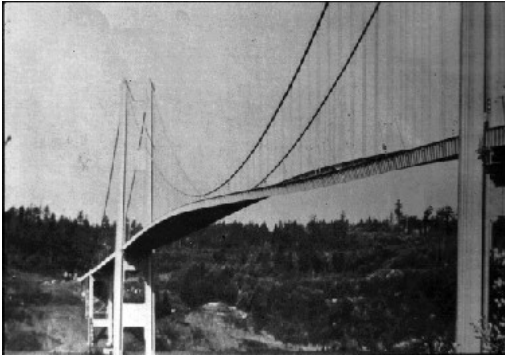


(a) Spalling fatigue failure



(b) Helicopter rotor failure

Figure 1.1: Fatigue phenomena in rotating systems



(a) Bridge oscillation



(b) Bridge collapse

Figure 1.2: Flutter phenomena in Tacoma Bridge disaster

Another example about the importance related to the modal study during the design process regards the Tacoma Bridge historical collapse occurred on November 7<sup>th</sup> 1940, Figure 1.2. Here is what concern civil structure in the vibration field. In this situation, the construction was excited at its critical velocity by a constant wind speed of  $62 \frac{km}{h}$ , establishing a fluid dynamic instability phenomena called flutter.

## 1.2 Vibration theory for multi-dof systems

### 1.2.1 Basics of vibration problem

A mass is considered vibrating when its displacement around the equilibrium position is small enough; it means the order of some  $mm$  for linear displacements, while less or equal to  $1^\circ$  for angular displacement, such that the first order Taylor series approximation is valid:

$$\sin(\theta) \approx \theta + o(\theta^3) \quad \text{and} \quad \cos(\theta) \approx 1 + o(\theta^2) \quad (1.1)$$

A real system generally has an infinite number of dofs, therefore it is possible to find an infinite number of natural frequencies. The common approach used for studying its dynamic behaviour is to consider each part characterised by lumped parameter masses. In such way it is possible to write a force balance equation for each of the lumped masses. Being all the masses linked to each others, the system of  $N$  equations obtained from each mass force balance equation, is linearly dependent. The following result is obtained expressing the equation system in a matrix form:

$$[M] \{\ddot{x}\} + [C] \{\dot{x}\} + [K] \{x\} = \{f\} \quad (1.2)$$

where the matrix  $\mathbf{M}^1$  is the matrix of mass properties, the  $\mathbf{C}$  matrix is the one of damping coefficients, the  $\mathbf{K}$  is the stiffness coefficient matrix and in the end the  $f$  vector is the vector of applied external forces. The vectors  $\ddot{\mathbf{x}}$ ,  $\dot{\mathbf{x}}$  and  $\mathbf{x}$  are respectively the accelerations, velocities and displacements of the system. Having the system a  $N$ -dofs, the  $\mathbf{M}$ ,  $\mathbf{C}$  and  $\mathbf{K}$  are square matrices  $N \times N$ , the vectors  $\ddot{\mathbf{x}}$ ,  $\dot{\mathbf{x}}$  and  $\mathbf{x}$  and  $\mathbf{f}$  are  $N \times 1$  vectors.

The term  $\mathbf{M}\ddot{\mathbf{x}}$  identifies the inertia part, the term  $\mathbf{C}\dot{\mathbf{x}}$  identifies the energy dissipation part of the equation (1.2), while the term  $\mathbf{K}\mathbf{x}$  identifies the portion of potential energy stored through spring elements or equivalent stiffness properties.

When it is possible, consider the damping matrix of the system as null. Therefore there will not be dissipation of energy during the motion, and equation (1.2) becomes:

$$[M] \{\ddot{x}\} + [K] \{x\} = \{f\} \quad (1.3)$$

and the system is called conservative, otherwise is commonly defined dissipative. When it is possible to express the damping matrix as a linear combination of mass and stiffness matrix

$$\mathbf{C} = \beta \mathbf{M} + \gamma \mathbf{K} \quad (1.4)$$

where  $\alpha$  and  $\beta$  are real constant coefficients, or it is valid the relation

$$\mathbf{C}\mathbf{M}^{-1}\mathbf{K} = \mathbf{K}\mathbf{M}^{-1}\mathbf{C} \quad (1.5)$$

the system is called proportionally damped.

### 1.2.2 Free response solution for a conservative system

Recalling that a system is named conservative if the damping matrix  $\mathbf{C}$  is null, therefore it is valid the equation (1.3). The term free response refers to system in which the external force vector  $\mathbf{f}$  is null too. Therefore the equation (1.2) turns to be

$$[M] \{\ddot{x}\} + [K] \{x\} = 0 \quad (1.6)$$

The solution for the upper second order equation is a solution like

---

<sup>1</sup>for simplicity up to now the matrices will be denoted with **capital bold** characters, while the vectors with **small bold** one.

$$\mathbf{x}(t) = \mathbf{x}e^{j\omega t} \quad (1.7)$$

where  $\mathbf{x}$  is the vector  $N \times 1$  of the amplitude of each  $i$  mass,  $j = \sqrt{-1}$  is the imaginary number and  $\omega$  is the vector of each natural frequency.

Deriving two times the solution proposed by the equation (1.7) and substituting the values in (1.6) it is obtained the following equation

$$(-\omega^2 \mathbf{M} + \mathbf{K})\mathbf{x}e^{j\omega t} = 0 \quad (1.8)$$

The latter equation is respected for  $\mathbf{x} = 0$ , known as trivial solution which correspond to the steady state response not of our interest, or for

$$\det(-\omega^2 \mathbf{M} + \mathbf{K}) = 0 \quad (1.9)$$

Equation (1.9) is known as eigenvalues problem equation, where the only unknown is the term  $\omega$ . The values of system natural frequencies are obtained solving the eigenvalues problem, resulting on  $N$  natural frequencies.

Once all the  $N$  natural frequencies are obtained, substituting each  $\omega_i$ , with  $i = 1 \div N$  indicates each natural frequency, in the (1.8), the only unknown is the vector  $\mathbf{x}$ . The latter vector is known as vibration mode for the  $i$  natural frequency. Mathematically the values of  $\omega$  are the eigenvalues, and the values of  $\mathbf{x}$  are the eigenvectors of the eigen problem (1.8). It has to be noticed that each vector  $\mathbf{x}$  is a  $N \times 1$  vector. The physical meaning of  $\mathbf{x}$  is to show how each mass move with respect the others for the given natural frequency.

Generally the natural frequencies, as well as the modes, can be complex number depending on the system properties. For conservative problems both eigenvalues and eigenvectors are real numbers, it means that the masses have synchronous motion, therefore the phase shift between the masses can be  $0^\circ$  or  $180^\circ$ .

Once modes and natural frequencies are computed, considering the Euler transformation, it is possible to express the displacement as:

$$\mathbf{x}(t) = \sum_{i=1}^N a_i \mathbf{x}_i \sin(\omega_i t + \phi_i) \quad (1.10)$$

where the term  $a_i$  and  $\phi_i$  are constant terms evaluated considering the given system initial conditions.

### 1.2.3 State space theory

The state space theory is a powerful method for expressing the general vibrating problem in a new coordinate space, reducing the problem from a second order differential equations to a first one. This kind of transformation is particularly useful for non-conservative and non-proportional systems.

The state space theory consist in rewriting the vibration matrix second order problem, into a new one where the reference system is modified in such a way

$$y_1 = x \quad \text{and} \quad y_2 = \dot{x} \quad (1.11)$$

Following the upper substitution in (1.3) it is obtained the new expression

$$\mathbf{M}\dot{\mathbf{y}}_2 + \mathbf{K}\mathbf{y}_1 = \mathbf{f} \quad (1.12)$$

It can be noticed that

$$\dot{y}_1 = y_2 = \dot{x} \quad (1.13)$$

therefore expressing the (1.12) and (1.13) in matrix form, remembering that the expression (1.12) is a matrix expression too, it is obtained the following result

$$\begin{bmatrix} \mathbf{I} & 0 \\ 0 & \mathbf{M} \end{bmatrix} \begin{Bmatrix} \dot{\mathbf{y}}_1 \\ \dot{\mathbf{y}}_2 \end{Bmatrix} + \begin{bmatrix} 0 & -\mathbf{I} \\ \mathbf{K} & 0 \end{bmatrix} \begin{Bmatrix} \mathbf{y}_1 \\ \mathbf{y}_2 \end{Bmatrix} = \begin{Bmatrix} 0 \\ \mathbf{f} \end{Bmatrix} \quad (1.14)$$

elaborating the upper formulation it is obtained the general formulation

$$\mathbf{A}\dot{\mathbf{y}} + \mathbf{B}\mathbf{y} = \mathbf{b} \quad (1.15)$$

It is precised to notice that the new matrices  $\mathbf{A}$  and  $\mathbf{B}$  are matrices of coefficients related with the system properties with dimension  $2Nx1$ . These two matrices are also called state matrices. The formulation of  $\mathbf{A}$  and  $\mathbf{B}$  are not general, them depend on the way of how the two equations (1.11) and (1.12) are written.

#### 1.2.4 Non-conservative system solution through state space theory

Recalling that a system is defined non-conservative if a dissipating energy term appear through the damping matrix  $\mathbf{C}$ , such that it still be valid the equation

$$\mathbf{M}\ddot{\mathbf{x}} + \mathbf{C}\dot{\mathbf{x}} + \mathbf{K}\mathbf{x} = 0 \quad (1.16)$$

Recalling the substitution (1.11) and the equivalence (1.13) opportunely re-elaborate as

$$\mathbf{K}\dot{\mathbf{y}}_1 - \mathbf{K}\mathbf{y}_2 = 0 \quad (1.17)$$

A matrix equation is obtained in the form

$$\begin{bmatrix} \mathbf{K} & 0 \\ 0 & \mathbf{M} \end{bmatrix} \begin{Bmatrix} \dot{\mathbf{y}}_1 \\ \dot{\mathbf{y}}_2 \end{Bmatrix} + \begin{bmatrix} 0 & \mathbf{K} \\ \mathbf{K} & \mathbf{C} \end{bmatrix} \begin{Bmatrix} \mathbf{y}_1 \\ \mathbf{y}_2 \end{Bmatrix} = \begin{Bmatrix} 0 \\ 0 \end{Bmatrix} \quad (1.18)$$

which is again an equation of the type (1.15).

For such kind of equation it is considered a solution like (1.7), therefore deriving one time and substituting in (1.18), it is obtained

$$(\lambda\mathbf{A} + \mathbf{B})\mathbf{y} = 0 \quad (1.19)$$

Solving the eigenvalues problem in the equation (1.19),  $2N$   $\lambda$  values are obtained. Generally these eigenvalues are complex numbers, making possible to evaluate the natural frequencies and damping coefficient following the formulation

$$\lambda_i = \xi_i\omega_i \pm j\omega_i\sqrt{1 - \xi_i^2} \quad (1.20)$$

Being the eigenvalues in general complex number, substituting these values in the eigenvalue problem (1.19),  $2N$  eigenvectors  $\mathbf{y}$  are obtained. The physical meaning of these values refers to the reciprocal masses amplitudes for the real part of  $y_i$ , while the imaginary part will give information relative to the phase shift between each mass. The solution procedure is analogue to the eigenvalues and eigenvectors problems previously described.

### 1.2.5 Theory of experimental modal analysis for frequency response

As previously mentioned, in practical situation the estimation of natural frequencies is not a direct computation, being the system properties generally unknown for real applications.

The real experimental procedure will differ from the method previously presented. Usually information about one or more input forces, and the output system accelerations or displacements are available for test bench analysis.

Considering for simplicity a conservative system, excited with an harmonic force of a given frequency  $\omega_f$ , of the type  $\mathbf{f}(t) = \mathbf{f}_0 e^{j\omega_f t}$ . The system equation of motion is the type (1.3). Being the system conservative it is reasonable suppose the steady state response function like

$$\mathbf{x}(t) = \mathbf{x} e^{j\omega_f t} \quad (1.21)$$

that is oscillating at the same forced frequency with a different amplitude and possible phase shift.

Again deriving and substituting in the equation of motion, the following expression is obtained

$$(\mathbf{K} - \omega_f^2 \mathbf{M}) \mathbf{x} e^{j\omega_f t} = \mathbf{f}_0 e^{j\omega_f t} \quad (1.22)$$

Expressing the latter equation in a different way highlighting the response vector  $\mathbf{x}$

$$\mathbf{x} = (\mathbf{K} - \omega_f^2 \mathbf{M})^{-1} \mathbf{f}_0 \quad (1.23)$$

The right hand side term between parenthesis is usually called receptance matrix:

$$\alpha(\omega_f) = (\mathbf{K} - \omega_f \mathbf{M})^{-1} \quad (1.24)$$

It is possible to express each receptance matrix term in relation to single-frequency response function. Throughout the definition of matrix multiplication, the  $ik^{th}$  receptance term can be defined by the ratio

$$\alpha_{ik}(\omega_f) = \frac{u_i}{f_k} \quad (1.25)$$

if and only if  $f_i \neq 0 \forall i = 1 \div N \vee i \neq k$ .

Considering the matrix  $S_m$  of modal vectors normalised with respect to the mass matrix, such that the following statements still be valid for a conservative or proportionally damped system

$$S_m^T M S_m = I \quad (1.26)$$

$$S_m^T K S_m = \text{diag}[\omega_i^2] \quad (1.27)$$

and substituting in (1.24), it is obtained

$$\alpha(\omega_f) = S_m [\text{diag}(\omega^2 - \omega_f^2)]^{-1} S_m^T \quad (1.28)$$

Considering each  $ik^{th}$  term, obtained partitioning the  $S_m$  matrix into columns

$$\alpha_{ik}(\omega_f) = \sum_{r=1}^N (\omega_r^2 - \omega_f^2)^{-1} [s_r s_r^T]_{ik} \quad (1.29)$$

where the term  $[s_r s_r^T]_{ik}$  is known as modal constant or residue for the considered mode. Equalling the equations (1.28) and (1.29) it is possible to get the natural frequencies of the system.

For proportionally damped systems the equation (1.29) is slightly different [3]

$$\alpha(\omega_f) = \sum_{r=1}^N (\omega_r^2 + 2j\xi_r \omega_r \omega_f - \omega_f^2)^{-1} s_r s_r^T \quad (1.30)$$

while for non-proportionally damped ones will turn

$$\alpha(\omega_f) = \sum_{r=1}^N \left\{ \frac{s_r s_r^T}{j\omega_f - \lambda_r} + \frac{s_r^* s_r^{*T}}{j\omega_f - \lambda_r^*} \right\} \quad (1.31)$$

where the terms with the asterisk refer to the complex conjugate ones.

## Chapter 2

# FEM Theory for CAE Studies

### 2.1 Introduction

The FEM analyses theory was firstly applied in civil and aerospace engineering field starting from 40s. The theory quickly expanded to several applications not only for engineering usage, but also in mathematical and physical studies. Actually this model is wildly used for solving real continuous problems simplifying them as discrete trough finite elements.

The aim of this work consists in applying the FEM in order to solve complex systems of differential equation in the vibration field, commonly known as modal analysis. A lot of textbooks regarding FEM exist and they focus the attention mainly in structural analyses. Anyway two works were used as guideline in the analytically modal study presented in this monography.

The application of FEM method for modal analysis is well exposed in [10]. Here, procedures, suggestions and typical mistakes done by engineers in executing analytic studies are exposed step by step. A good explanation of general problem setting up is exposed in the first chapter.

A general approach to the modal analyses is presented by [2]. The topic is presented starting from basics vibration and FEM theory. Typical FEM errors and solutions to reduce them are presented.

The following sections regard the steps about how to set up a correct modal analysis in modern CAE software and a mathematical model for FEM error reduction. It has to be noticed that in modern CAE software such models are embedded in solver procedure.

The following chapters show analytic modal analysis results obtained in the first part of the work through the same CAE program.

### 2.2 Analytic modal study: steps procedure

The analytic modal analysis for a real structure could be a very complex procedure, and in most of the cases, quite impossible for manually solving. For this reason the CAE software make use of FEM theory in order to simplify the problem solution with a significant time decreasing. Nevertheless these programs helps the engineering workload, they do not substitute it and a step by step procedure is recommended.

As it is exposed in [10], the program solver only helps the engineer which in any case has to make relevant decision in order to set up the correct problem so that analytic results face experimental outcomes. The modal study can be divided in the following steps:

- CAD model definition: it establishes geometry and structure dimensions;
- model preparation for model study: it means simplify the real geometry ignoring trivial features, e.g. small holes, fillets, groove;
- material declaration for each part of the model;
- setting constrains and eventual external loads;
- internal boundary conditions between model elements, usually set by default from the solver. Therefore, it is important to set other eventual current links;
- FE definition, i.e. type of element (e.g. maximum or minimum size, geometry);
- mesh generation, consist in divide the model in previously selected FE;
- study solver setting up procedure:
  - define number of vibration modes required or frequency range;
  - setting up the convergence criterion;
- problem execution;
- result post processing and review.

Some of the upper features are usually automatically done by the internal program solver. Remembering that the software is only useful for assist the engineer in obtaining results, each of these points has to be critically analysed so that the analytic result of each step has physical meaning and the last outcomes can be validated with experimental ones.

Some precaution can be taken during the study setting up in order to minimise the possibility of inconsistent results, as well as correction can be made after updating some features.

There are also mathematical models applicable for evaluating the coherence between analytic and experimental results [4, 5]. The most known and discussed in literature is the Updating model. With such model it is possible to have a comparison between experimental analyses and analytic ones, based on results parameters, such as modal shapes or eigenvalues solution. Such comparison is able to identify eventual erroneous FEs which will be updated in a successive FEM analysis.

In the following section each procedure step will be discussed considering the application for the actual study model presented in the subsequent chapter.

## 2.3 Geometry definition

Software for 3D modelling, usually known as software CAD, are nowadays widely used in scholar and industry environment. The design process is much more rapid and unequivocal and the modelling final result is a virtual 3D model which reproduces with high detail level the true structure geometry.

Programs such as PTC Creo<sup>®</sup>, PRO Engineer<sup>®</sup>, SolidWorks<sup>®</sup>, Unigraphics NX<sup>®</sup>, Catia<sup>®</sup> are the most used, and all of them have similar features. PTC Creo<sup>®</sup> is the software used in this work both for modelling and for simulating.

The 3D model gives the possibility to visualise the final product previously designed, but each model can be more or less detailed depending on the following design step. Considering for example the most known part of a design process, the production. Here the designer can give product information to production plant, such as dimensions and geometrical features. At this point the final part produced should reflect exactly the virtual model, therefore the 3D drawing detail level has to be very high. Lets now suppose to use the 3D model for an analytic study. In this case the virtual representation can ignore some small features but general geometry information has to be kept.

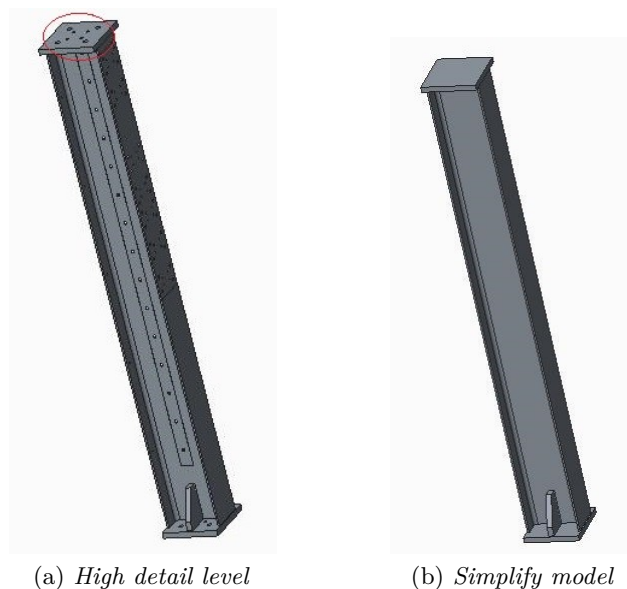


Figure 2.1: Beam element for detail levels example

Figure 2.1 shows an example of geometry model simplification. In particular, Figure 2.1 represents the beam element for the external structure of the study model exposed in the following chapter. For the analytic study some details such as holes, grooves, small section reductions in all components have been ignored.

The importance of simplifying the geometry is mainly due to eliminate, or at least reduce the possibility of error in the following study steps, such as mesh generation. Usually, curve elements or holes are critical geometries for FE generation and also for nodes congruence. Nevertheless, avoiding the presence of such kind of element guarantee a simpler geometry which directly affect the time required for the simulation. All these aspects influence the

number and quality of the FE. It is important to remember that the number of FE directly affect number of dof and, therefore, the time required to solve the system of equation. This topic will be recalled in the following sections.

An other important simplification consist in considering the geometry symmetry with respect the fundamental model planes, as it is exposed in [2] chapter 10<sup>th</sup>, which discuss the example of a body car frame dynamic study with FEM. Half of the whole structure was studied with a consequent reduction of elements and therefore computational time.

Fundamental is to consider also the presence of boundary conditions, such as in the latter example. Important geometry simplification such as symmetry condition require the application of analogous boundary condition in order to avoid erroneous results.

## 2.4 Material definition

Defining the material for each part of the model consist mainly in assign the physical properties. The most important material properties are density  $\rho$ , elasticity (or Young's) modulus  $E$ , Poisson coefficient  $\nu$ , maximum strength  $\sigma$ . These properties are of fundamental importance in most of analytic simulation. Defining the model geometry and the material for each part gives the possibility to compute mass and inertia properties.

In the field of interest for this work, modal analysis require mass and stiffness properties. Fundamental for such kind of problems is the definition of density, and Young modulus. With these latter parameters it is possible to get the mass and stiffness matrices which will guarantee the solution of the eigenvalues problem as exposed in section 1.2.

The majority of CAE softwares has an embedded material library in which the most common industrial material are present with their common properties. Anyway it is possible to create or edit materials making personal libraries, to be used in future simulations.

## 2.5 Constrain, loads and boundary conditions definitions

The constrain relation and boundary condition between structure parts is a crucial point in the modal study. Critical mistakes and erroneous results can appear, if wrong or not coherent choices are made in this part of the study definition.

In particular [2] identify two most common FEM modelling errors:

- mistakes due to wrong constrains or boundary condition applications;
- mistakes in mesh creation.

The definition of particular boundary conditions or constrains between model parts leads to set defined displacement or tension status between each FE node. It means that choosing a wrong boundary condition imply to define a displacement or a tension status which does not correspond with the actual physical one.

In particular [2] affirms that such kind of setting up error leads to wrong physical properties distribution due to mistakes in the FE nodes distribution or constrain. It is not possible to update these types of errors in successive corrections and it is also difficult to

recognise these situations. In the following chapter a situation comparable with this topic will be exposed.

An example from [2] of two different way of coupling two beams is shown in Figure 2.2.

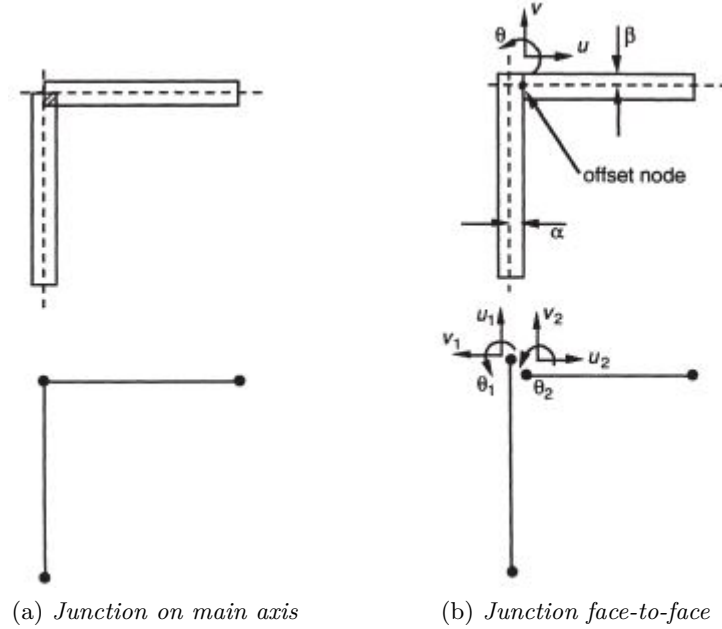


Figure 2.2: Example of two beams junction for FEM generation

Figure 2.2a shows the case of junctions in correspondence of two main axes. Applying such kind of junction implies a superposition of material between both beams, as well as a lack in the opposed side of the superposition. The CAE mesh generator will produce an erroneous mesh element distribution with a superposition of elements too and a possible incoherence in the nodes contact between elements. Moreover, in such kind of situation, also the mass and stiffness properties distribution are affected, and therefore, the system of equation solution will be wrong.

The solution proposed in Figure 2.2b is to move the junction point in such way that the beam faces are now in contact and a contact boundary condition will be applied. This kind of contact implies in null displacements between the two contact elements nodes, usually called bonded. In such a way, the elements distribution will be easier controlled and superposition will be avoided.

Loads application on the structure will not affect the modal properties. Note that the FRFs will be instead affected by eventual external loads.

## 2.6 Basic theory for finite elements

The finite elements study has the objective of divide the structure under investigation in small geometrical elements. Each element is characterised by nodes and edges which define a surface, as shown in Figure 2.3.

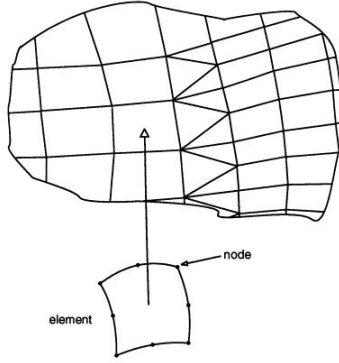


Figure 2.3: Example of finite elements

A fundamental feature for a correct FE analysis is the connection between elements, and some rules are mandatory for a correct division in elements. First of all each element node has to be linked with one or more nodes or being part of the system boundary, or rather, it is not admitted a superposition of elements, the only contact point between elements can be between nodes.

The number of nodes establishes the system degree of freedom. Therefore, it is possible to determine an equation of motion for each node. The displacement for nodes in contact has to be the same because of the material continuity, it is not possible to admit a separation in the material except in presence of cracks (it is a particular study case).

The FE division gives the possibility of system properties discretization, therefore to compute structure mass and stiffness. The elements are unequivocally identified in the space. Once material properties are defined along the study process, mass and stiffness are determined according with:

$$\mathbf{m} = \iiint_{-1}^1 \mathbf{N}^T \rho \mathbf{N} \det(\mathbf{J}) d\epsilon_1 d\epsilon_2 d\epsilon_3 \quad (2.1)$$

$$\mathbf{k} = \iiint_{-1}^1 \mathbf{B}^T \mathbf{D} \mathbf{B} \det(\mathbf{J}) d\epsilon_1 d\epsilon_2 d\epsilon_3 \quad (2.2)$$

where  $d\epsilon_i$  is the element differential position with respect to its local coordinate, the matrix  $\mathbf{N}$ , called form function matrix, identify each element position with respect its local coordinates, the matrix  $\mathbf{B}$  is the form function matrix first derivative with respect to general coordinates, the matrix  $\mathbf{D}$  expresses the elasticity properties and in the end the matrix  $\mathbf{J}$  is the so called Jacobian matrix, defined as:

$$\mathbf{J} = \begin{bmatrix} \frac{dx}{d\epsilon_1} & \frac{dy}{d\epsilon_1} & \frac{dz}{d\epsilon_1} \\ \frac{dx}{d\epsilon_2} & \frac{dy}{d\epsilon_2} & \frac{dz}{d\epsilon_2} \\ \frac{dx}{d\epsilon_3} & \frac{dy}{d\epsilon_3} & \frac{dz}{d\epsilon_3} \end{bmatrix} \quad (2.3)$$

It is possible to notice, from the equation (2.3), how a small variation in the FE space distribution can generate a sensible change in system mass and stiffness properties.

Regarding the elements types, the FE can have a quadrilateral and/or triangular geometry in 2D space, while them can be tetrahedral and/or hexagonal in 3D space.

## 2.7 Mesh generation

The system surface division in FE is defined as mesh. Therefore, once elements types and dimensions are defined, the system surface must be divided in a grid of small elements.

In most of the cases the procedure for mesh generation is automatically done by the software [10]. The engineer work is check and eventually correct the software mesh, or apply mathematical models in order to evaluate the possibility of incongruity between results due to error in mesh generation or constrain attribution.

### 2.7.1 Possible mesh generation failures

One of the most common source of error in modal analysis is due to mistakes in mesh generation (as exposed in 2<sup>nd</sup> chapter of [2] and discussed in section 2.5).

Several possible reasons are here exposed. As discussed in section 2.5, some of the most common mistakes regard the wrong relations definitions between system parts, or a extremely coarse mesh, which means a mesh with big dimensions, or FE superposition.

## 2.8 A posteriori adaptive FE error estimation technique

Several mathematical theories for FE error estimation have been proposed in the years. According with [1], the majority of these techniques are a posteriori adaptive methodologies based on the energy norm computation.

A method is defined adaptive when the error is controlled by subsequent system degree of freedom increasing in specified areas under investigation. A posteriori means to apply the technique in iterative process basing the following computation on a previous step.

This theory affirm that an error index  $\eta$  gives the error estimation with respect an energy norm such that the following expression still being valid:

$$C_1\eta \leq \| e \| \leq C_2\eta \quad (2.4)$$

In the equation (2.4) the values  $C_1$  and  $C_2$  are constants close to 1, and the energy is defined as  $e = u - U$ , where  $u$  is the theoretical exact value and  $U$  is the FEM approximation of  $u$ .

The last section from the second chapter in [2] proposes a solution for the norm energy value computation, based in [1]. This work proposes to compute the energy norm with respect to the evaluated structure stress value. The energy norm is defined as:

$$\| e_\sigma \| = \sqrt{\int_{\Omega} e_\sigma^T \mathbf{D}^{-1} e_\sigma d\Omega} \quad (2.5)$$

where the energy is defined by the difference between the theoretically exact value of the stress applied to the structure  $\sigma$ , and the evaluated FEM one  $\hat{\sigma}$ , such that:

$$e_\sigma = \sigma - \hat{\sigma} \quad (2.6)$$

The main obstacle faced in this procedure is a correct evaluation of  $\sigma$ , which is not provided by a FEM analysis. A way to overcome this initial problem is to estimate a  $\sigma^*$  value which approximate the theoretical  $\sigma$  in a closer form with respect to  $\hat{\sigma}$ . [2] proposes to evaluate the  $\sigma^*$  value by means of a smoothed tension value  $\bar{\sigma}^*$  interpolated using a displacement shape function  $\mathbf{N}$ :

$$\sigma^* = \mathbf{N}\bar{\sigma}^* \quad (2.7)$$

The least squared method is considered for the residual value  $(\sigma^* - \hat{\sigma})$ , in order to evaluate the smoothed values:

$$\int_{\Omega} \mathbf{N}^T (\sigma^* - \hat{\sigma}) d\Omega = 0 \quad (2.8)$$

Substituting the equation (2.7) in (2.8) and expressing the value of the smoothed stress, it is obtained:

$$\bar{\sigma}^* = \left( \int_{\Omega} \mathbf{N}^T \mathbf{N} d\Omega \right)^{-1} \int_{\Omega} \mathbf{N}^T \hat{\sigma} d\Omega \quad (2.9)$$

Up to this point, it is possible to express the error index in a percentage value as:

$$\eta = \frac{\| e_{\sigma} \|}{\left( \int_{\Omega} \sigma^{*T} \mathbf{D}^{-1} \sigma^* d\Omega \right)^{-1}} \times 100 \quad (2.10)$$

## Chapter 3

# PTC Creo<sup>®</sup> review

### 3.1 Introduction

The software PTC Creo<sup>®</sup> is the CAD/CAE software used in this work for the vertical axis test bench modelling and tests analysis. This software has the great advantage of offering a completely free student version edition with the full modelling features and a didactic simulate package for analytic analysis.

Several dedicated software exist for analytic simulation and in particular dynamic and modal analysis, such as MSC/Nastran<sup>®</sup> or Ansys<sup>®</sup>. Anyway it was decided to use the software PTC Creo<sup>®</sup> because of its intuitive and guided user interface without neglecting the result accuracy.

A brief PTC Creo<sup>®</sup> exposition is presented in this chapter. The main PTC Creo Parametric<sup>®</sup> feature and a comparison between the most known commercial software will be shown. A PTC Creo Simulate<sup>®</sup> review will be presented.

#### 3.1.1 PTC Creo<sup>®</sup> environment

All the PTC Creo<sup>®</sup> applications follow the same interface scheme, only changing the disposable features.

In general it is possible to recognise the following parts in each PTC Creo<sup>®</sup> working windows, an example is shown in Figure 3.1:

- Model Tree: in the red box;
- Tools Bar: in green box;
- Rapid Menu: in the blue box;
- Work Sheet: major area without box.

#### Model Tree

The Model Tree is a dedicated part which shows all the design or simulation work flow. In particular, each part design is shown in time history sequence, all the features created; in



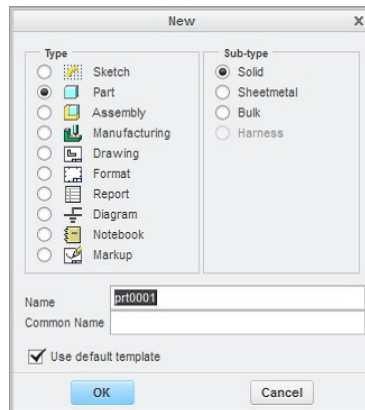


Figure 3.2: PTC Creo Parametric® first dialog windows

### 3.2.1 Sketch tab

The design procedure starts from here and the user working interface is opened. In general each design process, part or assembly design process, will be characterised by a slightly different dialog windows, anyway the main tabs are shown in Figure 3.1. The interface is divided into eighth main windows which guide the user in the modelling process. The starting point for the 3D design process is to draw a 2D sketch from the same task in the main "Model" tab (Figure 3.1). Here the software open a dialog window in which all the sketch features are inside. First of all it is require to specify in which plane the sketch will be drawn.

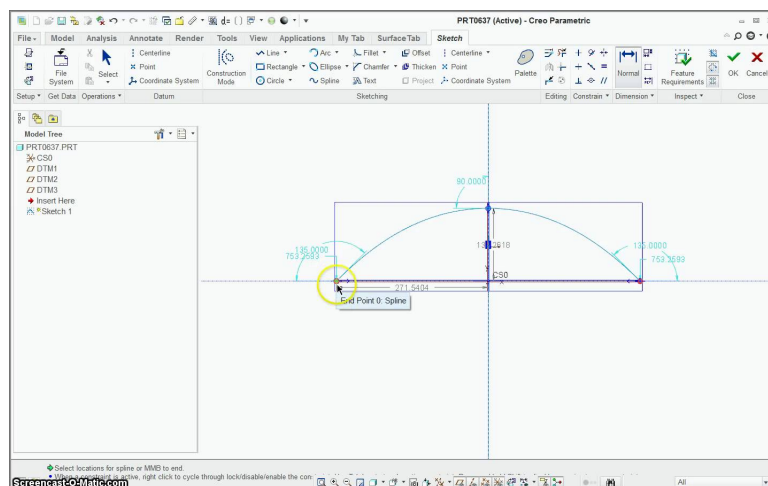


Figure 3.3: PTC Creo Parametric® sketch features

It is now possible to start defining the part geometry, drawing it with line, circle, square etc. (Figure 3.3). Dimension and constrain tabs allow to define the sketch relations between drawn geometrical features. When the sketch is fully constrained, in other words the sketch is unequivocally fixed in relation to the main plane reference system, it is possible transform

the geometry in a 3D design.

### Comments and comparisons between software

Most of the commercial softwares used in educational or industrial fields, present the same features and dialog windows structures. Nevertheless all these programs are slightly different.

In particular shortcuts commands are different from the SolidWorks®, Unigraphics NX® and Inventor® programs.

The automatic relation between sketch features is not present in PTC Creo Parametric®, as well as in Unigraphics NX® and in comparison with SolidWorks® and Inventor®. Here all the possible reference between the sketch and the main reference system are required and not directly found out by the program.

A great contrast point between PTC Creo Parametric® and other softwares is the dimensions definition. Here, a dimension set can be easily updated only with drag and drop. This is a confusing software characteristic. In other programs, once a distance is set, the point or the feature is unequivocally related with respect another sketch element. It means that the user can not drag and drop the feature anymore. It is a synonym of element constrain and it is helpful for determining the sketch full constrain. Therefore it is more difficult to visualise when the sketch is fully constrained and therefore pass to the following design step.

### 3.2.2 Model tab

In the model tab it is possible to edit an existing 3D feature creating holes, repetition or mirroring, or it is possible to extrude a 2D sketch into a 3D feature. All the commands are shown in the tab as it is displayed in Figure 3.1.

All the features exposed in the PTC Creo® Model tab are quite the same for other commercial programs. Small difference exist in the way to define the specified command.

### 3.2.3 Assembly procedure

It is possible to connect more than a part creating an assembly, which will represent the CAD model reproduction of a future product. In order to create an assembly it is required to choose the proper file extension once the software is launched (Figure 3.2).

Again the procedure for creating assemblies is similar between the different softwares. Anyway the way to define constrains between parts is slightly different, the procedure is well guided by the program interface.

In PTC Creo Parametric® the assembly construction is made opening the assembly environment from the dialog window in Figure 3.2, such that a work windows like Figure 3.1 will be shown. Here pressing the button Assembly, in the main tab Model and in the environment Component, it is possible to choose which part will be included in the assembly.

Once the part is chosen, a dialog window for the component placement will appear, as it is shown in Figure 3.4. It is possible to define the relation between the the new part and the existing assembly.

There are some different features regarding the complexity in resetting constraints between parts previously set. In PTC Creo® this process is not fully accessible, being required to right click on the desired part shown in Model Tree, and define "Edit Actions: edit definition for the selected object". Clicking there makes appear again the Component Placement dialog window and the part position is again editable.

### 3.2.4 Drawing model

The innovative part of the CAD/CAE software is the possibility to extract digital drawings directly from the 3D part, enormously reducing the engineer workload due to manual drawings. The final output is the same for all the commercial softwares, a .pdf file with all levels of details required for the following design step.

## 3.3 PTC Creo Simulate®

The program Simulate of the package PTC Creo® is dedicated to analytic structural, thermal, modal, dynamic and motion simulations. This is one of the differences, for example with the program SolidWorks®, which has a dedicated program for each of required analysis, in the premium package.

The PTC Creo Simulate® student version is not available in the free package, only a demon version is disposable, which is not fully available in all its features.

The fully student 3.0 release of the software was used for the modal analyses execution which will be shown in the next chapters.

### 3.3.1 Simulate environment

As it was exposed in section 3.1.1, all the PTC Creo® packages have the same working environment characterised by a Model Tree, Tools Bar, Rapid Menu and Work Sheet, as it is shown in Figure 3.1.

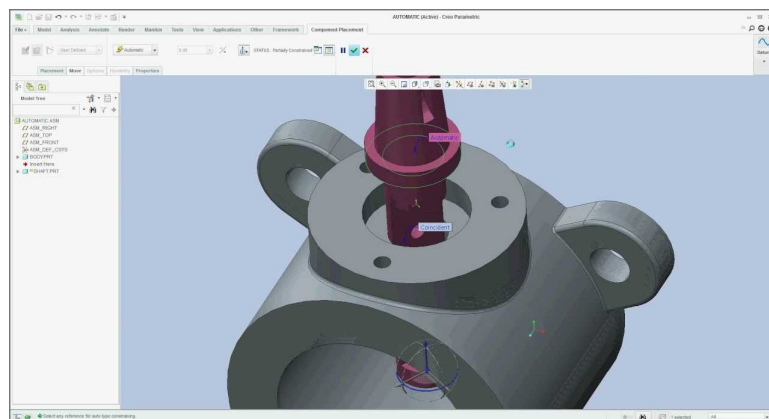


Figure 3.4: Assembly dialog window for components assembly

The main difference between the Simulate and Parametric packages are the different features, in particular, those are reduced in number for the Simulate one .

### Model Tree

The Model Tree shows all the CAD parts which are made up of the eventual assembly, the material assigned to each part, the constrains set, the mesh information and the analysis, as it is shown in Figure 3.5

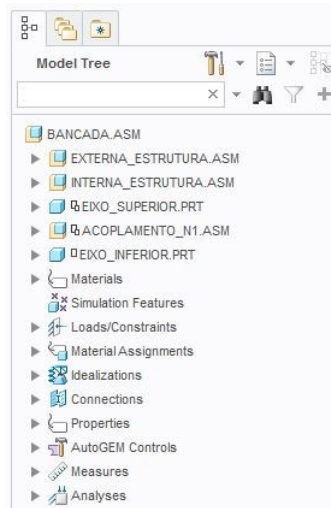


Figure 3.5: Model Tree for PTC Creo Simulate®

The Model Tree, therefore, make accessible all the simulation steps setup, so that they can be easily modified.

### Rapid Menu

The Rapid Menu is composed by five main tabs: Home, Refine Model, Inspect, Tools and View, as shown in Figure 3.6.

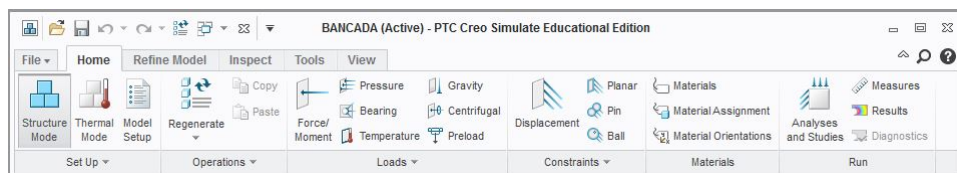


Figure 3.6: Rapid menu - Home tab

### Tools Bar

For a simulation setup, all the tools are collected in the first two tabs Home (Figure 3.6) and Refine Model (Figure 3.7)

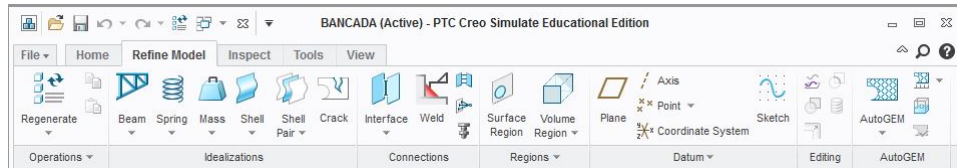


Figure 3.7: Simulation tools for Refine Mode tab

### 3.3.2 Description of the simulation setup process

As shown in Figure 3.6, the main two studies that can be set up are Structure or Thermal study. For this work, the Structure one was selected.

#### Model study setup

In this environment the Model Setup option allows to define the main study, therefore, the type of study: the FEM mode analysis will create mesh model file in Ansys® or MSC/Nastran® extension; the general interface conditions are set by default to bonded (Figure 3.8).

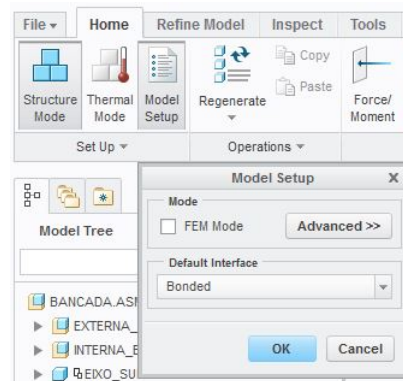


Figure 3.8: Setup options for Structure study

The Tools Bar gives a great help in setting a correct study. The steps are defined by the sequence displayed in Figures 3.6 and 3.7.

#### External loads and constrains

In the Home tab it is possible to define eventual external loads applied to the structure under evaluation, after the constrains and the materials.

#### Material definition

For the material definition, it is possible to choose from a predefined library present in the software, as shown in Figure 3.9. This library contains only the engineering most common materials with the relative average properties. For specific materials, such as Al7000 series,

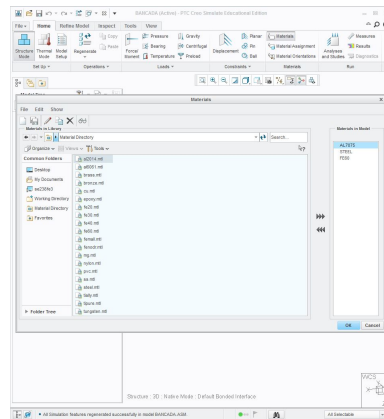


Figure 3.9: PTC Creo Simulate® material library

the user needs to create its own material. This is not a difficult process, but quite time spending. A solution could be search the required material in online users communities.

### Geometry redefinition

Once the previous features are set, it is possible to move to the Refine Model tab (Figure 3.7), which allows to redefine some model parts in order to assign determined structural behaviours, such as beams, springs or masses.

Particular attention has to be given to the definition of new contact constrains between elements parts. By default, the contact between all the model parts is bounded. If a contact is updated a different mass and stiffness distribution will be assign once the mesh is created, as it is exposed in section 2.7.1.

The next set of options in the Refine Model tab refers to new surface or volume identification in model parts. These geometrical features can be created after the creation of a sketch that will define the general shape of the new geometrical feature. This step can be important if a different dimension mesh is required in the same part. It is recommendable to create a new geometrical feature in the PTC Creo Parametric® environment, because geometrical features created in Simulate can not be deleted or modified.

### Mesh generation

It is possible to find the mesh setting options in Refine Model tab.

PTC Creo Simulate® has a automatic mash generator: the AutoGEM feature. This tool automatically creates FEs according with the engineer specification. If no inputs are given to the software, it automatically creates elements with a maximum dimension of  $10mm$ .

Three are the principal and most used FEs definitions: maximum elements dimension, minimum element dimensions and mapped mash. It is possible to set the elements required considering surfaces, volumes, defining the geometry to discretize through points or edges selections or selecting the whole component.

The first two options will generate triangular and tetraedric elements whose dimensions, maximum or minimum respectively, is tried to be reached by AutoGEM. Notice that the

constrain set during the geometry element definition is a goal for the AutoGEM tool, namely, it tries to approach such requirement. If the automatic generator is not able to create the specified elements, it will automatically reshape the discretization making a comparison between the element size and the whole part volume; in such case also a warning message will be displayed.

The mapped mesh consist in divide the part surface in quadrangular or cubic elements for planar surfaces, or triangular or tetrahedric ones for circular surfaces. This type of division gives the possibility of reducing the computational time, because the structure will be divided in less elements, therefore less number of nodes, without losing accuracy in the results. Such type of mesh elements is particularly suitable for element with planar symmetry in movement elements, in which high pressure contact holds or small thickness are present.

Even if the Model Tree is built, it is possible to visualise and eventually modify any design parameter. The mesh distribution is the only feature which can not automatically be displayed when the user selects it. A complex and not intuitive procedure is required for mesh visualisation; each time it is necessary to open the AutoGEM tool and to load or reconstruct it.

### 3.3.3 The analysis

It is possible to find the Analysis and Study tool in the Home tab. With the last tool it is finally possible to choose and setting the type of study required.

Table 3.1 shows a brief exposition of the possible types of analyses.

Table 3.1: PTC Creo Simulate® analysis types

Product	Analysis Type
Structure analyses	<ul style="list-style-type: none"> <li>- Linear Static Analysis</li> <li>- Non Linear Static Analysis with Large Deformation</li> <li>- Non Linear Static Analysis with Contacts</li> <li>- Non Linear Static Analysis with Elastoplastic Materials</li> <li>- Non Linear Static Analysis with Hyperelastic Materials</li> <li>- Prestress Static</li> <li>- Buckling</li> <li>- Modal</li> <li>- Prestress Modal</li> <li>- Fatigue</li> </ul>
Thermal	<ul style="list-style-type: none"> <li>- Steady-State Thermal</li> <li>- Transient Thermal</li> </ul>
Vibration (only for parts)	<ul style="list-style-type: none"> <li>- Dynamic Time Response</li> <li>- Dynamic Frequency Response</li> <li>- Dynamic Random Response</li> <li>- Dynamic Shock Response</li> </ul>

Once the Analysis and Study option is selected, a dialog windows appears.

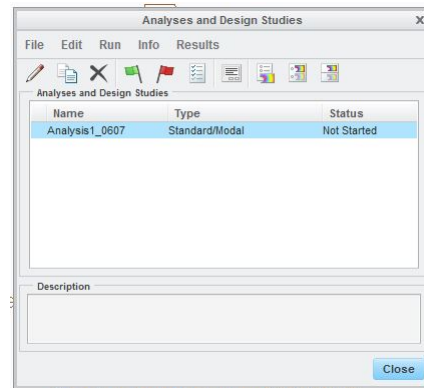


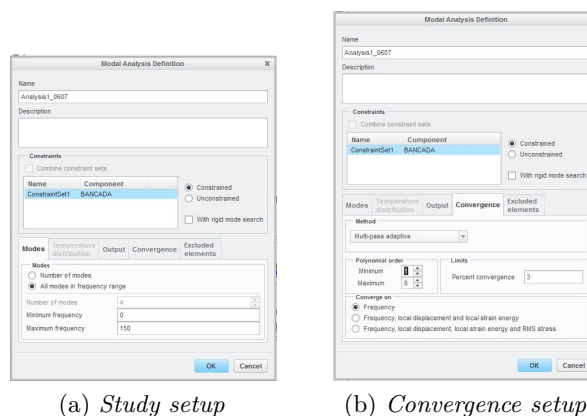
Figure 3.10: Analysis dialog windows

In the dialog window, shown in Figure 3.10, the File tab exposes all the possible type of analyses according with Table 3.1, for the selected Product.

In this case, the possible feature for the Modal Analysis of the Structure package is shown.

### Modal analysis definition

There are two types of analysis which can be selected for a Modal study in Simulate: the first one consists in choosing the number of modes the solver has to evaluate without any restriction regarding the frequency range, the second one permits to set a frequency range in which the solver has to evaluate all the natural structure modes (Figure 3.11a). It is common in modal analyses studies to evaluate critical conditions due to low natural frequencies. Those are the most dangerous circumstances, thinking to the Tacoma Bridge disaster or a starter rotor where low rotational speeds can match natural frequencies. This is also the case of interest for this study, which will be discussed in the following chapter, where structure natural frequencies below  $100Hz$  are investigated.



(a) Study setup

(b) Convergence setup

Figure 3.11: Modal analysis definition

An important feature to be selected for a correct modal study is the type of convergence criterion. It will determine when the solver has to end the simulation process. It is important to establish the proper convergence model in order to avoid erroneous results but from the opposite side to loss time for the simulation process end.

The PTC Creo Simulate® gives the possibility of three convergence criterion (Figure 3.11b):

- Quick Check;
- Single-Pass Adaptive;
- Multi-Pass Adaptive.

Even being the adaptive criterion one of the most commonly used for analysis and discussed in literature [2], here it is possible to notice the main relevant difference between PTC Creo Simulate® and commercial dedicated software like MSC/Nastran® or Ansys®; for such kind of programs the convergence criterion selection is greater.

### **Quick Check**

This convergence criterion is the faster one. It is usually recommended in first analysis in order to check problem setup consistence. The solver runs once the analysis for a polynomial of 3<sup>rd</sup> order.

### **Single-Pass Adaptive**

With such type of analysis the solver resolves the problem in two subsequent iterative procedure. Starting from a polynomial of the 3<sup>rd</sup> order, the solution and its error estimation are computed. The solver automatically increases the polynomial order considering the latter error magnitude.

If this type of convergence is chosen, it is fundamental the engineer critical interpretation of the results, establishing if the obtained level of error match the requirements, and therefore, the results can be considered acceptable. If the error level is not sufficiently low, the engineer can consider the hypothesis to move to a Multi-Pass Adaptive convergence.

### **Multi-Pass Adaptive**

This is the most complete and computer memory time consuming criterion of convergence offered by Simulate.

Various inputs are required for setting the problem. First of all, it is required to choose the convergence to be computed, in particular, it is possible to select between:

- convergence on frequency;
- convergence on frequency, local displacement and local stain energy;
- convergence on frequency, local displacement, local strain energy and RMS stress.

All these items are referred to a percentage index of the error, as exposed in section 2.8 and [1, 2]. This percentage is a parameter chosen by the analyst. It is easy to understand that each of the three convergence choices implies an higher time for end the simulation.

The second feature to be selected is the polynomial order both for the first iteration and the maximum order (Figure 3.11b).

The solver starts the iterative adaptive procedure solving the problem with a polynomial of the order established. As well as the Single-Pass procedure, the subsequent steps are automatically set by the solver increasing the polynomial order according with the error level.

The solver stops in two cases: the convergence is reached and the results are generated, or the convergence is not reached for the maximum polynomial order set, anyway the results computed up to that level are disposable.

A third possibility of solver break without disposable result can occur and it is common for all the three convergence criterion in case All modes in frequency range analysis method is set: it is the case in which the solver does not find any mode in that frequency range.

### 3.3.4 Result visualiser tool

The results obtained from any kind of analysis can be visualised in a proper program, PTC Creo Result®.

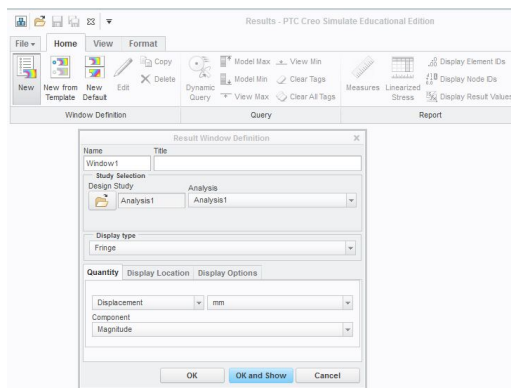


Figure 3.12: PTC Creo Result® user interface

Again the user interface is the common one of all Creo packages with the exception in the case of Model Tree.

Selecting the New command in the Home tab, a dialog window, like the one shown in Figure 3.12, appears. It is possible to choose the result from a analysis file, to be displayed. In the case of modal analysis, it is possible to display the modal displacements, structure stresses, to draw plots for specified points on the structure, all this for required natural frequencies or combination of them.

Several layouts can be chosen from a predefined list, or new ones can be created.

# Chapter 4

## Analytic modal analysis results

### 4.1 Introduction

In this chapter the modal analysis settings up and results will be discussed. Several analysis, each time with a higher level of detail, were run. The analytic study for each part of the complete test bench model were computed.

The model under investigation is a test bench for vertical shafts. The structure is composed by an external structure, made of four double T beams bolted on a base, and a superior frame frame, made of four welded steel rectangular parts. The external structure is provided of four structural elements aiming to support the superior shaft and sensors supports for future experimental analyses; these structural elements also guarantees more stiffness.

An internal structure, independent on the external one, is present inside the latter. The aim is to house the electrical motor and support the inferior shaft.

The whole CAD model is shown in Figure 4.1.

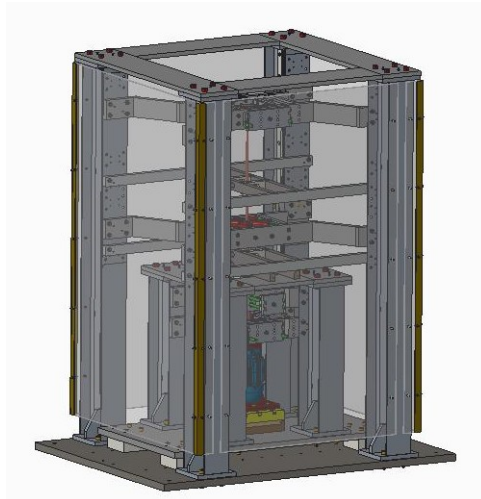


Figure 4.1: Test bench for vertical shafts 3D CAD model

Same procedure, described in Chapter 2, is used for setting up the analyses. In this case the geometry, therefore the 3D models were provided.

As shown in Figure 4.1, this model has an high level of details, for this reason, all small geometrical features, such as holes, and structural elements, like screws and bolts, have been removed. Even existing in PTC Creo<sup>®</sup> a tool for hiding such kind of features only for CAE simulation, the models have been permanently simplified so that these could be used also with others simulating softwares.

In the following sections all the simulation results are exposed. The analyses for each sub-assembly model are firstly presented, up to the final one concerning the global model. The following structures are studied:

- External simplified structure;
- External complete structure;
- Internal structure;
- Superior shaft;
- Inferior shaft;
- shafts assembly;
- Global structure.

One analyses with Ansys AIM 18<sup>®</sup>, only for the External simplified structure is run. The reason behind this choice is to compare the fist result obtained with PTC Creo Simulate<sup>®</sup> in order to evaluate eventual discrepancies between results.

In general, three simulation for each structure, with an increasing quality of the mesh, were executed. It is possible to classify the analyses for each model as:

- Coarse mesh: elements size with higher dimensions;
- Medium mesh: elements size with mean dimensions lower than the coarse, therefore an higher number of elements;
- Fine mesh: smallest elements size and highest number of elements in relation with all the simulations.

The final simulations target is to investigate the system properties in its low frequency field, in the range between  $0 \div 150Hz$ . It is required in order to mitigate the effects of an eventual excitation of the natural frequencies of the structure during the shaft operation. The presence of substructure natural frequencies and modes in the global model are investigated.

## 4.2 External simplified structure

The first analysis concerns the external structure without any internal supports.

Seven analyses were run for this model. The first three results are obtained defining a different contact relation between the model parts. A simulation with Ansys AIM 18<sup>®</sup> is executed, in order to check the previous results. Than other three simulation with PTC Creo Simulate<sup>®</sup> and default connection between model parts were run.

The geometry, boundary conditions with respect the absolute reference system and material definitions are in common in the seven simulations.

### Geometry

The model is composed by five elements, as Figure 4.2 shows, and described in Table 4.1.

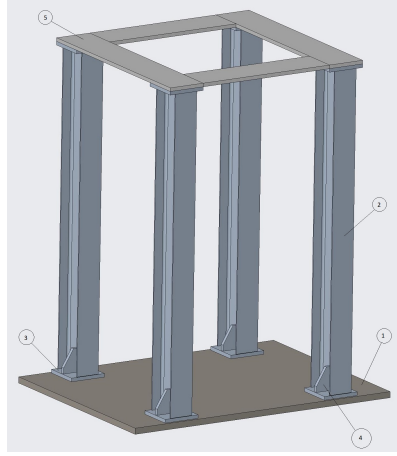


Figure 4.2: Simplified external structure CAD model

Table 4.1: List of materials for simplified external structure

Id.	Name	Quantity	Material
1	Base	1	Structural steel
2	Double T beam	4	Structural steel
3	Beam backing base	8	Structural steel
4	Beam support	8	Structural steel
5	Superior frame	1	Structural steel

### Material

The material is the same for all parts. Structural steel is the material selected from PTC Creo Simulate<sup>®</sup> material library. The principal properties of interest are reported in Table 4.2

Table 4.2: Structural steel properties from PTC Creo Simulate®

Density $\rho [\frac{kg}{m^3}]$	Young modulus $E[GPa]$	Poisson coefficient $\nu[-]$
7827	199.95	0.27

### Boundary conditions

A fixed boundary conditions between the base bottom part and the solver absolute reference system is considered. It means that the structure can not translate and rotate and it is fixed to the ground. This constrain would reproduce the link between base and ground throughout the four supports, which here are not taken into account. Figure 4.3 shows in green the constrain location.

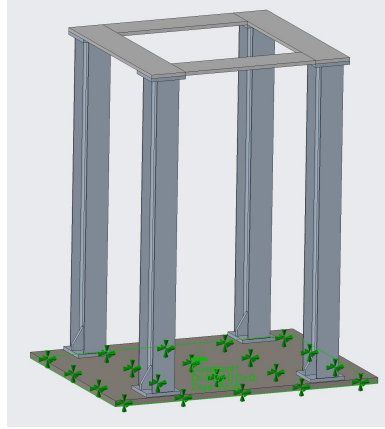


Figure 4.3: External simplified structure, boundary condition

### 4.2.1 First analysis for simplified external structure: coarse mesh

#### Contact relation between parts

A Rigid Link between the beam backing bases and grounded base, as well as the superior frame and beams, was set for the first three analyses. Overwritten contact relations appear in brown colour in Figure 4.4.

As it is exposed in the PTC Creo® online helper [11]: *"a Rigid Link is suggested for a component whose rigidity is far greater than the others, and whose only contribution is to maintain set displacements between attached components. Components so connected are free to move in any manner, but will maintain their relative positions."*

#### Mesh element definition

Different kinds of FEs are chosen for this analysis. In particular, mapped mesh is set for the base and the superior frame, while maximum element size is selected for beams and

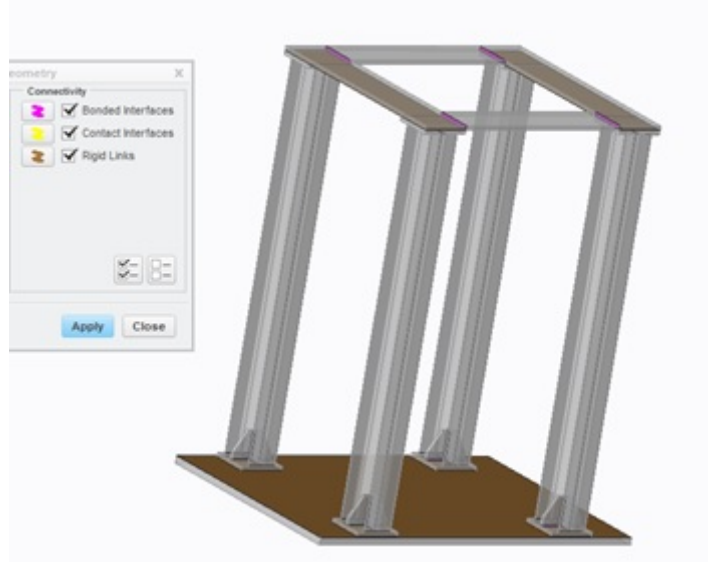


Figure 4.4: Redefinition of contact between external simplified structure parts

relative backing bases and support parts.

The reason to select differentiate meshes is due to the part symmetry; both base and superior frame are rectangular parts, therefore, it is possible to reduce the number of elements and dofs choosing a mapped mesh. Table 4.3 reports the element dimensions set.

Table 4.3: Simplified external structure, coarse mesh, FE size

Id.	Name	Type of FE	FE dimension [mm] or $n^\circ$
1	Base	Mapped	2
2	Double T beam	Max element size	100
3-4	Beam backing and support	Max element size	80
5	Superior frame	Mapped	2

### Mesh generation and analysis parameters

Figure 4.5 shows the AutoGEM mesh obtained. Not all the features set are correctly executed, in fact the base and the part of the superior frame have not a mapped discretization.

A warning message is displayed during the mesh auto-generation. This message informs that not all the specified features are correctly executed. A rearranging discretization is adopted in order to correctly connect each FE nodes between contact parts.

For this study the following results from the AutoGEM are obtained, and the relative study settings are established:

- Number of points: 4980;

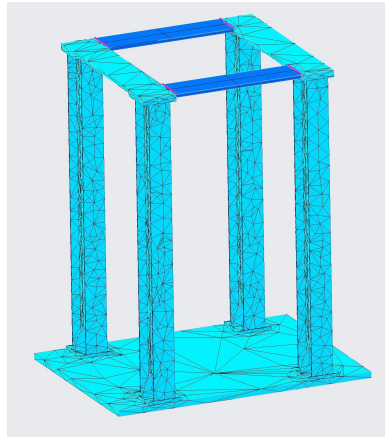


Figure 4.5: Coarse mixed mesh, simplified external structure

- Number of edges: 25145;
- Number of solid elements: 15553;
- Convergence criterion: Single-Pass Adaptive;
- Analysis definition: ten first modes.

## Results

The Single-Pass Adaptive solver, as it was exposed in section 3.3.3, runs the iterative computation process twice.

Ten first modes as analysis definition is considered because, in this first approach to modal analysis, the number of natural frequencies under  $100Hz$  is not fully known.

A number of equations equal to 267069 with a maximum polynomial order of 4 is executed in the first step. In the second step the polynomial order is increased up to 7 with 290052 equations to be solved.

Table 4.4 shows the natural frequencies values obtained and the relative RMS error percentage computed with respect to the natural frequency.

From the results in Table 4.4, it is possible to notice that only the first four natural frequencies are in a range between  $0 \div 150Hz$ , which can be considered the critical range. Moreover, the error percentage is sufficiently small to consider those results valid. Anyway, other simulations are run in order to compare the results and confirm the existence of even small differences between final values, due to change in the number of FE.

### 4.2.2 Second analysis for simplified external structure: medium mesh

#### Contact relation between parts

Again for the second analysis, the same contact relation exposed in section 4.2.1 is set. Figure 4.4, shows the location, as well the previous analysis.

Table 4.4: Natural frequencies and RMS errors, external simplified structure: coarse mesh

Mode	Natural Frequency $\omega_n [Hz]$	Error $\eta\%$
1	19.78	0.5
2	62.20	0.3
3	73.72	0.4
4	127.48	0.5
5	157.64	0.6
6	205.80	0.5
7	212.94	0.6
8	214.37	0.5
9	219.65	0.2
10	234.65	0.4

### Mesh element definition

Based on the same scheme of the previous analysis, mapped mesh is set for the base and the superior frame, while maximum element size is selected for beams and relative backing bases and support parts. The only difference is the dimensions and number of elements. Table 4.5 shows the data set up.

Table 4.5: Simplified external structure, medium mesh, FE size

Id.	Name	Type of FE	FE dimension [mm] or $n^\circ$
1	Base	Mapped	3
2	Double T beam	Max element size	70
3-4	Beam backing and support	Max element size	30
5	Superior frame	Mapped	3

### Mesh generation and analysis parameters

Figure 4.6 shows the AutoGEM mesh obtained. Not all the features set were correctly executed, in fact the base and the part of the superior frame have not a mapped discretization.

For this study the following results from the AutoGEM are obtained, and the relative study settings are established:

- Number of points: 7152;
- Number of edges: 36367;
- Number of solid elements: 22865;
- Convergence criterion: Single-Pass Adaptive;

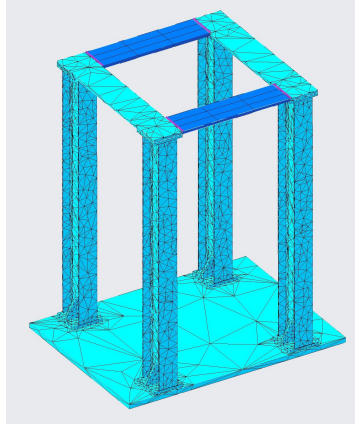


Figure 4.6: Medium mixed mesh, simplified external structure

- Analysis definition: ten first modes.

## Results

Increasing the number of FE, also the number of equations will increase. For this reason the number of equation for the first iteration is 3377859 with a maximum polynomial order of 4. In the second step the polynomial order is increased up to 8 with 428088 equations to be solved.

Table 4.6 shows the natural frequencies values obtained and the relative RMS error percentage computed with respect to the natural frequency.

Table 4.6: Natural frequencies and RMS errors, external simplified structure: medium mesh

Mode	Natural Frequency $\omega_n [Hz]$	Error $\eta\%$
1	19.70	0.4
2	62.13	0.2
3	73.66	0.2
4	127.08	0.4
5	157.09	0.4
6	205.16	0.3
7	212.15	0.3
8	212.28	0.3
9	216.23	0.2
10	234.22	0.2

Again, from Table 4.6, it is possible to notice that only the first four natural frequencies are in a range between  $0 \div 150Hz$ . The error percentage is sufficiently small to consider those results valid.

Very small difference in the the results exists for the field of interest.

### 4.2.3 Third analysis for simplified external structure: fine mesh

#### Contact relation between parts

The same contact relation exposed of section 4.2.1 is set. Figure 4.4, shows the location, as well the previous analyses.

#### Mesh element definition

Again, mapped mesh is set for the base and the superior frame, while maximum element size is selected for beams and relative backing bases and support parts. The only difference is the dimensions and number of elements. Table 4.7 shows the data set.

Table 4.7: Simplified external structure, fine mesh, FE size

<b>Id.</b>	<b>Name</b>	<b>Type of FE</b>	<b>FE dimension [mm] or <math>n^\circ</math></b>
1	Base	Mapped	8
2	Double T beam	Max element size	20
3-4	Beam backing and support	Max element size	18
5	Superior frame	Mapped	8

#### Mesh generation and analysis parameters

Figure 4.7 shows the AutoGEM mesh obtained. Not all the features set were correctly executed, in fact the base and the part of the superior frame have not a mapped discretization.

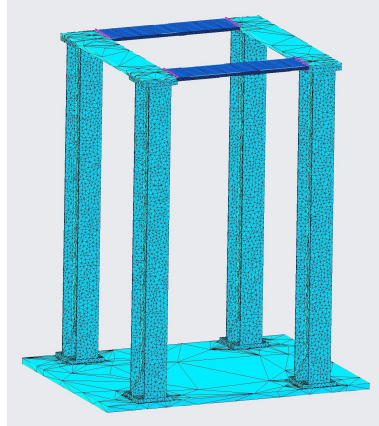


Figure 4.7: Fine mixed mesh, simplified external structure

For this study the following results from the AutoGEM are obtained, and the relative study settings are established:

- Number of points: 24440;

- Number of edges: 122162;
- Number of solid elements: 74123;
- Convergence criterion: Single-Pass Adaptive;
- Analysis definition: ten first modes.

## Results

Increasing the number of FE, also the number of equations will increase. For this reason the number of equation for the first iteration is 1265712 with a maximum polynomial order of 4. In the second step the polynomial order is increased up to 7 with 1323858 equations to be solved.

Table 4.8 shows the natural frequencies values obtained and the relative RMS error percentage computed with respect to the natural frequency.

Table 4.8: Natural frequencies and RMS errors, external simplified structure: fine mesh

Mode	Natural Frequency $\omega_n [Hz]$	Error $\eta\%$
1	19.65	0.1
2	62.09	0.2
3	73.62	0.3
4	126.87	0.1
5	156.79	0.1
6	204.74	0.2
7	210.39	0.2
8	211.83	0.2
9	213.64	0.1
10	233.95	0.3

Again, from Table 4.8, it is possible to notice that only the first four natural frequencies are in a range between  $0 \div 150Hz$ . The error percentage is sufficiently small to consider those results valid.

Very small difference in the the results exists for the field of interest.

### 4.2.4 External simplified vibration modes: rigid link contact

This section shows only the vibration modes in the frequency range between  $0 \div 150Hz$ .

Figure 4.8 shows the vibration modes. All the three simulations turn the same modes, exposed in Figure 4.8, the only difference is in the natural frequencies values, as it is discussed in the previous sections.

The main displacements concern the beams, as expected. The first three modes are of interest and are the ones which could appear in real applications. It is possible that the mode in Figure 4.8d will not be present in real application, because of the strong assumption regarding the geometry simplifications.

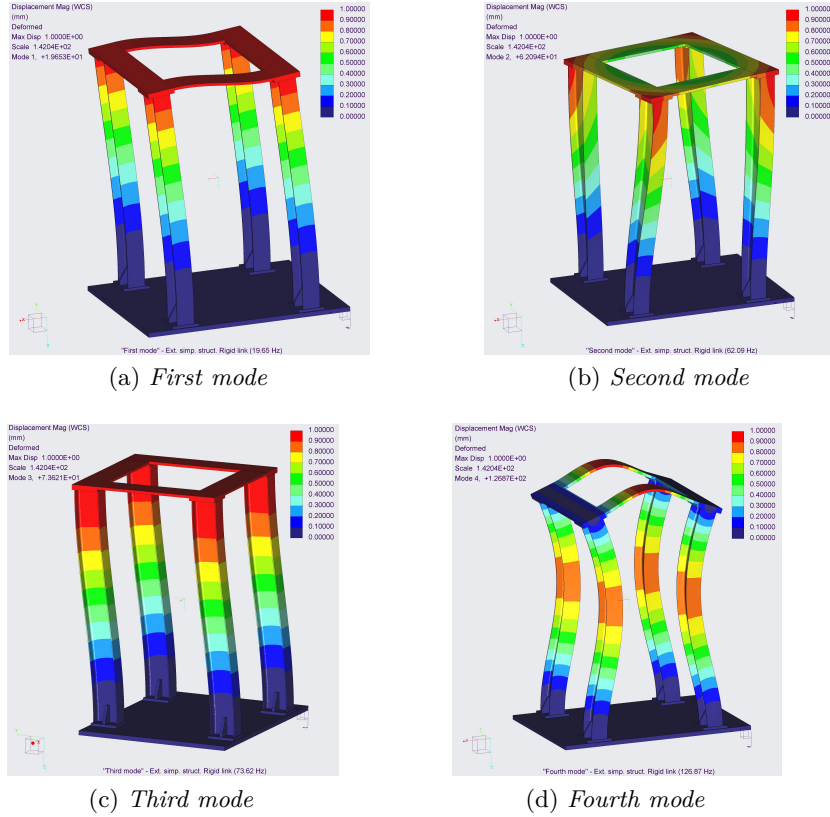


Figure 4.8: External simplified structure vibration modes: rigid link contact

The mode in Figure 4.8b is the most dangerous vibration mode. Torsional displacement could lead to catastrophic structural collapses, and for this reason should be avoided increasing the structure stiffness. In the following analyses the study of this mode will be of interest.

#### 4.2.5 Fourth analysis for simplified external structure: Ansys AIM 18<sup>®</sup>

##### Contact relation between parts

From here on only default contact relation between parts are considered. The default configuration is the bonded one. Bonded contact imply that all the parts in contact have a null relative displacement. Moreover, the nodes belonging to two different parts in contact are joined, meaning null displacement between the two FEs.

##### Mesh element definition

Ansys AIM 18<sup>®</sup> give the possibility to choose several FE settings. For the proposed analysis, general FE definition is set up for the whole geometry. Here the FEs settings are described:

- Starting FE dimension: 25mm;
- Increasing element ratio: 1.5;
- Mesh quality increasing ratio for Adaptive solver: 1.

In particular, the starting dimension set the minimum element size, the increasing ratio define the ratio between the biggest and the smallest FE, the last item define the way how the solver increase the mesh quality for the following steps in the adaptive method.

### Mesh generation and analysis parameters

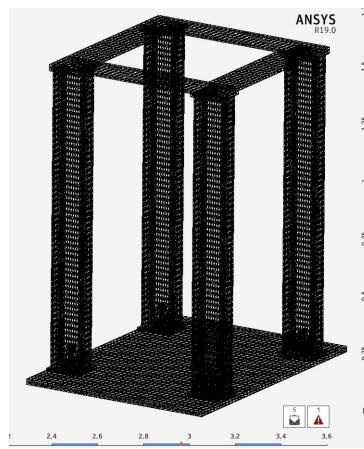


Figure 4.9: Very fine mesh, simplified external structure: Ansys AIM 18<sup>®</sup>

Tetragonal and hexagonal FEs have been created in this analysis. In particular, comparing the number of nodes obtained in the final mesh, this type of discretization can be very well defined. Figure 4.9 shows the mesh discretization.

The following parameters have been selected for this analysis:

- Number of points: 79973;
- Number of solid elements: 12328;
- Convergence criterion: Adaptive;
- Analysis definition: six first modes.

### Results

From this study, the results in Table 4.9, in term of natural frequencies are obtained.

The results from Table 4.9 show a big difference between the first three simulations (Tables 4.4 - 4.6 - 4.8). The main reason behind it can be attributed to wrong connections definitions.

For this reason, other three analyses were accomplished.

Table 4.9: Natural frequencies, external simplified structure: Ansys AIM 18<sup>®</sup>

Mode	Natural Frequency $\omega_n [Hz]$
1	19.336
2	38.828
3	43.715
4	125.80
5	129.552
6	154.292

#### 4.2.6 External simplified vibration modes: Ansys AIM 18<sup>®</sup> results

In this section are shown only the vibration modes in the first five modes corresponding with frequency range between  $0 \div 150 Hz$ .

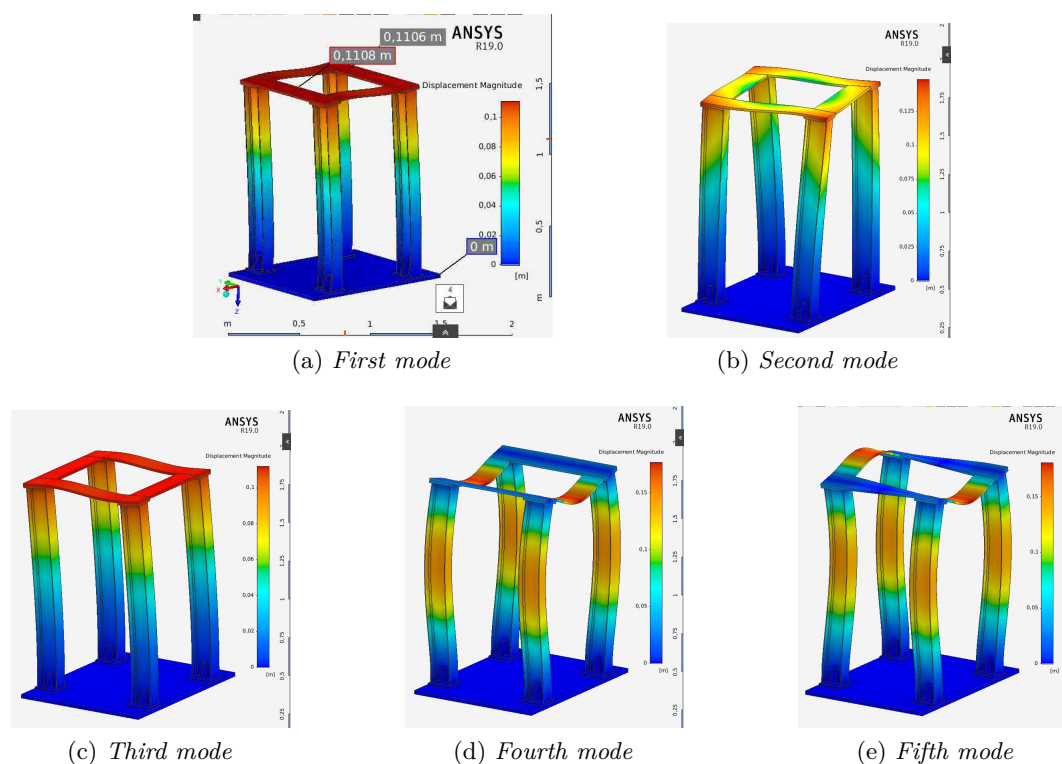


Figure 4.10: External simplified structure vibration modes: Ansys AIM 18<sup>®</sup>, bounded contact

Figure 4.10 shows the vibration modes. The first four modes are exactly equal to the ones shown in Figure 4.8. The main differences regards the natural frequencies values,

which are far from the previous results, and the presence of a fifth modes under the  $150Hz$  (Figure 4.10e).

Again, the main displacements regards the beams, and of interest will be the analysis of the mode in Figure 4.10b in the following studies.

Concerning to the modes in Figures 4.10d - 4.10e, it is reasonable to consider those as an exception related to the geometry simplified assumptions.

## 4.2.7 Fifth analysis for simplified external structure: medium mesh

### Contact relation between parts

Default contact conditions are used for this analysis, therefore bounded connection between parts is set.

### Mesh element definition

Triangular and tetraedrical FEs have been chosen for the whole structure. The only difference is the dimensions and therefore, number of elements; Table 4.10 shows the maximum dimension selected for each part.

Table 4.10: Simplified external structure, medium mesh, triangular and tetragonal FEs size

Id.	Name	Type of FE	FE dimension [mm]
1	Base	Max element size	88
2	Double T beam	Max element size	70
3-4	Beam backing and support	Max element size	30
5	Superior frame	Mapped	50

### Mesh generation and analysis parameters

Figure 4.11 shows the AutoGEM mesh obtained. In this case the mesh generation did not turn out any mistake. All elements are congruent with the model and constrains imposed.

For this, results from the AutoGEM are obtained, and the relative study settings are established:

- Number of points: 8108;
- Number of edges: 41088;
- Number of solid elements: 25661;
- Convergence criterion: Multi-Pass Adaptive;
- Analysis definition: frequency range between 0 and  $150Hz$ ;
- Convergence criterion: percentage error with respect the frequency value up to 2%.

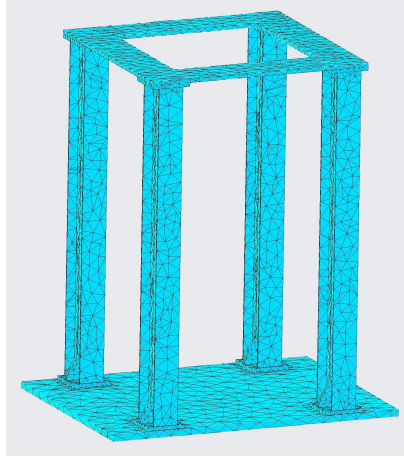


Figure 4.11: Medium triangular and tetragonal mesh, simplified external structure

## Results

The Multi-Pass Adaptive convergence criterion runs the solver up to reach the convergence limit or the maximum polynomial order set. The solver automatically increase the polynomial order in order to reach the convergence. Table 4.11 reports the steps.

Table 4.11: Multi-Pass Adaptive steps, simplified external structure, medium mesh

Pass	Number of equations	Polynomial order	Percentage error [%]
Pass 1	23 469	1	100
Pass 2	144 363	2	100
Pass 3	683 205	4	2.5
Pass 4	1 336 212	5	0.1

The number of natural frequencies, in the range  $0 \div 150Hz$ , is five. Table 4.12 shows the natural frequencies values obtained and the relative RMS error percentage computed with respect to the natural frequency.

Comparing the results in Table 4.12 with ones in Table 4.9, only few differences can be noticed. This validates the hypothesis of wrong assumption in contact relations for the first three simulations.

Anyway other two simulations are run in order to evaluate eventual discrepancies due to different mesh discretization.

Table 4.12: Natural frequencies and RMS errors, external simplified structure: medium triangular and thertaedrical mesh

Mode	Natural Frequency $\omega_n [Hz]$	Error $\eta\%$
1	19.27	0.1
2	38.76	0.1
3	43.63	0.1
4	125.58	0.1
5	129.39	0.1

#### 4.2.8 Sixth analysis for simplified external structure: fine triangular and theraedral mesh

##### Contact relation between parts

Default contact conditions are used for this analysis, therefore bounded connection between parts is set.

##### Mesh element definition

Triangular and tetraedrical FEs have been chosen for the whole structure. The only difference is the dimensions and therefore, number of elements; Table 4.13 shows the maximum dimension selected for each part.

Table 4.13: Simplified external structure, fine mesh, triangular and thetraagonal FEs size

Id.	Name	Type of FE	FE dimension [mm]
1	Base	Max element size	60
2	Double T beam	Max element size	50
3-4	Beam backing and support	Max element size	20
5	Superior frame	Mapped	30

##### Mesh generation and analysis parameters

Figure 4.12 shows the AutoGEM mesh obtained. In this case the mesh generation did not turn out any mistake. All elements are congruent with the model and constrains imposed.

For this study the following results from the AutoGEM are obtained, and the relative study settings are established:

- Number of points: 11881;
- Number of edges: 59784;

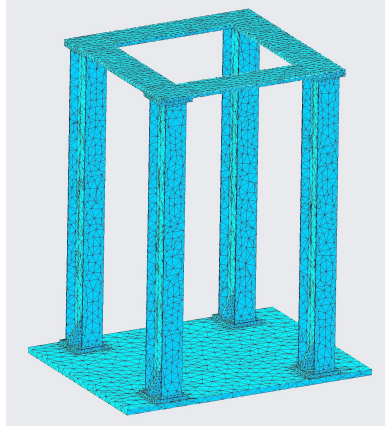


Figure 4.12: Fine triangular and tetragonal mesh, simplified external structure

- Number of solid elements: 37156;
- Convergence criterion: Multi-Pass Adaptive;
- Analysis definition: frequency range between 0 and  $150Hz$ ;
- Convergence criterion: percentage error with respect the frequency value up to 2%.

## Results

In Table 4.14 the solver steps up to reaching the convergence are reported.

Table 4.14: Multi-Pass Adaptive steps, simplified external structure, fine mesh

Pass	Number of equations	Polynomial order	Percentage error [%]
Pass 1	34 011	1	100
Pass 2	208 755	2	100
Pass 3	1 004 145	4	4.4
Pass 4	1 922 652	5	0.1

The number of natural frequencies, in the range  $0 \div 150Hz$ , is five. Table 4.15 shows the natural frequencies values obtained and the relative RMS error percentage computed with respect to the natural frequency.

The results in Table 4.15 are equivalent to the ones in Table 4.12, even with small reductions in FEs dimensions. Only small differences are present for the higher natural frequencies on the order of hundredth.

Anyway one more simulation is run. This last simulation is on the basis of the one in section 4.2.3, in order to double check the influence of redefined contact between parts influence.

Table 4.15: Natural frequencies and RMS errors, external simplified structure: fine triangular and thertaedrical mesh

Mode	Natural Frequency $\omega_n [Hz]$	Error $\eta\%$
1	19.27	0.1
2	38.75	0.0
3	43.63	0.0
4	125.54	0.1
5	129.35	0.1

### 4.2.9 Seventh analysis for simplified external structure: fine mixed mesh

This analysis was based on the study exposed in section 4.2.3. The same FEs setting where maintained, the only difference is in the contact relations. Also the study set up, therefore the convergence criterion and the type of study, is maintained.

#### Contact relation between parts

Default contact conditions are used for this analysis, therefore bounded connection between parts is set.

#### Mesh element definition

Mapped mesh is set for the base and the superior frame, while maximum element size is selected for beams and relative backing bases and support parts. The set up is shown in Table 4.7.

#### Mesh generation and analysis parameters

As well as exposed in section 4.2.3, Figure 4.7 shows the AutoGEM mesh obtained. Not all the features required were executed correctly, in fact the base and the part of the superior frame have not a mapped discretization.

A warning message was displayed during the mesh auto-generation. This message informed that not all the specified features were correctly executed. A rearranging discretization was adopted in order to correctly connect each FE nodes between contact parts.

Results from the AutoGEM are obtained, and the relative study settings are established:

- Number of points: 24440;
- Number of edges: 122162;
- Number of solid elements: 74123;
- Convergence criterion: Single-Pass Adaptive;

- Analysis definition: ten first natural frequencies.

## Results

Again a Single-Pass Adaptive criterion is selected, therefore two iterations have been run. The number of equations, for the first step, is 1302600 with a maximum polynomial order of 4. In the second step the polynomial order was increased up to 6 with 1334916 equations to be solved.

Table 4.16 shows the natural frequencies values obtained and the relative RMS error percentage computed with respect to the natural frequency.

Table 4.16: Natural frequencies and RMS errors, external simplified structure, based on section 4.2.3

Mode	Natural Frequency $\omega_n [Hz]$	Error $\eta\%$
1	19.29	0.1
2	38.80	0.2
3	43.67	0.2
4	125.64	0.1
5	129.56	0.2
6	154.16	0.1
7	155.71	0.1
8	199.33	0.1
9	199.42	0.1
10	216.08	0.3

The first five results in Table 4.16 are equivalent to the ones in Table 4.15, even with small reductions in FEs dimensions.

Once more these results confirm that defining different contact conditions can lead to different or erroneous results, because of the different relation between the FEs.

### 4.2.10 External simplified vibration modes: rigid link contact

In this section only the vibration modes in the first five modes corresponding with frequency range between  $0 \div 150Hz$  are shown.

Figure 4.13 shows the vibration modes. The first four modes are quite similar to those shown in Figures 4.8 - 4.10. The main differences regard the natural frequencies values, in comparison with the first three analyses.

The results obtained from these latter simulations, and the results from Ansys, are perfectly coherent in terms of vibration modes, as it is possible to notice comparing Figures 4.13 and 4.10, and also in terms of natural frequencies values.

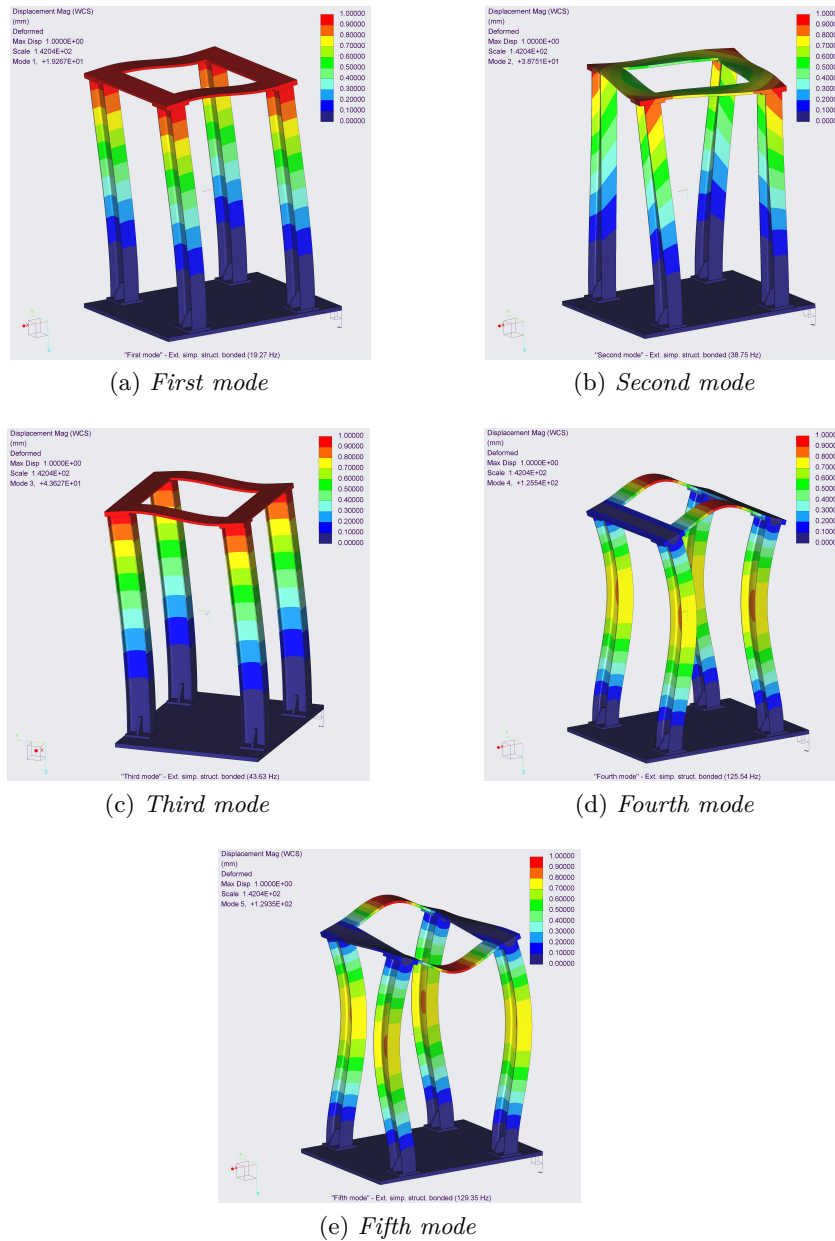


Figure 4.13: External simplified structure vibration modes: bounded contact

### 4.3 Full external structure

For the full external structure model, three simulations were run. Only the software PTC Creo Simulate<sup>®</sup> is used.

The aim of studying natural frequencies and modes for the full structure, is to compare them with the simplify structure results and verify the influence of FEs dimension on the

results.

### Geometry

The full external structure is composed of the same parts of the model in Figure 4.2, with four additional inferior supports which connect the base with the ground, and four internal structures, as shown in Figure 4.14.

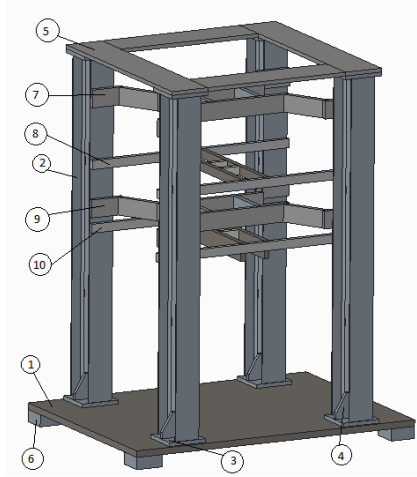


Figure 4.14: Full external structure CAD model

Table 4.17: Bill of materials for full external structure

Id.	Name	Quantity	Material
1	Base	1	Structural steel
2	Double T beam	4	Structural steel
3	Beam backing	8	Structural steel
4	Beam support	8	Structural steel
5	Superior frame	1	Structural steel
6	Support	4	Structural steel
7	Bearing structure	1	Structural steel
8	Superior sensor support	1	Structural steel
9	Electric exciter support	1	Structural steel
10	Inferior sensor support	1	Structural steel

### Material

The material used is the same for all parts. It is the structural steel from the PTC Creo Simulate<sup>®</sup> material library, which properties are shown in Table 4.2.

## Boundary conditions

A fixed boundary conditions between the bottom part of the four supports and the solver absolute reference system is considered. It means that the structure can not translate and rotate and is fixed to the ground. Figure 4.15 shows in purple the constrain location.

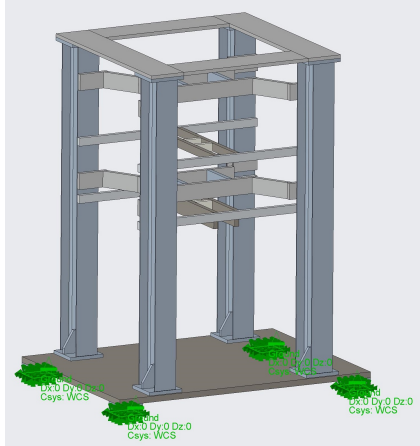


Figure 4.15: Complete external structure boundary condition

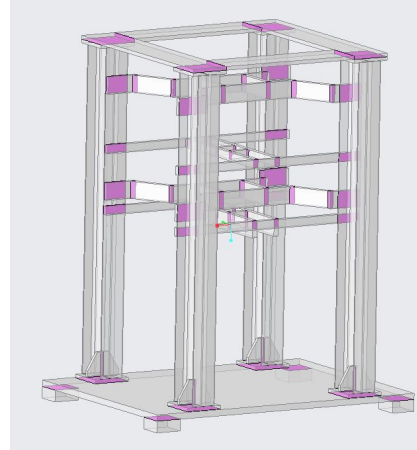


Figure 4.16: Complete external structure bounded contact

## Contact relation between parts

Default bounded contact between each assembly element is defined for all the simulations run. Figure 4.16 shows where the bounded link is automatically recognised by the software, where the surfaces are depicted of pink.

### 4.3.1 First analysis for complete external structure: coarse mesh

#### Mesh element definition

A maximum element size constrain is set for the FEs definition for all the model parts, considering the main sub-assemblies as a whole, for example the superior sensor support in Table 4.17.

Starting from the assumption of setting lower FE size for the smaller model elements, the values reported in Table 4.18 are set as coarse mesh for the first analysis.

#### Mesh generation and analysis parameters

Figure 4.17 shows the AutoGEM mesh obtained. The solver dialog window does not report any problem in mesh generation. All elements are congruent with the model and constrains imposed.

For this study the following results from the AutoGEM are obtained, and the relative study settings are established:

Table 4.18: Complete external structure, coarse mesh, FE size

Id.	Name	Type of FE	FE dimension [mm]
1-6	Base and Supports	Max element size	150
2	Double T beam	Max element size	80
3-4	Beam backing and support	Max element size	60
5	Superior frame	Max element size	75
7-9	Bearing structure and Electric exciter support	Max element size	75
8-10	Superior and Inferior sensors supports	Max element size	70



Figure 4.17: Coarse mesh, complete external structure

- Number of points: 6192;
- Number of edges: 29910;
- Number of solid elements: 17773;
- Convergence criterion: Multi-Pass Adaptive;
- Analysis definition: frequency range between 0 and 150Hz;
- Convergence criterion: percentage error with respect the frequency value up to 1%.

## Results

The criterion convergence was not satisfied by the solver because of the lower value of the highest polynomial order (equal to 7). Anyway acceptable results are obtained, with a convergence percentage near to 1.7% of the theoretical frequency exact value. Table 4.19 reports the solver steps up to reaching the convergence.

Table 4.19: Multi-Pass Adaptive steps, complete external structure, coarse mesh

Pass	Number of equations	Polynomial order	Percentage error [%]
Pass 1	18 528	1	100
Pass 2	108 198	2	100
Pass 3	537 417	4	26.6
Pass 4	1 075 677	6	3.1
Pass 5	1 849 908	7	1.7

The number of natural frequencies, in the range  $0 \div 150Hz$ , is seven. Table 4.20 shows the natural frequencies values obtained and the relative RMS error percentage computed with respect to the natural frequency.

Table 4.20: Natural frequencies and RMS errors, complete external structure: coarse mesh

Mode	Natural Frequency $\omega_n [Hz]$	Error $\eta\%$
1	23.86	0.3
2	29.65	0.3
3	31.00	0.5
4	74.17	1.7
5	80.38	1.2
6	98.74	0.3
7	111.63	0.5

The results obtained and shown in Table 4.20 differs in number and values with respect the previous model analysed (Table 4.15, considered the most reliable one, being the quality mesh higher).

Such kind of results are expected, supposing that the internal structures lend higher stiffness to the model, moreover additional vibration modes should appear due to the introduction of new structural elements.

### 4.3.2 Second analysis for complete external structure: medium mesh

#### Mesh element definition

A maximum element size constrain is set for the FEs definition, for all the model parts, considering the main sub-assemblies as a whole, as well as the previous simulation.

Again lower FE size for the smaller model elements, the values reported in Table 4.21 are set as medium mesh for the second analysis

Table 4.21: Complete external structure, medium mesh, FE size

Id.	Name	Type of FE	FE dimension [mm]
1-6	Base and Supports	Max element size	100
2	Double T beam	Max element size	75
3-4	Beam backing and support	Max element size	50
5	Superior frame	Max element size	65
7-9	Bearing structure and Electric exciter support	Max element size	65
8-10	Superior and Inferior sensors supports	Max element size	60

### Mesh generation and analysis parameters

Figure 4.18 shows the AutoGEM mesh obtained. The solver dialog window does not report any problem in mesh generation. All elements are congruent with the model and constraints imposed.



Figure 4.18: Medium mesh, complete external structure

For this study the following results from the AutoGEM are obtained, and the relative study settings are established:

- Number of points: 7269;
- Number of edges: 35230;
- Number of solid elements: 21044;
- Convergence criterion: Multi-Pass Adaptive;
- Analysis definition: frequency range between 0 and 150Hz;
- Convergence criterion: percentage error with respect the frequency value up to 1%.

## Results

The convergence criterion was satisfied in five consecutive pass, reaching the 1% error in the frequency content. Table 4.22 reports the solver steps up to reaching the convergence.

Table 4.22: Multi-Pass Adaptive steps, complete external structure, medium mesh

Pass	Number of equations	Polynomial order	Percentage error [%]
Pass 1	21 747	1	100
Pass 2	127 341	2	100
Pass 3	650 586	4	25.6
Pass 4	1 292 625	6	2.7
Pass 5	2 191 233	7	1

Table 4.23 shows the natural frequencies values obtained and the relative RMS error percentage computed with respect to the natural frequency.

Table 4.23: Natural frequencies and RMS errors, complete external structure: medium mesh

Mode	Natural Frequency $\omega_n [Hz]$	Error $\eta\%$
1	23.84	0.2
2	29.70	0.2
3	31.08	0.3
4	73.69	1
5	80.14	0.6
6	98.72	0.2
7	112.45	0.4

Even the convergence in the previous analysis was not reached, in particular for the fourth mode, it is possible to notice that no significant difference are appreciable between the previous results and the latter one. The fourth mode differ for less than  $1Hz$  between the two simulations.

For completeness a third analysis was executed.

### 4.3.3 Third analysis for complete external structure: fine mesh

#### Mesh element definition

Table 4.24 shows the data set for the fine mesh under investigation. Again only maximum element size definition is used for all the model parts.

Table 4.24: Complete external structure, fine mesh, FE size

Id.	Name	Type of FE	FE dimension [mm]
1-6	Base and Supports	Max element size	90
2	Double T beam	Max element size	70
3-4	Beam backing and support	Max element size	40
5	Superior frame	Max element size	55
7-9	Bearing structure and Electric exciter support	Max element size	55
8-10	Superior and Inferior sensors supports	Max element size	50

### Mesh generation and analysis parameters

Figure 4.19 shows the AutoGEM mesh obtained. The solver dialog window does not report any problem in mesh generation. All elements are congruent with the model and constraints imposed.

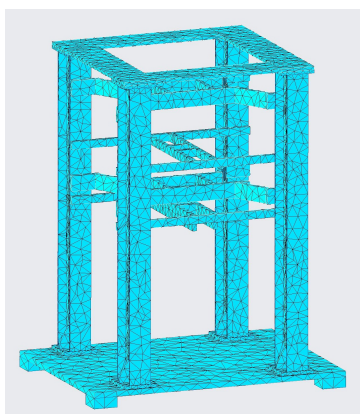


Figure 4.19: Fine mesh, complete external structure

For this study the following results from the AutoGEM are obtained, and the relative study settings are established:

- Number of points: 8470;
- Number of edges: 41296;
- Number of solid elements: 24847;
- Convergence criterion: Multi-Pass Adaptive;
- Analysis definition: frequency range between 0 and 150Hz;
- Convergence criterion: percentage error with respect the frequency value up to 1%.

## Results

The convergence for this study was reached in five consecutive steps. Table 4.25 reports the solver steps up to reaching the convergence.

Table 4.25: Multi-Pass Adaptive steps, complete external structure, fine mesh

Pass	Number of equations	Polynomial order	Percentage error [%]
Pass 1	25 317	1	100
Pass 2	149 034	2	100
Pass 3	769 419	4	21.9
Pass 4	1 526 382	6	2.4
Pass 5	2 588 784	1	

The number of natural frequencies, in the range  $0 \div 150Hz$ , is seven. Table 4.26 shows the natural frequencies values obtained and the relative RMS error percentage computed with respect to the natural frequency.

Table 4.26: Natural frequencies and RMS errors, complete external structure: fine mesh

Mode	Natural Frequency $\omega_n [Hz]$	Error $\eta\%$
1	23.82	0.2
2	29.68	0.2
3	31.05	0.3
4	73.65	1
5	80.08	0.6
6	98.67	0.2
7	112.35	0.3

The results obtained are in perfect accordance with the previous analysis. It is of interest to notice how increasing the mesh quality, the convergence is reached with an higher level in all the results, even being the time consumed considerably much higher.

### 4.3.4 Complete external vibration modes

In this section are shown the vibration modes for the complete external structure

Figure 4.20 shows the beams vibration modes. The first three modes are equal to the ones found out in the external simplified structure (Figure 4.8). Also here, the second torsional mode is present, with almost the same natural frequency, only  $5Hz$  lower than the simplified structure.

Again, quite strange modes appear for higher values of natural frequencies (Figures 4.20d - 4.20e), even being these different form the simplified structure (Figures 4.13d - 4.13e).

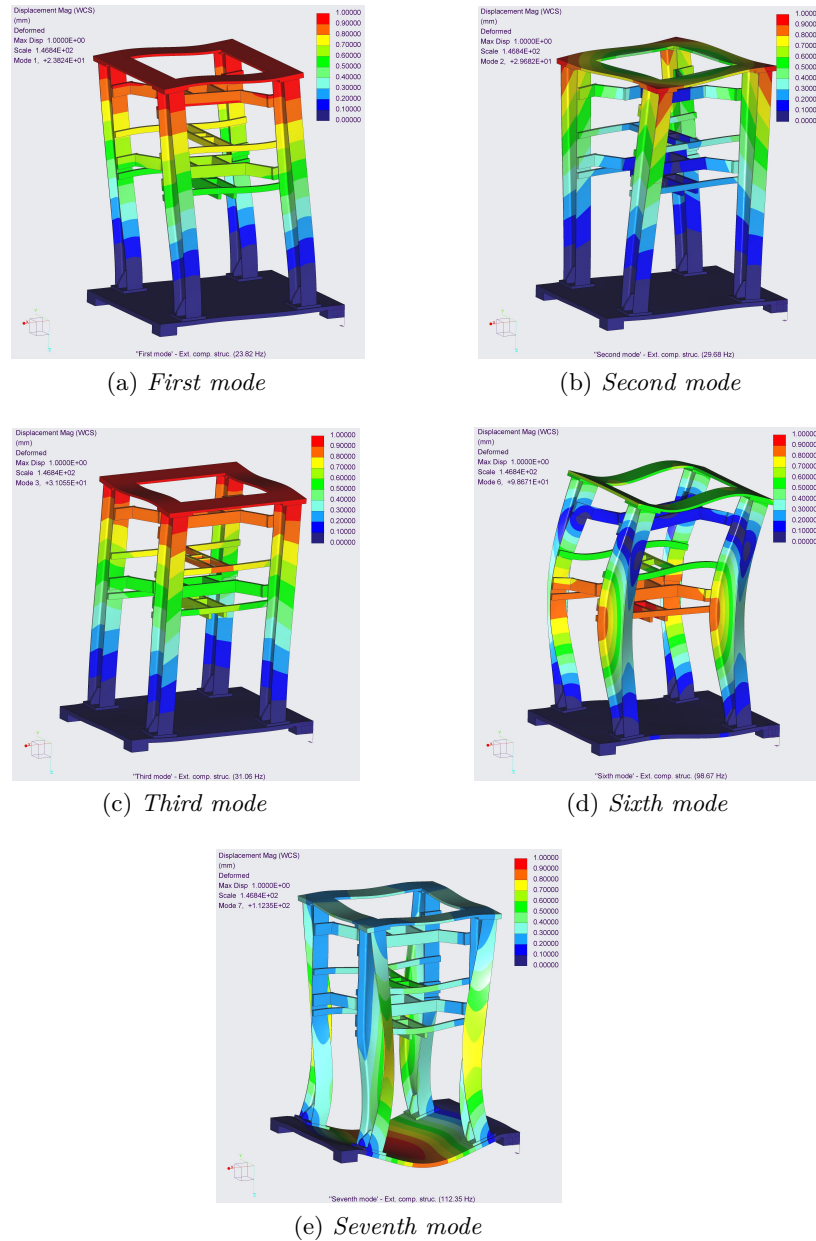


Figure 4.20: Complete external structure, beams vibration modes

The base vibration is appreciable too in this model, because of the base support presence. The element is ignored in the simplified structure, therefore, this vibration is not present, being the base directly constrained to the ground.

Figure 4.21 shows the modes relative to the internal structure. As it is expected, two new vibration modes appears due to the presence of other elements in the geometry.

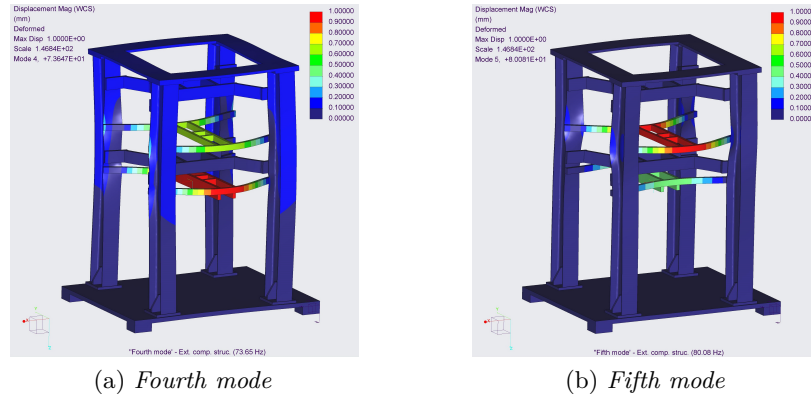


Figure 4.21: Complete external structure, internal structures vibration modes

## 4.4 Internal structure

The internal structure modal analysis is done only with PTC Creo Simulate<sup>®</sup>, and three analyses with increasing quality mesh are executed.

The aim is to investigate the internal structure vibration modes and check their presence in the global model.

### Geometry

The internal structure is basically equal to the external one, in terms of parts geometry and types of components, with reduced dimensions. Figure 4.22 and Table 4.27 show the parts which compose the model.

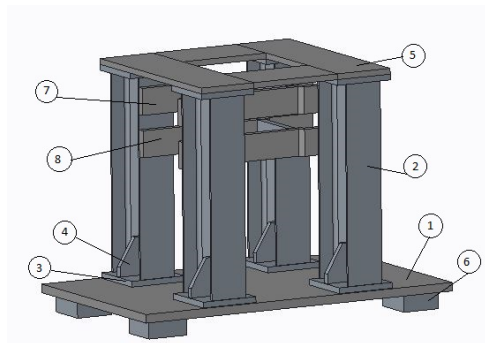


Figure 4.22: Internal structure CAD model

### Material

The material used is the same for all parts. It is the structural steel from the PTC Creo Simulate<sup>®</sup> material library, which properties are shown in Table 4.2.

Table 4.27: Bill of materials for internal structure

Id.	Name	Quantity	Material
1	Base	1	Structural steel
2	Double T beam	4	Structural steel
3	Beam backing base	8	Structural steel
4	Beam support	8	Structural steel
5	Superior frame	1	Structural steel
6	Support	4	Structural steel
7	Superior bearing structure	1	Structural steel
8	Inferior bearing structure	1	Structural steel

### Boundary conditions

A fixed boundary conditions between the bottom part of the four supports and the solver absolute reference system is considered. It means that the structure can not translate or rotate and is fixed to the ground, and it would represent the connection between the external structure base and the internal structure supports. Figure 4.23 shows in green the constrain location.

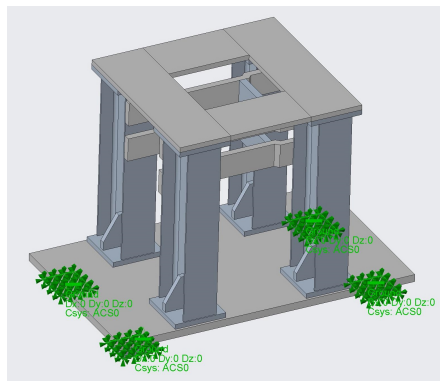


Figure 4.23: Internal structure boundary condition

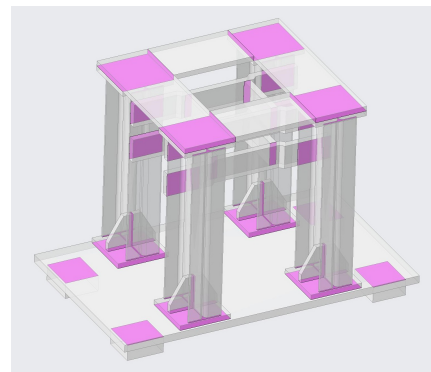


Figure 4.24: Internal structure bounded contact

### Contact relation between parts

Default bounded contact between each assembly element is defined for all the simulations run. Figure 4.24 shows where the bounded link is automatically recognised by the software, where the surfaces are depicted in pink.

#### 4.4.1 First analysis for internal structure: coarse mesh

##### Mesh element definition

A maximum element size constrain is set for the FEs definition, for all the model parts, considering the main sub-assemblies as a whole, for example the superior and inferior bearing structure in Table 4.27.

Starting from the assumption of setting lower FE size for the smaller model elements, the values reported in Table 4.28 are set as coarse mesh for the first analysis.

Table 4.28: Internal structure, coarse mesh, FE size

Id.	Name	Type of FE	FE dimension [ <i>mm</i> ]
1-6	Base and Supports	Max element size	150
2	Double T beam	Max element size	90
3-4	Beam backing and support	Max element size	70
5	Superior frame	Max element size	80
7-8	Superior and Inferior bearing structures	Max element size	80

##### Mesh generation and analysis parameters

Figure 4.25 shows the AutoGEM mesh obtained. The solver dialog window does not report any problem in mesh generation. All elements are congruent with the model and constrains imposed.

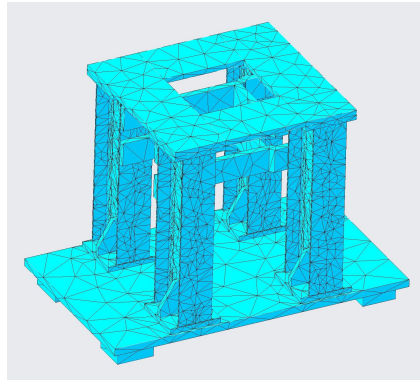


Figure 4.25: Coarse mesh, internal structure

For this study the following results from the AutoGEM are obtained, and the relative settings are established:

- Number of points: 4746;
- Number of edges: 23463;

- Number of solid elements: 14225;
- Convergence criterion: Multi-Pass Adaptive;
- Analysis definition: frequency range between 0 and 150Hz;
- Convergence criterion: percentage error with respect the frequency value up to 2.5%.

## Results

The convergence was reached after four iteration. The solver is not able to reach any acceptable solutions, in the range of frequency between  $0 \div 150Hz$ , in the first iteration. The solver finds out solutions, from the second iteration. Table 4.29 reports the solver steps up to reaching the convergence.

Table 4.29: Multi-Pass Adaptive steps, internal structure, coarse mesh

Pass	Number of equations	Polynomial order	Percentage error [%]
Pass 1	14 190	1	-
Pass 2	84 519	2	100
Pass 3	253 617	3	13.5
Pass 4	560 520	4	2.4

The number of natural frequencies, in the range  $0 \div 150Hz$ , is three. Table 4.30 shows the natural frequencies values obtained and the relative RMS error percentage computed with respect to the natural frequency.

Table 4.30: Natural frequencies and RMS errors, internal structure: coarse mesh

Mode	Natural Frequency $\omega_n [Hz]$	Error $\eta\%$
1	113.18	2.4
2	128.71	1.5
3	133.86	1.1

The results obtained, and shown in Table 4.30, are coherent with what is expected. Being lower the global structure dimension, therefore being also lower the total mass, the system stiffness will be higher (being proportional to the inverse of the geometrical feature), therefore the expected natural frequencies should be higher than for the external structure.

### 4.4.2 Second analysis for internal structure: medium mesh

#### Mesh element definition

A maximum element size constrain is set for the FEs definition, for all the model parts.

Table 4.31 shows the FEs set up for the medium mesh analysis.

Table 4.31: Internal structure, medium mesh, FE size

<b>Id.</b>	<b>Name</b>	<b>Type of FE</b>	<b>FE dimension [<i>mm</i>]</b>
1-6	Base and Supports	Max element size	90
2	Double T beam	Max element size	70
3-4	Beam backing and support	Max element size	50
5	Superior frame	Max element size	60
7-8	Superior and Inferior bearing structures	Max element size	60

### Mesh generation and analysis parameters

Figure 4.26 shows the AutoGEM mesh obtained. The solver dialog window does not report any problem in mesh generation. All elements are congruent with the model and constrains imposed.

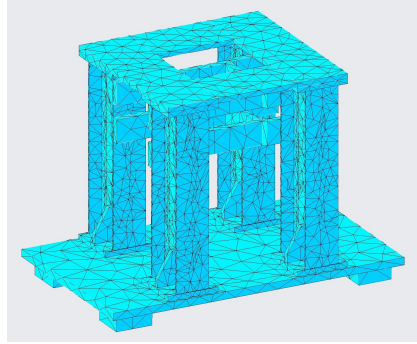


Figure 4.26: Medium mesh, internal structure

The following results, from the AutoGEM are obtained for this study, and the relative settings are established:

- Number of points: 5491;
- Number of edges: 27238;
- Number of solid elements: 16585;
- Convergence criterion: Multi-Pass Adaptive;
- Analysis definition: frequency range between 0 and  $150Hz$ ;
- Convergence criterion: percentage error with respect the frequency value up to 1%.

### Results

The convergence was reached after four iteration. The solver is not able to reach any acceptable solutions, in the range of frequency between  $0 \div 150Hz$ , in the first iteration.

The solver finds out solutions, from the second iteration. Table 4.32 reports the solver steps up to reaching the convergence.

Table 4.32: Multi-Pass Adaptive steps, internal structure, medium mesh

Pass	Number of equations	Polynomial order	Percentage error [%]
Pass 1	16 380	1	-
Pass 2	97 923	2	100
Pass 3	294 339	3	6.5
Pass 4	653 712	4	1.3

The number of natural frequencies, in the range  $0 \div 150Hz$ , is three. Table 4.33 shows the natural frequencies values obtained and the relative RMS error percentage computed with respect to the natural frequency.

Table 4.33: Natural frequencies and RMS errors, internal structure: medium mesh

Mode	Natural Frequency $\omega_n [Hz]$	Error $\eta\%$
1	112.06	0.5
2	127.90	0.3
3	133.19	0.3

The results in Table 4.33 are not so far from the ones in Table 4.30, which differs for less than  $1Hz$  even being the latter ones with considerably higher level of confidence .

### 4.4.3 Third analysis for internal structure: fine mesh

#### Mesh element definition

A maximum element size constrain is set for the FEs definition, for all the model parts.

Table 4.34 shows the FEs set up for the fine mesh analysis.

#### Mesh generation and analysis parameters

Figure 4.27 shows the AutoGEM mesh obtained. The solver dialog window does not report any problem in mesh generation. All elements are congruent with the model and constrains imposed.

The following results from the AutoGEM are obtained, and the relative study settings are established:

- Number of points: 6607;
- Number of edges: 33013;
- Number of solid elements: 20261;

Table 4.34: Internal structure, fine mesh, FE size

<b>Id.</b>	<b>Name</b>	<b>Type of FE</b>	<b>FE dimension [<i>mm</i>]</b>
1-6	Base and Supports	Max element size	70
2	Double T beam	Max element size	45
3-4	Beam backing and support	Max element size	35
5	Superior frame	Max element size	40
7-8	Superior and Inferior bearing structures	Max element size	45

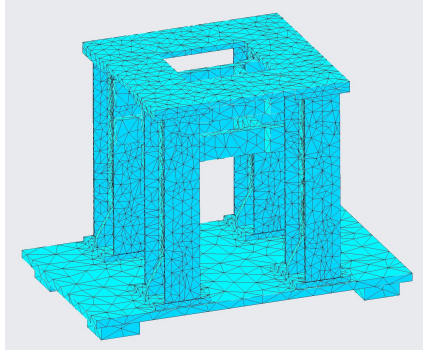


Figure 4.27: Fine mesh, internal structure

- Convergence criterion: Multi-Pass Adaptive;
- Analysis definition: frequency range between 0 and  $150Hz$ ;
- Convergence criterion: percentage error with respect the frequency value up to 1%.

## Results

The convergence was reached after four iteration. The solver was not able to reach any acceptable solutions in the first iteration, in the range of frequency between  $0 \div 150Hz$ . From the second iteration the solver finds out solutions. Table 4.35 reports the solver steps up to reaching the convergence.

The number of natural frequencies, in the range  $0 \div 150Hz$ , found out, is three. Table 4.36 shows the natural frequencies values obtained and the relative RMS error percentage computed with respect to the natural frequency.

The results in Table 4.33 are coherent with the previous analyses.

### 4.4.4 Internal structure vibration modes

In this section the vibration modes for the internal structure are shown.

Figure 4.28 shows the beams vibration modes. The modes are coherent with the external geometry, in the sense that the whole structure vibration is analogous between the two

Table 4.35: Multi-Pass Adaptive steps, internal structure, fine mesh

Pass	Number of equations	Polynomial order	Percentage error [%]
Pass 1	19 713	1	-
Pass 2	118 560	2	100
Pass 3	357 279	3	5.1
Pass 4	793 863	4	1

Table 4.36: Natural frequencies and RMS errors, internal structure: fine mesh

Mode	Natural Frequency $\omega_n [Hz]$	Error $\eta\%$
1	112.32	1
2	128.05	0.6
3	133.39	0.7

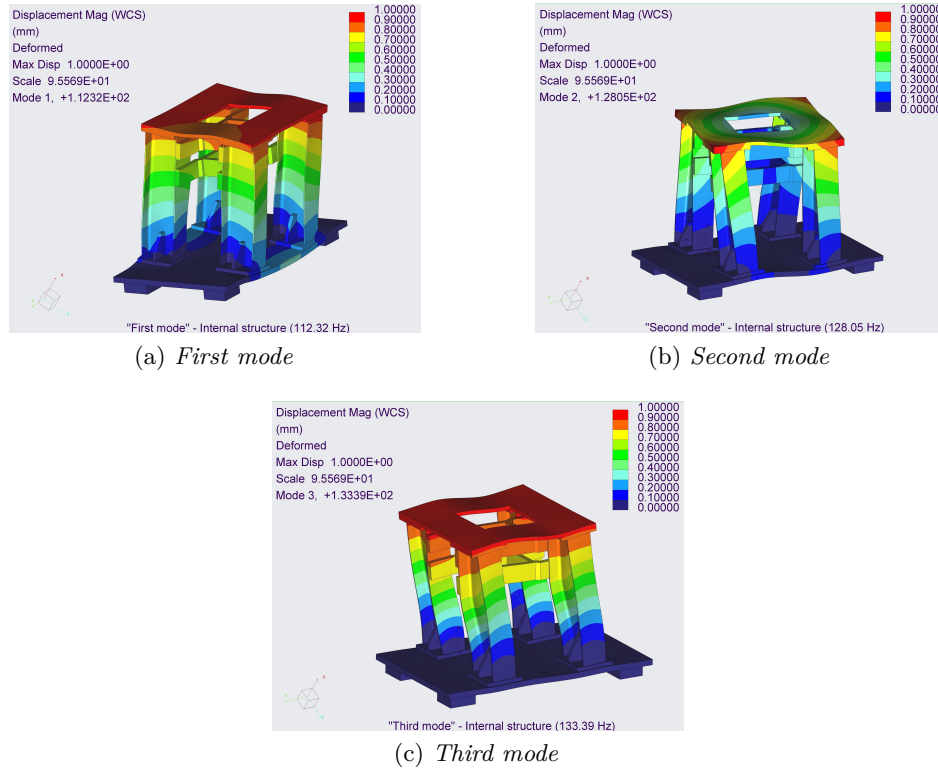


Figure 4.28: Internal structure, vibration modes

models. Two vibration modes in the lateral planes, and a torsional mode are present, only

with the difference of a higher natural frequency values.

Also here, it is appreciable a small base vibration due to the supports presence.

## 4.5 Superior shaft

The superior shaft modal analysis is done only with PTC Creo Simulate<sup>®</sup>. Two analyses with increasing quality mesh are executed.

The aim is to investigate the superior shaft vibration modes and check their presence in the shafts assembly, as well as the global model.

### Geometry

The superior shaft is a cylindrical bar of steel. The model is simplified deleting all wholes, rounds and chamfers.

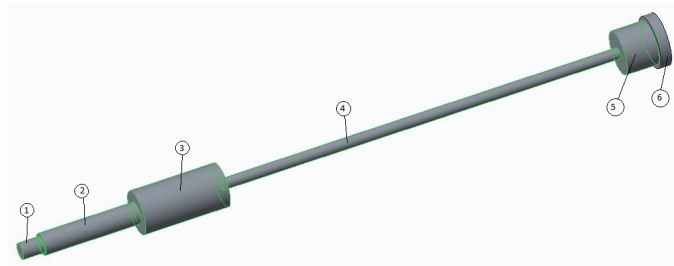


Figure 4.29: Superior shaft CAD model

The geometry was divided in six volumes, as it is shown in Figure 4.29, in green. This division turns useful for the subsequent FEs definitions. For this type of analyses a different elements size is chosen for the different volumes. Table 4.37 shows the names for the future identification in the mesh definition

Table 4.37: Superior shaft volume division

<b>Id.</b>	<b>Name</b>
1	Coupling superior shaft - elastic junction
2	Shaft corp 1
3	Electric exciter zone
4	Shaft corp 2
5	Bearing coupling
6	Shaft head

### Material

The structural steel, from the PTC Creo Simulate<sup>®</sup> material library, is the material used, whose properties are shown in Table 4.2.

### Boundary conditions

The so called Pin constrain is set for the superior shaft. The Pin constrain is definable for cylindrical surfaces, usually in rotating operational condition [11].

Two directions can be constrained: the rotation along the main shaft, and the axial translation. Both directions are set as fixed in correspondence of bearing coupling, as Figure 4.30 shows in green.

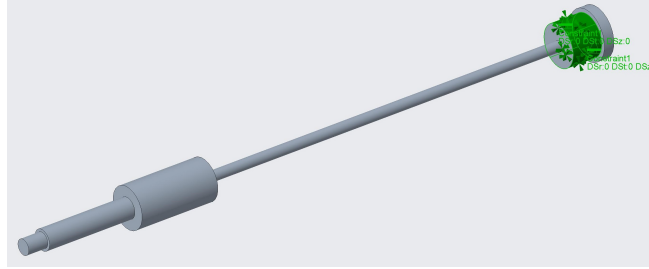


Figure 4.30: Superior shaft boundary condition

### 4.5.1 First analysis for superior shaft: coarse mesh

#### Mesh element definition

A maximum element size constrain is set for the FEs definition, for the different volumes defined. Lower FEs size are set for the smaller volumes, for volumes in which higher displacement are supposed and for ones in which there is coupling between the shaft and the elastic junction. Table 4.38 shows the data set.

Table 4.38: Superior shaft, coarse mesh, FE size

Id.	Name	Type of FE	FE dimension [mm]
1	Coupling superior shaft - elastic junction	Max element size	7.5
2	Shaft corp 1	Max element size	10
3	Electric exciter zone	Max element size	15
4	Shaft corp 2	Max element size	5
5	Bearing coupling	Max element size	20
6	Shaft head	Max element size	24

#### Mesh generation and analysis parameters

Figure 4.31 shows the AutoGEM mesh obtained. The solver dialog window does not report any problem in mesh generation. All elements are congruent with the model and constrains imposed.

The following results, from the AutoGEM, are obtained, and the relative settings are established:

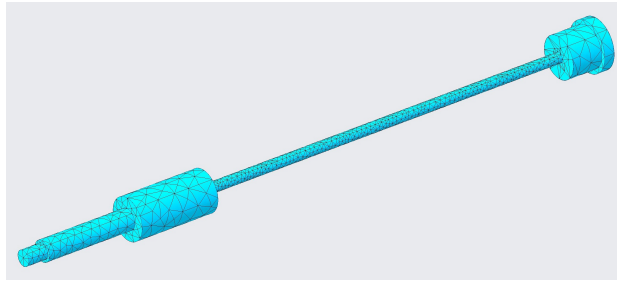


Figure 4.31: Coarse mesh, superior shaft

- Number of points: 1583;
- Number of edges: 8042;
- Number of solid elements: 5443;
- Convergence criterion: Multi-Pass Adaptive;
- Analysis definition: frequency range between 0 and 150Hz;
- Convergence criterion: percentage error with respect the frequency value up to 1%.

## Results

The convergence was reached after four iteration. Table 4.39 reports the solver steps up to reaching the convergence.

Table 4.39: Multi-Pass Adaptive steps, superior shaft, coarse mesh

Pass	Number of equations	Polynomial order	Percentage error [%]
Pass 1	4653	1	100
Pass 2	28 551	2	100
Pass 3	155 850	4	51.1
Pass 4	309 315	5	0.1

The number of natural frequencies, in the range  $0 \div 150Hz$ , is four. Table 4.40 shows the natural frequencies values obtained and the relative RMS error percentage computed with respect to the natural frequency.

Even being only two the natural frequencies found out, they correspond to two different modes shape. In fact the natural frequencies differs only for the second or third decimal number, and correspond to the vibration in two different planes (symmetry of the shaft), for this reason the solver splits the results.

Table 4.40: Natural frequencies and RMS errors, superior shaft: coarse mesh

Mode	Natural Frequency $\omega_n [Hz]$	Error $\eta\%$
1	8.97	0.0
2	8.97	0.1
3	105.96	0.1
4	105.97	0.1

### 4.5.2 Second analysis for superior shaft: medium mesh

#### Mesh element definition

Following the same criterion used in previous simulation, Table 4.41 shows the data set.

Table 4.41: Superior shaft, medium mesh, FE size

Id.	Name	Type of FE	FE dimension [mm]
1	Coupling superior shaft - elastic junction	Max element size	6
2	Shaft corp 1	Max element size	7.5
3	Electric exciter zone	Max element size	12.5
4	Shaft corp 2	Max element size	3.5
5	Bearing coupling	Max element size	17
6	Shaft head	Max element size	20

#### Mesh generation and analysis parameters

Figure 4.32 shows the AutoGEM mesh obtained. The solver dialog window does not report any problem in mesh generation. All elements are congruent with the model and constrains imposed.

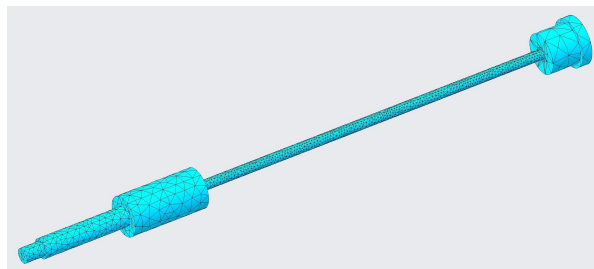


Figure 4.32: Medium mesh, superior shaft

The following results from the AutoGEM are obtained, and the relative study settings are established:

- Number of points: 3459;
- Number of edges: 18831;
- Number of solid elements: 13260;
- Convergence criterion: Multi-Pass Adaptive;
- Analysis definition: frequency range between 0 and  $150Hz$ ;
- Convergence criterion: percentage error with respect the frequency, local edge displacement and strain energy value up to 5%.

### Results

The convergence was not reached with respect the local edge displacement, which stayed the maximum in all the iterative passage. Anyway the convergence in the frequency and strain energy values was reached in the fourth passage. Table 4.42 reports the solver steps up to reaching the convergence and the values of the error computed with respect the RMS strain energy.

Table 4.42: Multi-Pass Adaptive steps, superior shaft, medium mesh

Pass	Number of equations	Polynomial order	Percentage error [%]
Pass 1	10 266	1	100
Pass 2	66 489	2	100
Pass 3	388 260	4	31.2
Pass 4	754 785	5	1.5
Pass 5	117 918	6	2.3
Pass 6	1 812 567	7	1.6
Pass 7	2 687 877	8	1.4

The number of natural frequencies, in the range  $0 \div 150Hz$ , is four. Table 4.43 shows the natural frequencies values obtained and the relative RMS error percentage computed with respect to the natural frequency.

Table 4.43: Natural frequencies and RMS errors, superior shaft: coarse mesh

Mode	Natural Frequency $\omega_n [Hz]$	Error $\eta\%$
1	8.96	0.0
2	8.96	0.0
3	105.91	0.0
4	105.91	0.0

The result were confirmed with this second simulation. The choice to run a second analysis and also with a so strict convergence criterion, was completely arbitrary and not recommended. Also the previous results could be considered sufficiently reliable.

### 4.5.3 Superior shaft vibration modes

In this section the vibration modes for the superior shaft are shown.

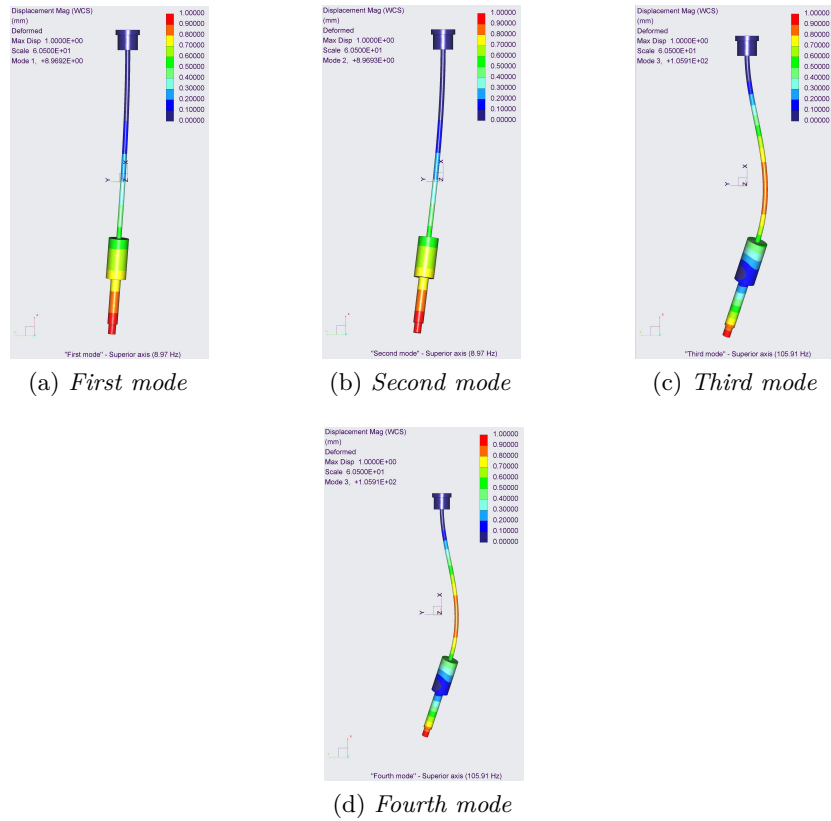


Figure 4.33: Superior shaft, vibration modes

Figure 4.33 shows the superior shaft vibration modes. As it was previously commented for the natural frequencies, the modes are equal in couples. The only difference between the two modes  $\omega_{n1} = 8.96Hz$ , as well as  $\omega_{n2} = 105.91Hz$ , is the vibration plane. It means that the real vibration mode is a superposition, obtaining an higher displacement.

## 4.6 Inferior shaft

The inferior shaft modal analysis is done only with PTC Creo Simulate<sup>®</sup>, and just one analysis is executed.

## Geometry

The superior shaft is a cylindrical bar of steel.

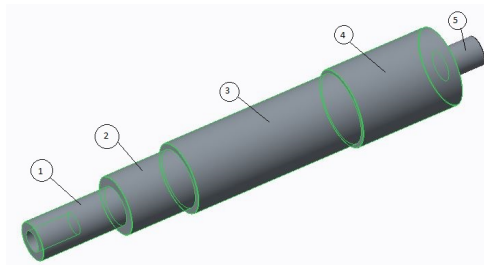


Figure 4.34: Superior shaft CAD model

The geometry was divided in five volumes, as it is shown in Figure 4.34 in green. This division turns useful for the subsequent FEs definitions. For this type of analyses a different elements size is chosen for the different volumes. Table 4.44 shows the names for the future identification in the mesh definition

Table 4.44: Inferior shaft volume division

<b>Id.</b>	<b>Name</b>
1	Coupling inferior shaft - electric motor
2	Bearing coupling 1
3	Shaft corp
4	Bearing coupling 2
5	Coupling inferior shaft - elastic junction

## Material

The structural steel, from the PTC Creo Simulate<sup>®</sup> material library, is the material used, which properties are shown in Table 4.2.

## Boundary conditions

For the inferior shaft a constrain defined Pin constrain is set.

Both the two directions, rotation around the axis and translation along the axis, are set as fixed in correspondence of the bearing coupling 2 (Table 4.44), as Figure 4.35 shows in green.

### 4.6.1 Analysis for inferior shaft

#### Mesh element definition

A maximum element size constrain is set for the FEs definition, for the different volumes defined. Lower FEs size are set for the smaller volumes, for volumes in which higher

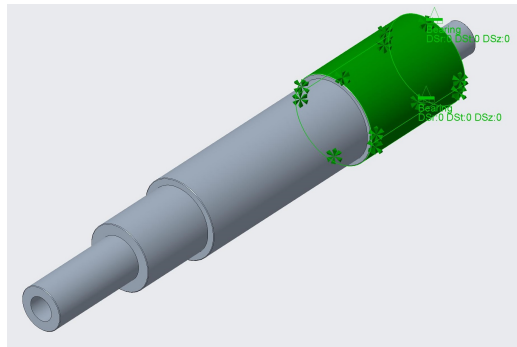


Figure 4.35: Inferior shaft boundary condition

displacement are supposed and for ones in which couplings are present. Table 4.45 shows the data set.

Table 4.45: Inferior shaft, FE size

<b>Id.</b>	<b>Name</b>	<b>Type of FE</b>	<b>FE dimension [mm]</b>
1	Coupling inferior shaft - electric motor	Max element size	10
2	Bearing coupling 1	Max element size	15
3	Shaft corp	Max element size	18
4	Bearing coupling 2	Max element size	20
5	Coupling inferior shaft - elastic junction	Max element size	7.5

### Mesh generation and analysis parameters

Figure 4.36 shows the AutoGEM mesh obtained. The solver dialog window does not report any problem in mesh generation. All elements are congruent with the model and constrains imposed.

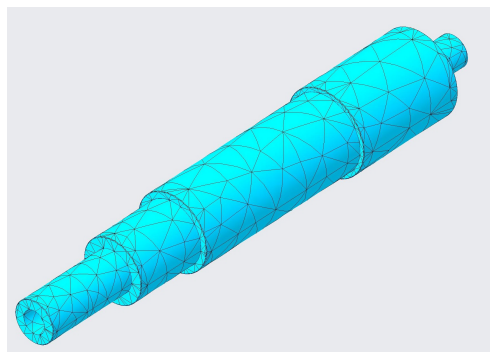


Figure 4.36: Coarse mesh, inferior shaft

For this study the following results from the AutoGEM are obtained, and the relative study settings are established:

- Number of points: 766;
- Number of edges: 3693;
- Number of solid elements: 5237;
- Convergence criterion: Quick Check.

## Results

Several analyses have been computed with an Adaptive convergence criterion, considering the range of frequencies of interest. All these analyses turned out no results in that frequency range. For these reason a Quick Check study was done. Table 4.46 shows the results obtained.

Table 4.46: Natural frequencies, inferior shaft

Mode	Natural Frequency $\omega_n[Hz]$
1	1241.8
2	1241.9
3	4720.0
4	4721.8

All the results are largely out from the range of frequencies of interest. For this reason no more analyses have been run.

It is interesting to notice that, exactly as the superior shaft, four natural frequencies were found out, and are equal in couple, meaning that the mode shapes will be different in the plane but will occur for the same natural frequencies.

Being the natural frequencies out of the field of interest, it is reasonable to suppose null, or very low, inferior shaft displacement in the global assembly as well as the shafts assembly. For this reason vibration modes are not exposed.

## 4.7 Shafts assembly

The shafts assembly modal analysis is done only with PTC Creo Simulate<sup>®</sup>, and two analyses with increasing quality mesh are executed.

The aim is to investigate the shafts assembly vibration modes and check their presence in the global model; moreover the presence of superior shaft modes and natural frequencies are investigated in the assembly.

## Geometry

The assembly is made of the superior shaft, whose modal analyses results are exposed in Section 4.5, the inferior shaft, whose modal analysis results are exposed in Section 4.6, and the elastic junction, as Figure 4.37 shows and Table 4.47 reports the list of materials.

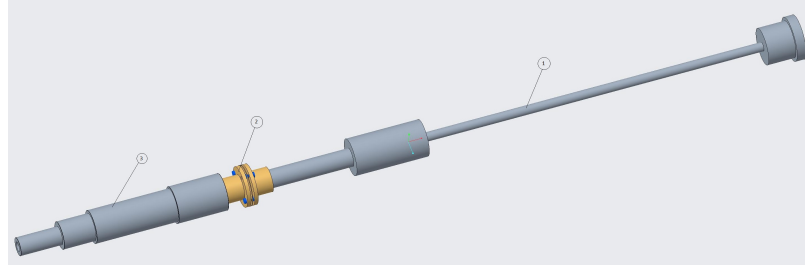


Figure 4.37: Shafts assembly CAD model

Table 4.47: List of materials for shafts assembly

Id.	Name	Quantity	Material
1	Superior shaft	1	Structural steel
2	Inferior shaft	1	Structural steel
3	Elastic junction	1	Aluminium - class: Al 7075

## Material

The material used for the shafts is the Structural steel from the PTC Creo Simulate<sup>®</sup>, whereas the elastic junction material is manually defined. The aluminium properties, for the class Al 7075, are reported in Table 4.48.

## Boundary conditions

The boundary conditions imposed to the model would reproduce the bearing constrain and the coupling between the inferior shaft and the electric motor. Figure 4.38 shows, with the green colour, the boundary conditions position.

In particular, a Pin constrain is imposed, both for the superior and inferior shafts, in the position where bearings are located (Figure 4.38). A constrain in axial translation is imposed in the inferior shaft bottom part and in the superior shaft head volume.

## Contact relation between parts

Default bounded contact between shafts and elastic junction was maintained, as Figure 4.39 shows with pink colour.

Moreover, it is possible to observe, in Figure 4.37, a blue element in presence of elastic junction holes. A bolted link is set up in that position in order to reproduce the real elastic junction contact. A structural steel M4 is selected.

Table 4.48: Material properties for modal analyses simulations

Material	Density $\rho [\frac{kg}{m^3}]$	Young modulus $E[GPa]$	Poisson coefficient $\nu[-]$
Structural steel	7827	199.95	0.27
Al 7075	2850	72	0.33

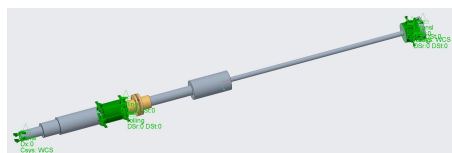


Figure 4.38: Shafts assembly boundary condition



Figure 4.39: Shafts assembly bounded contact

### 4.7.1 First analysis for shafts assembly: coarse mesh

#### Mesh element definition

A maximum element size constrain is set for the FEs definition, for all the model parts.

The same volume division for the superior and inferior shafts is considered, according with Tables 4.37 and 4.44. Again lower element sizes are set up for lover volumes and for parts in which there are contacts.

Table 4.49 reports the values assigned. The values 1.x refer to superior shaft volumes, while the values numbered as 2.x refer to the inferior shaft.

#### Mesh generation and analysis parameters

Figure 4.40 shows the AutoGEM mesh obtained. The solver dialog window does not report any problem in mesh generation. All elements are congruent with the model and constrains imposed.

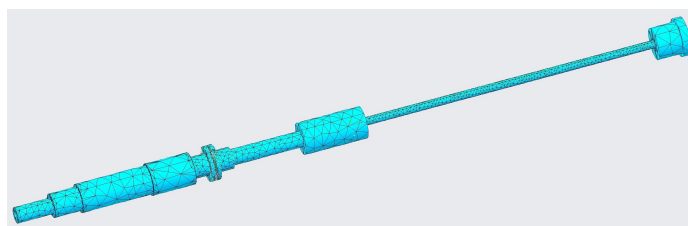


Figure 4.40: Coarse mesh, shafts assembly

For this study the following results from the AutoGEM are obtained, and the relative settings are established:

- Number of points: 3107;
- Number of edges: 15556;

Table 4.49: Shafts assembly, coarse mesh, FE size

<b>Id.</b>	<b>Name</b>	<b>Type of FE</b>	<b>FE dimension [mm]</b>
1.1	Coupling superior shaft - elastic junction	Max element size	7.5
1.2	shaft corp 1	Max element size	10
1.3	Electric exciter zone	Max element size	15
1.4	shaft corp 2	Max element size	5
1.5	Bearing coupling	Max element size	20
1.6	shaft head	Max element size	24
2.1	Coupling inferior shaft - electric motor	Max element size	10
2.2	Bearing coupling 1	Max element size	15
2.3	shaft corp	Max element size	18
2.4	Bearing coupling 2	Max element size	20
2.5	Coupling inferior shaft - elastic junction	Max element size	7.5
3	Elastic junction	Max element size	7.5

- Number of solid elements: 10068;
- Number of spring elements: 4;
- Convergence criterion: Multi-Pass Adaptive;
- Analysis definition: frequency range between 0 and 150Hz;
- Convergence criterion: percentage error with respect the frequency value up to 1%.

## Results

The convergence was reached after four iteration. The first iteration the solver was not able to reach any acceptable solutions in the range of frequency between 0 ÷ 150Hz. From the second iteration the solver finds out solutions. Table 4.50 reports the solver steps up to reaching the convergence.

Table 4.50: Multi-Pass Adaptive steps, shafts assembly, coarse mesh

<b>Pass</b>	<b>Number of equations</b>	<b>Polynomial order</b>	<b>Percentage error [%]</b>
Pass 1	8999	1	-
Pass 2	54 930	2	100
Pass 3	167 967	3	9.1
Pass 4	331 186	4	0.2

Two natural frequencies, in the range 0 ÷ 150Hz, have been found out. Table 4.51 shows the natural frequencies values obtained and the relative RMS error percentage computed with respect to the natural frequency.

Table 4.51: Natural frequencies and RMS errors, shafts assembly: coarse mesh

Mode	Natural Frequency $\omega_n [Hz]$	Error $\eta\%$
1	58.46	0.2
2	58.51	0.2

The results shows two vibration modes which appear around the same natural frequencies. Those values are a bit lower with respect the superior shaft first modes, even if the shape is maintained.

A natural frequencies reduction can be lead to the elastic junction presence, which influence the assembly vibration so that also its vibration modes are appreciable.

### 4.7.2 Second analysis for shafts assembly: medium mesh

#### Mesh element definition

On the bases of the previous analysis, a maximum element size is defined for shafts volumes and the elastic junction

Table 4.52 reports the values assigned. The values 1.*x* refer to superior shaft volumes, while the values numbered as 2.*x* refer to the inferior shaft.

Table 4.52: Shafts assembly, medium mesh, FE size

Id.	Name	Type of FE	FE dimension [mm]
1.1	Coupling superior shaft - elastic junction	Max element size	4
1.2	Shaft corp 1	Max element size	6.5
1.3	Electric exciter zone	Max element size	11.5
1.4	Shaft corp 2	Max element size	2
1.5	Bearing coupling	Max element size	16.5
1.6	Shaft head	Max element size	20
2.1	Coupling inferior shaft - electric motor	Max element size	6.5
2.2	Bearing coupling 1	Max element size	12.5
2.3	Shaft corp	Max element size	14.5
2.4	Bearing coupling 2	Max element size	17.5
2.5	Coupling inferior shaft - elastic junction	Max element size	3
3	Elastic junction	Max element size	3

#### Mesh generation and analysis parameters

Figure 4.41 shows the AutoGEM mesh obtained. The solver dialog window does not report any problem in mesh generation. All elements are congruent with the model and constrains imposed.

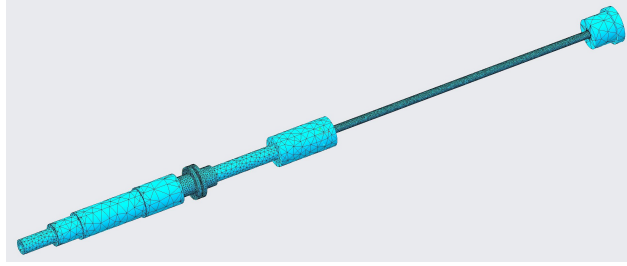


Figure 4.41: Medium mesh, shafts assembly

For this study the following results from the AutoGEM are obtained, and the relative study settings are established:

- Number of points: 16070;
- Number of edges: 91739;
- Number of solid elements: 66746;
- Number of springs elements: 4;
- Convergence criterion: Multi-Pass Adaptive;
- Analysis definition: frequency range between 0 and  $150Hz$ ;
- Convergence criterion: percentage error with respect the frequency value up to 1%.

## Results

The convergence was reached after four iteration. The first iteration the solver was not able to reach any acceptable solutions in the range of frequency between  $0 \div 150Hz$ . From the second iteration the solver finds out solutions. Table 4.53 reports the solver steps up to reaching the convergence.

Table 4.53: Multi-Pass Adaptive steps, shafts assembly, medium mesh

Pass	Number of equations	Polynomial order	Percentage error [%]
Pass 1	47 860	1	-
Pass 2	322 258	2	100
Pass 3	1 023 402	3	1.3
Pass 4	2 032 525	4	0.1

Two natural frequencies, in the range  $0 \div 150Hz$ , have been found out. Table 4.54 shows the natural frequencies values obtained and the relative RMS error percentage computed with respect to the natural frequency.

Analogous results, to the first simulation, are obtained with an higher level of confidence.

Table 4.54: Natural frequencies and RMS errors, shafts assembly: medium mesh

Mode	Natural Frequency $\omega_n [Hz]$	Error $\eta\%$
1	58.42	0.1
2	58.47	0.1

### 4.7.3 Shafts assembly vibration modes

In this section the vibration modes for the shafts assembly are shown.

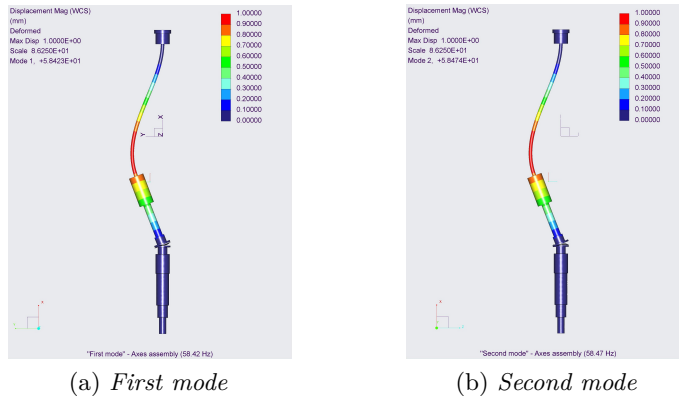


Figure 4.42: Shafts assembly, vibration modes

Figure 4.42 shows the shafts assembly vibration modes. The mode shown reflect the third and fourth superior shaft vibration modes, but occurs for a considerably lower natural frequency. The motivation behind can be attributed to the elastic junction modes, which superpose with the shaft ones.

The two modes appear for mostly equal natural frequencies and in the same plane. It means that, the mode will appear for a natural frequency around  $58.5 Hz$ , with a shape similar to Figure 4.42, with an higher amplitude and in a plane given by the composition of both.

## 4.8 Test bench structure

For the test bench model, three simulations were run. Only the software PTC Creo Simulate<sup>®</sup> is used.

The final objective, of studying the complete complete analytic model vibration behaviour, is to compare those results with the experimental analysis. Moreover, it is interesting to study the influence of all vibration modes, previously analysed, in the global structure.

## Geometry

The full test bench CAD model is basically made of all the previous models. Some simplifications were done in the internal and external structures analyses: the internal shafts support parts were omitted (Figure 4.43), whereas in these analyses all the components are considered.

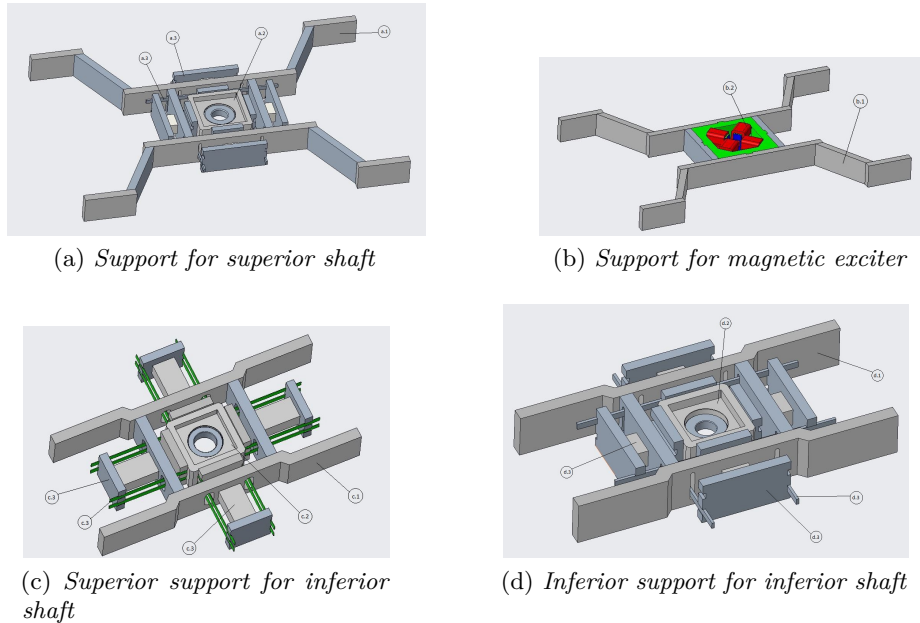


Figure 4.43: Shafts supports parts detail

Figure 4.44 shows the complete test bench CAD model. Table 4.55 lists all the parts with the respective material. Figure 4.44 does not show with sufficient level of details the shafts supports, which are shown in Figures 4.43a - 4.43b - 4.43c - 4.43d.

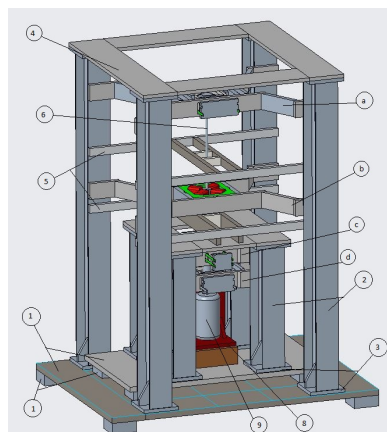


Figure 4.44: Test bench structure CAD model

Table 4.55: Table of test bench model parts

Id.	Name	Material
1	Base and supports	Structural steel
2	Double T beam	Structural steel
3	Beam backing and supports	Structural steel
4	Superior frame	Structural steel
a.1-b.1-c.1-d.1	Shafts support structure	Structural steel
a.2-c.2-d.2	Shafts supports	Aluminium - class: Al 7075
b.2	Magnetic exciter	-
a.3-c.3-d.3	Shafts supports balancing elements	Structural steel
5	Sensors supports	Structural steel
6	Superior and inferior shafts	Structural steel
7	Elastic junction	Aluminium - class: Al 7075
8	Motor support	Structural steel
9	Electric motor casing	Cast iron - FE60

## Material

The material used, for almost all the parts, is the Structural steel, from the PTC Creo Simulate<sup>®</sup>. Only for the elastic junction and the shafts supports elements, *a.2*, *c.2* and *d.2* in Figure 4.43, the material used is the aluminium - class Al 7075. Also the cast iron - FE60 is not present in the software material database, therefore, it was manually added and it is assigned to the electric motor casing.

All the material properties are listed in Table 4.56.

Table 4.56: Material properties for test bench modal analyses

Material	Density $\rho[\frac{kg}{m^3}]$	Young modulus $E[GPa]$	Poisson coefficient $\nu[-]$
Structural steel	7827	199.95	0.27
Al 7075	2850	72	0.33
FE60	7468	131	0.25

## Boundary conditions

A fixed boundary conditions between the bottom part of the four external structure supports and the solver absolute reference system is considered. It means that the structure can not translate or rotate and is fixed to the ground. Figure 4.45 shows in green the constrain location.

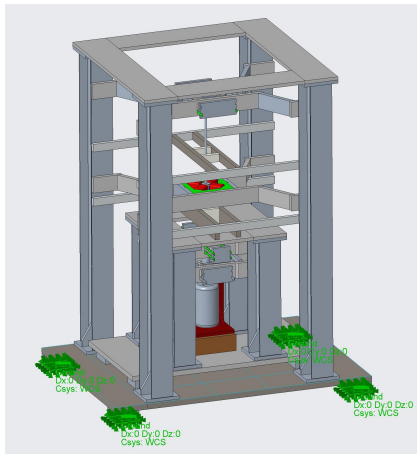


Figure 4.45: Test bench boundary condition constrains

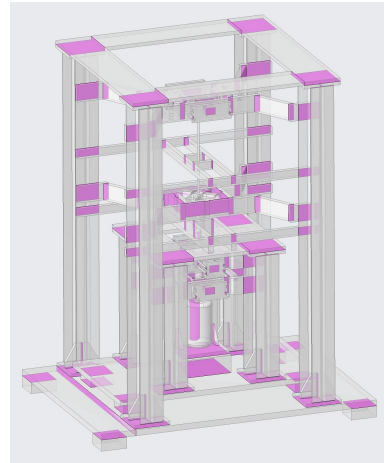


Figure 4.46: Test bench contact conditions between parts

### Contact relation between parts

Default bounded contact between each assembly element is defined for all the simulations run. Figure 4.46 shows where the bounded link is automatically recognised by the software, where the surfaces are depicted of pink.

A bolted contact is set up in correspondence of the elastic junction holes, as well as the shafts assembly analyses. Figure 4.37 shows bolts positions in the model.

## 4.8.1 First analysis for test bench: coarse mesh

### Mesh element definition

A maximum element size constrain is set for the FEs definition for all the model parts, considering the main sub-assemblies as a whole.

Starting from the assumption of setting lower FE size for smaller elements, as well as parts whose displacement is expected higher, the values reported in Table 4.57 have been set as coarse mesh for the first analysis.

### Mesh generation and analysis parameters

Figure 4.47 shows the AutoGEM mesh obtained. The solver dialog window does not report any problem in mesh generation. All elements are congruent with the model and constrains imposed.

For this study the following results from the AutoGEM are obtained, and the relative study settings are established:

- Number of points: 16541;
- Number of edges: 79331;
- Number of solid elements: 47277;

Table 4.57: Test bench structure, coarse mesh, FE size

Id.	Name	Type of FE	FE dimension [mm]
1	Base and supports	Max element size	130
2	Double T beam	Max element size	110
3	Beam backing and supports	Max element size	85
4	Superior frame	Max element size	90
a.1-b.1-c.1-d.1	Shafts support structure	Max element size	85
a.2-c.2-d.2	Shafts supports	Max element size	75
a.3-c.3-d.3	Shafts supports balancing elements	Max element size	70
5	Sensors supports	Max element size	75
6	Superior and inferior shafts	Max element size	70
7	Elastic junction	Max element size	60
8	Motor support	Max element size	100
9	Electric motor casing	Max element size	130

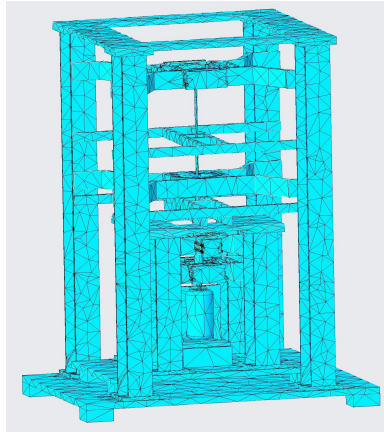


Figure 4.47: Coarse mesh, test bench structure

- Number of spring elements: 4;
- Number of masses (magnetic exciter): 8;
- Convergence criterion: Multi-Pass Adaptive;
- Analysis definition: frequency range between 0 and 150Hz;
- Convergence criterion: percentage error with respect the frequency value up to 3.5%.

## Results

The convergence is reached in four steps.

Table 4.58 reports the solver steps up to reaching the convergence.

Table 4.58: Multi-Pass Adaptive steps, test bench structure, coarse mesh

Pass	Number of equations	Polynomial order	Percentage error [%]
Pass 1	49 575	1	100
Pass 2	287 508	2	100
Pass 3	1 149 006	4	100
Pass 4	2 498 988	6	3

The number of natural frequencies, in the range  $0 \div 150Hz$ , is twenty one. Table 4.59 shows the natural frequencies values obtained and the relative RMS error percentage computed with respect to the natural frequency.

Table 4.59: Natural frequencies and RMS errors, test bench structure: coarse mesh

Mode	Natural Frequency $\omega_n [Hz]$	Error $\eta\%$	Mode	Natural Frequency $\omega_n [Hz]$	Error $\eta\%$
1	12.90	0.4	12	92.13	3
2	12.91	0.5	13	96.13	1.8
3	21.35	0.8	14	105.27	0.8
4	28.59	1.6	15	110.21	2.3
5	30.28	1.1	16	115.08	1.9
6	54.79	1.3	17	119.95	1.3
7	57.26	1	18	124.64	2.5
8	69.91	2	19	134.15	2.4
9	75.52	2.4	20	138.87	2.1
10	77.33	0.9	21	146.26	2.1
11	81.39	2.9			

Several natural frequencies have been found out and the majority face the sub-assemblies natural frequencies. Probably the first two natural frequencies will not face the real structure behaviour, being those the balance elements, for inferior shaft support, vibration modes.

## 4.8.2 Second analysis for test bench: medium mesh

### Mesh element definition

A maximum element size constrain is set for the FEs definition for all the model parts, considering the main sub-assemblies as a whole. Table 4.60 lists the data set up for the second analysis.

### Mesh generation and analysis parameters

Figure 4.48 shows the AutoGEM mesh obtained. The solver dialog window does not report any problem in mesh generation. All elements are congruent with the model and constrains

Table 4.60: Test bench structure, medium mesh, FE size

Id.	Name	Type of FE	FE dimension [mm]
1	Base and supports	Max element size	90
2	Double T beam	Max element size	75
3	Beam backing and supports	Max element size	60
4	Superior frame	Max element size	70
a.1-b.1-c.1-d.1	Shafts support structure	Max element size	65
a.2-c.2-d.2	Shafts supports	Max element size	60
a.3-c.3-d.3	Shafts supports balancing elements	Max element size	50
5	Sensors supports	Max element size	55
6	Superior and inferior shafts	Max element size	50
7	Elastic junction	Max element size	45
8	Motor support	Max element size	90
9	Electric motor casing	Max element size	95

imposed.

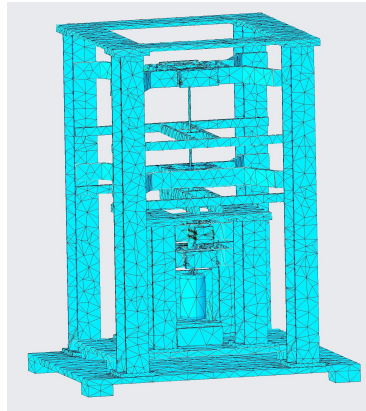


Figure 4.48: Medium mesh, test bench structure

For this study the following results from the AutoGEM are obtained, and the relative settings are established:

- Number of points: 18406;
- Number of edges: 88260;
- Number of solid elements: 52617;
- Number of spring elements: 4;

- Number of masses (magnetic exciter): 8;
- Convergence criterion: Multi-Pass Adaptive;
- Analysis definition: frequency range between 0 and  $150Hz$ ;
- Convergence criterion: percentage error with respect the frequency value up to 3.5%.

## Results

The convergence is reached in four steps.

Table 4.61 reports the solver steps up to reaching the convergence.

Table 4.61: Multi-Pass Adaptive steps, test bench structure, medium mesh

Pass	Number of equations	Polynomial order	Percentage error [%]
Pass 1	55 128	1	100
Pass 2	319 746	2	100
Pass 3	1 346 190	4	100
Pass 4	2 851 494	6	2.6

The number of natural frequencies, in the range  $0 \div 150Hz$ , is twenty one. Table 4.62 shows the natural frequencies values obtained and the relative RMS error percentage computed with respect to the natural frequency.

Table 4.62: Natural frequencies and RMS errors, test bench structure: medium mesh

Mode	Natural Frequency $\omega_n[Hz]$	Error $\eta\%$	Mode	Natural Frequency $\omega_n[Hz]$	Error $\eta\%$
1	12.91	0.4	12	91.42	1.7
2	12.92	0.4	13	95.66	1.3
3	21.30	0.6	14	105.31	0.7
4	28.47	1	15	109.64	1.4
5	30.20	0.7	16	113.58	2
6	54.83	1.5	17	119.72	1.1
7	57.39	1.6	18	124.01	1.3
8	69.85	1.7	19	133.31	1.4
9	74.06	2.6	20	138.62	1.7
10	77.15	0.6	21	145.36	1.2
11	81.37	2			

The natural frequencies are mostly equal to the previous analysis, except for some values which differ for around  $1.5Hz$ . Anyway it is possible to confirm the values obtained in Table 4.62.

For a double check a third analysis with a finer mesh is run.

### 4.8.3 Third analysis for test bench: fine mesh

#### Mesh element definition

A maximum element size constrain is set for the FEs definition for all the model parts, considering the main sub-assemblies as a whole. Table 4.63 lists the data set up.

Table 4.63: Test bench structure, fine mesh, FE size

<b>Id.</b>	<b>Name</b>	<b>Type of FE</b>	<b>FE dimension [mm]</b>
1	Base and supports	Max element size	70
2	Double T beam	Max element size	50
3	Beam backing and supports	Max element size	40
4	Superior frame	Max element size	45
a.1-b.1-c.1-d.1	Shafts support structure	Max element size	45
a.2-c.2-d.2	Shafts supports	Max element size	35
a.3-c.3-d.3	Shafts supports balancing elements	Max element size	25
5	Sensors supports	Max element size	30
6	Superior and inferior shafts	Max element size	30
7	Elastic junction	Max element size	25
8	Motor support	Max element size	65
9	Electric motor casing	Max element size	80

#### Mesh generation and analysis parameters

Figure 4.49 shows the AutoGEM mesh obtained. The solver dialog window does not report any problem in mesh generation. All elements are congruent with the model and constrains imposed.

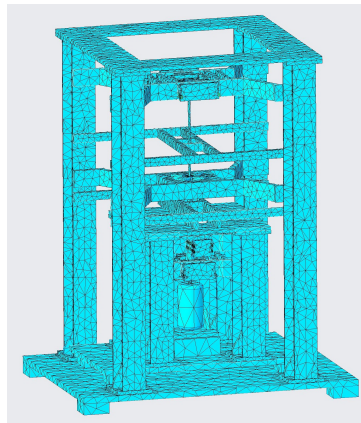


Figure 4.49: Fine mesh, test bench structure

For this study the following results from the AutoGEM are obtained, and the relative study settings are established:

- Number of points: 24881;
- Number of edges: 119684;
- Number of solid elements: 71519;
- Number of spring elements: 4;
- Number of masses (magnetic exciter): 8;
- Convergence criterion: Multi-Pass Adaptive;
- Analysis definition: frequency range between 0 and 150Hz;
- Convergence criterion: percentage error with respect the frequency value up to 3%.

## Results

The convergence is reached in four steps.

Table 4.64 reports the solver steps up to reaching the convergence.

Table 4.64: Multi-Pass Adaptive steps, test bench structure, fine mesh

Pass	Number of equations	Polynomial order	Percentage error [%]
Pass 1	74 535	1	100
Pass 2	433 395	2	100
Pass 3	2 176 149	4	100
Pass 4	4 301 817	6	1.5

The number of natural frequencies, in the range  $0 \div 150Hz$ , is twenty one. Table 4.65 shows the natural frequencies values obtained and the relative RMS error percentage computed with respect to the natural frequency.

In general, the natural frequencies values are stable and in accordance with the previous results. The results in Table 4.65 have higher level of confidence, therefore a lower error percentage.

### 4.8.4 Test bench vibration modes

In this section the vibration modes for the complete test bench in comparison with the sub-assemblies modes are shown.

The modes which have not relation with the substructure are shown and commented separately.

Table 4.65: Natural frequencies and RMS errors, test bench structure: fine mesh

Mode	Natural Frequency $\omega_n [Hz]$	Error $\eta\%$	Mode	Natural Frequency $\omega_n [Hz]$	Error $\eta\%$
1	12.87	0.3	12	91.13	1.2
2	12.90	0.4	13	95.22	0.8
3	21.26	0.3	14	104.99	0.5
4	28.41	0.6	15	109.29	1
5	30.15	0.4	16	112.78	1.1
6	54.67	0.5	17	119.48	0.8
7	57.20	0.4	18	123.65	0.8
8	69.59	0.9	19	132.98	1
9	73.43	1.5	20	138.06	1.1
10	76.98	0.3	21	144.64	0.7
11	79.94	0.9			

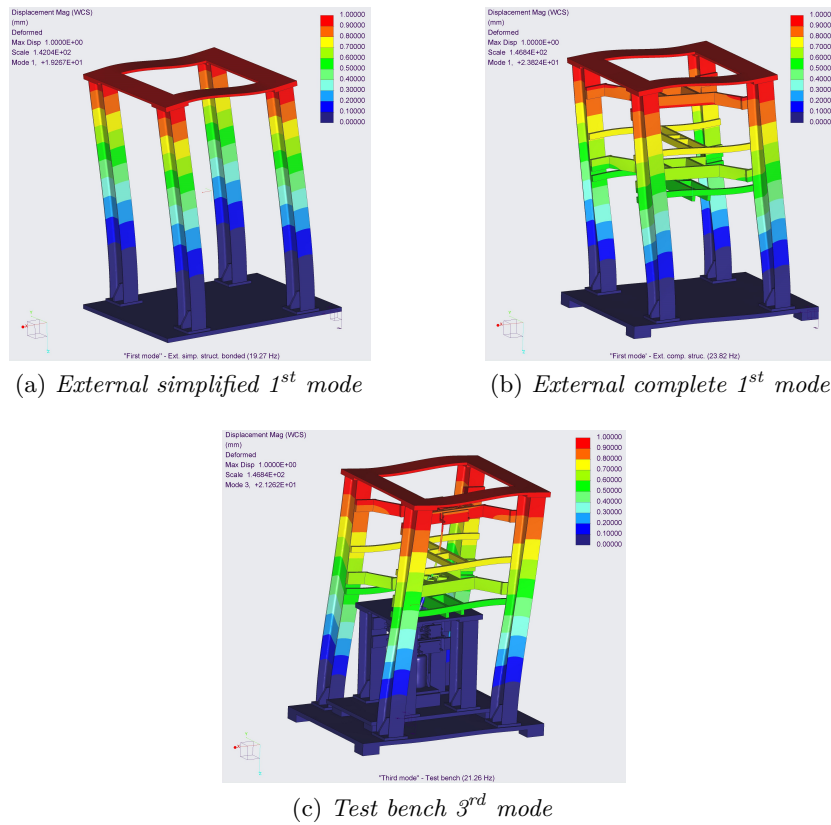


Figure 4.50: Comparison between models, 1<sup>st</sup> external structure mode

### First external structure mode

Figure 4.50 shows the comparison between the first external structure vibration mode, and the global structure, which correspond to the third vibration mode.

It is possible to notice how the mode is perfectly reproduced in the test bench model, and also the natural frequency is not so far from the complete external structure value.

### Second external structure mode

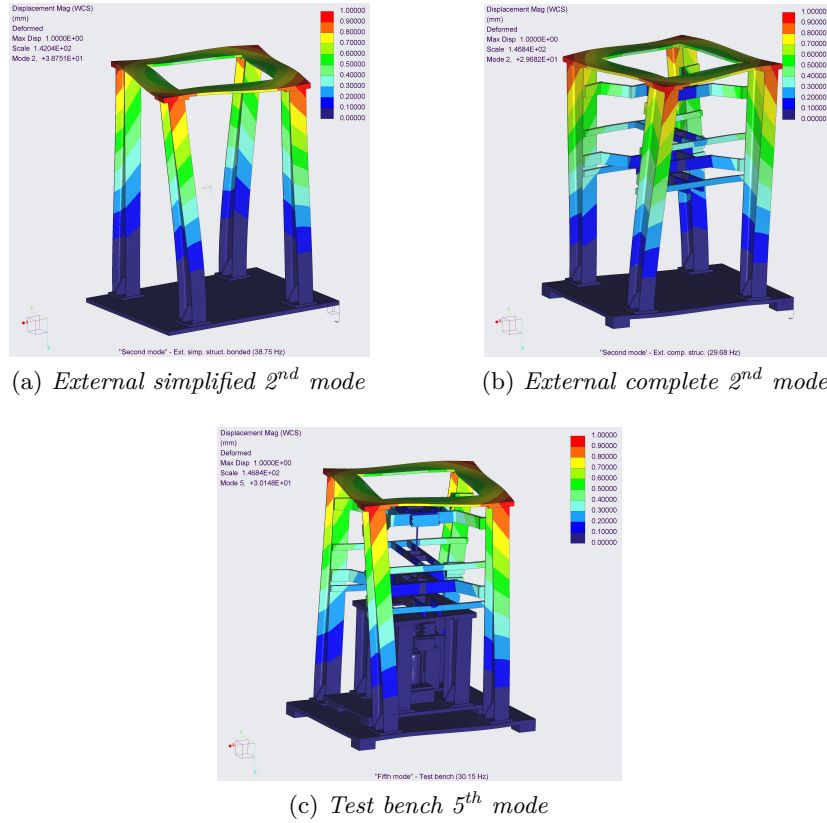


Figure 4.51: Comparison between models, 2<sup>nd</sup> external structure mode

Figure 4.51 shows the comparison between the second external structure vibration mode, and the global structure, which correspond to the fifth vibration mode.

It is possible to notice how the mode is also reproduced in the test bench model, and also the natural frequency is not so far from the complete external structure value.

### Third external structure mode

Figure 4.52 shows the comparison between the third external structure vibration mode, and the global structure, which correspond to the fourth vibration mode.

It is possible to notice how the mode is reproduced in the test bench model. A small change in the natural frequency value happen, as well as an inversion in the modes progression. The torsional vibration mode appears after the external structure third translation mode.

Analytic modal analysis results

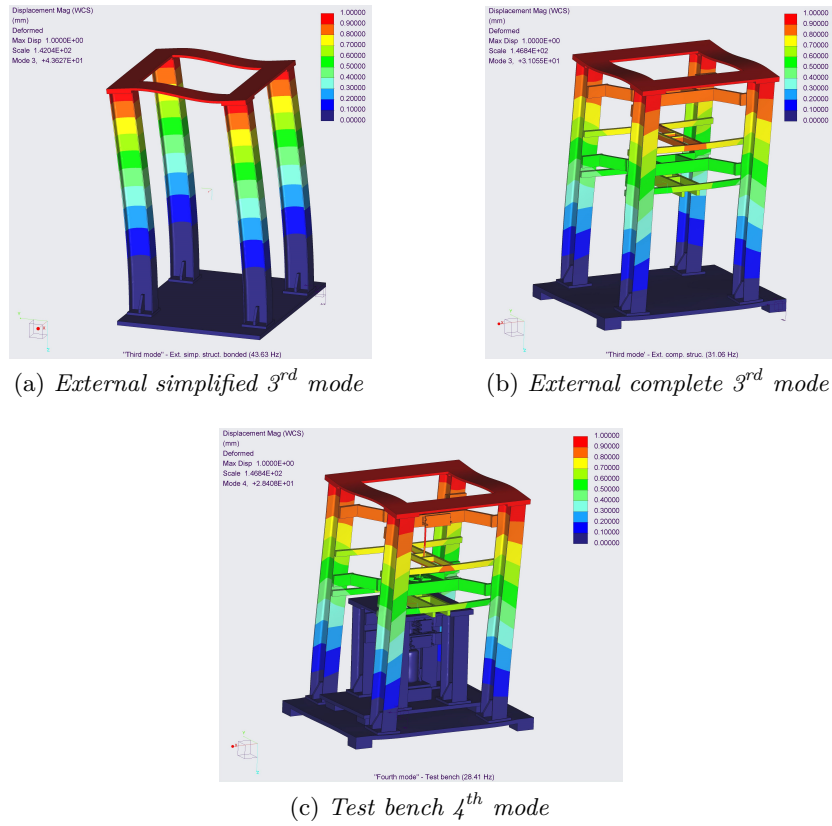


Figure 4.52: Comparison between models, 3<sup>rd</sup> external structure mode

Fourth external structure mode

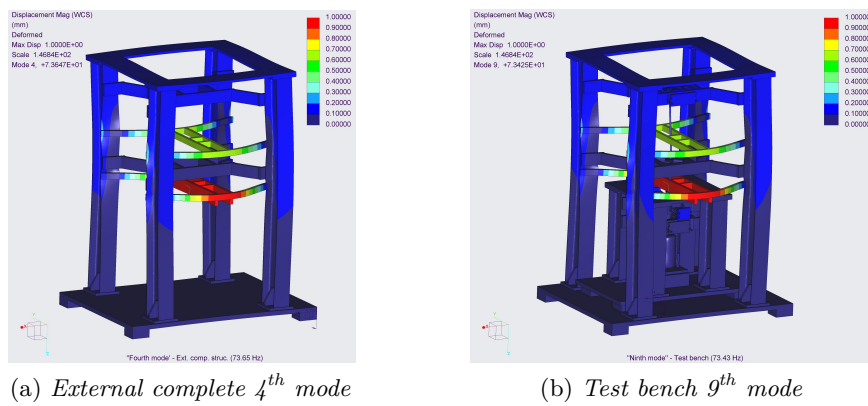


Figure 4.53: Comparison between models, 4<sup>th</sup> external structure mode

Figure 4.53 shows the comparison between the fourth external structure vibration mode,

and the global structure, which correspond to the ninth vibration mode.

It is possible to notice how the mode is reproduced in the test bench model, and also the natural frequency is not so far from the complete external structure value.

### Fifth external structure mode

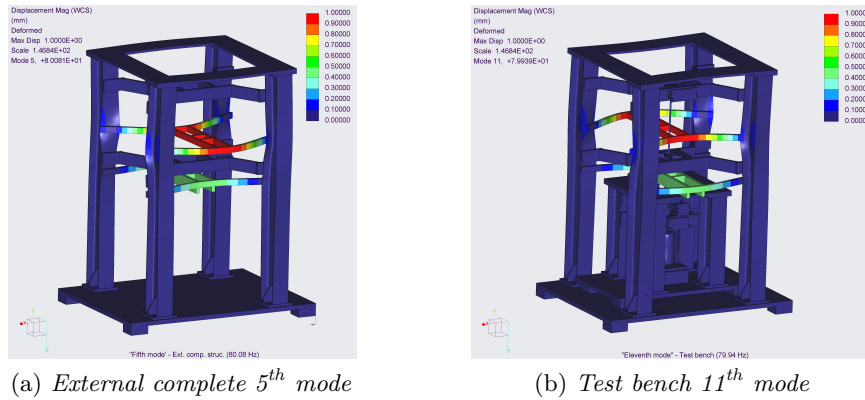


Figure 4.54: Comparison between models, 5<sup>th</sup> external structure mode

Figure 4.54 shows the comparison between the fifth external structure vibration mode, and the global structure, which correspond to the eleventh vibration mode.

It is possible to notice how the mode is reproduced in the test bench model, and also the natural frequency is not so far from the complete external structure value.

### Sixth external structure mode

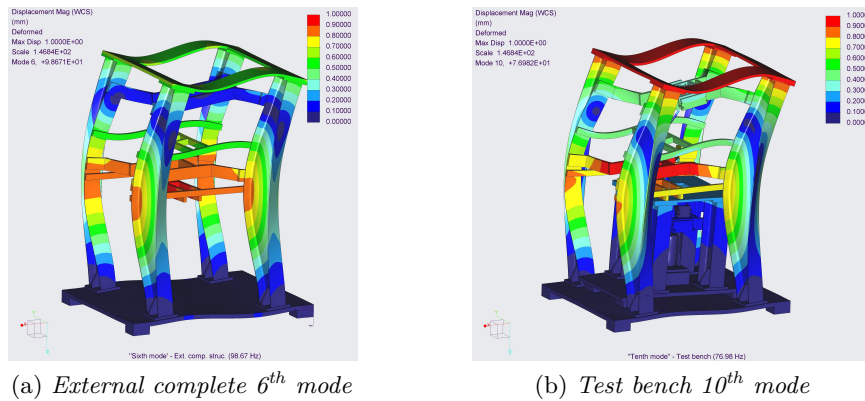


Figure 4.55: Comparison between models, 6<sup>th</sup> external structure mode

Figure 4.55 shows the comparison between the sixth external structure vibration mode, and the global structure, which correspond to the tenth vibration mode.

It is possible to notice how the mode is reproduced in the test bench model. Nevertheless, the natural frequency value is largely far from the external structure one, maybe caused by shafts assembly presence and the internal structure.

### Seventh external structure mode

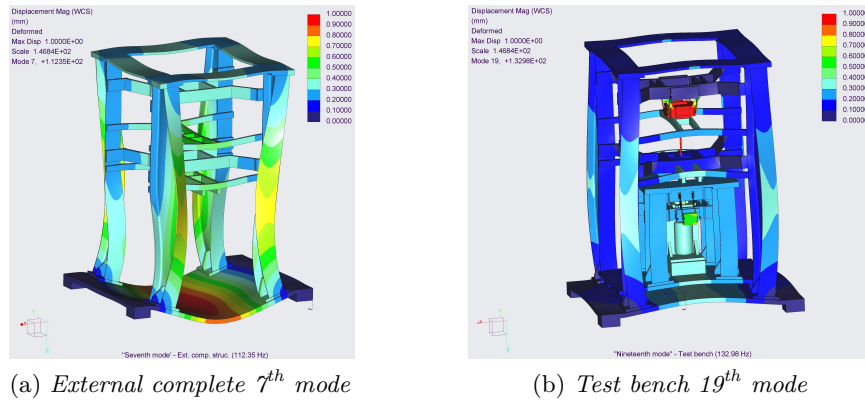


Figure 4.56: Comparison between models, 7<sup>th</sup> external structure mode

Figure 4.56 shows the comparison between the seventh external structure vibration mode, and the global structure, which is comparable with correspond to the nineteenth vibration mode.

The mode reproduce in certain way the last external structure vibration mode. The natural frequency value is largely far from the external structure one.

### First internal structure mode

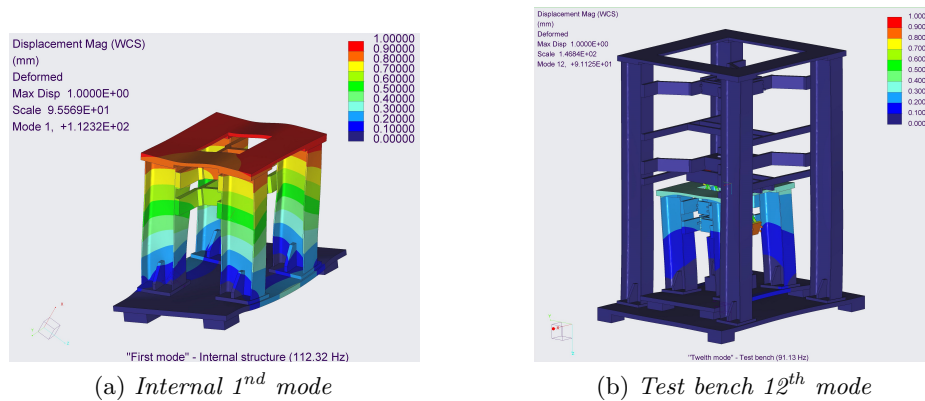


Figure 4.57: Comparison between models, 1<sup>st</sup> internal structure mode

Figure 4.57 shows the comparison between the first internal structure vibration mode, and the global structure, which correspond to the twelfth vibration mode.

It is possible to notice how the mode is reproduced with significant lower displacement in the test bench model. Also the natural frequency value is not so far from the internal structure one, even being around  $4Hz$  lower.

### Second internal structure mode

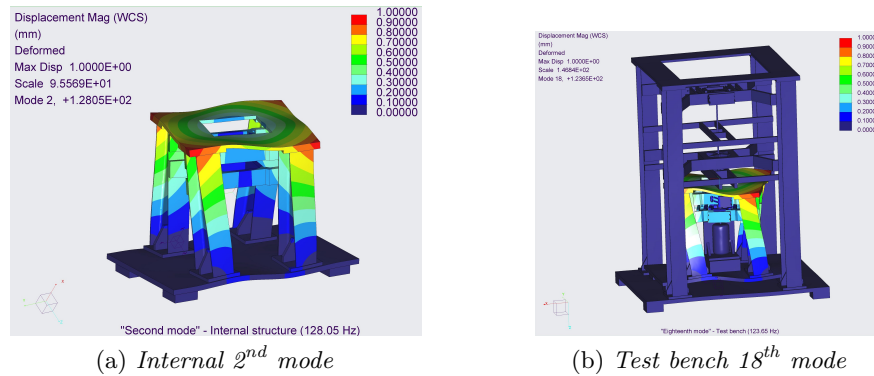


Figure 4.58: Comparison between models, 2<sup>nd</sup> internal structure mode

Figure 4.58 shows the comparison between the second internal structure vibration mode, and the global structure, which correspond to the eighteenth vibration mode.

It is possible to notice how the mode is well reproduced in the test bench model. Also the natural frequency value is not so far from the internal structure one.

### Third internal structure mode

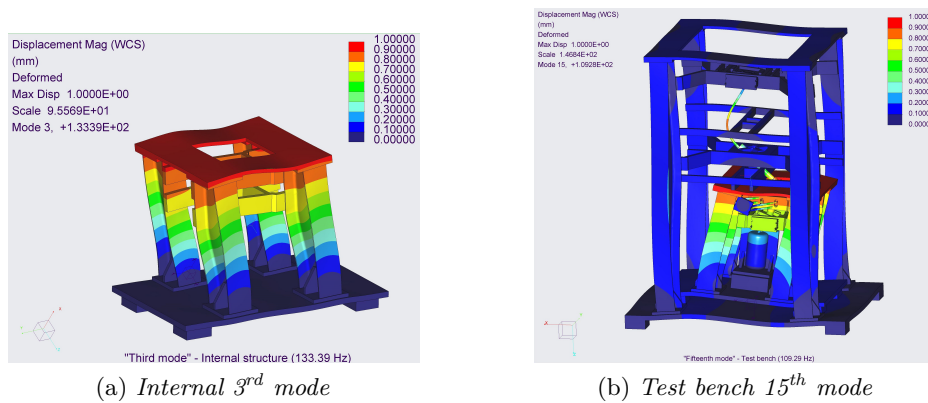


Figure 4.59: Comparison between models, 3<sup>rd</sup> internal structure mode

Figure 4.59 shows the comparison between the third internal structure vibration mode, and the global structure, which correspond to the fifteenth vibration mode.

It is possible to notice how the mode is well reproduced in the test bench model. Nevertheless, the natural frequency value is far from the internal structure one. Figure 4.59b

shows also a great displacement of the superior shaft, which could affect the final natural frequency value.

### Shafts assembly mode

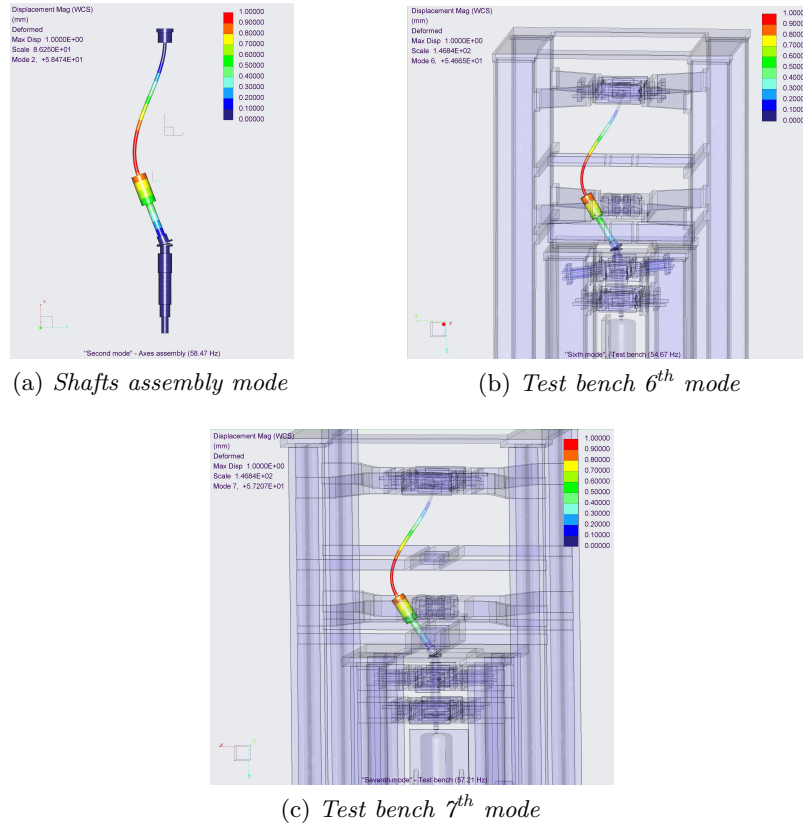


Figure 4.60: Comparison between models, shafts assembly mode

Figure 4.60 shows the comparison between the shafts assembly vibration mode, and the global structure, which correspond to the sixth and seventh vibration mode.

It is possible to notice how it is correctly reproduced in the test bench, and also the natural frequency value is not far from the complete external structure value. Also here the vibration is divided into two planes, even if the natural frequencies differs for  $3Hz$ . Probably also the stabiliser masses for the inferior shaft support, in the internal structure, influence the final value.

Other two modes, relative to the shafts assembly, are recognisable, in modes eighth and twentieth. The superior support for the inferior shaft, in the internal structure, contribution to the vibration mode, in Figure 4.61, is much more evident.

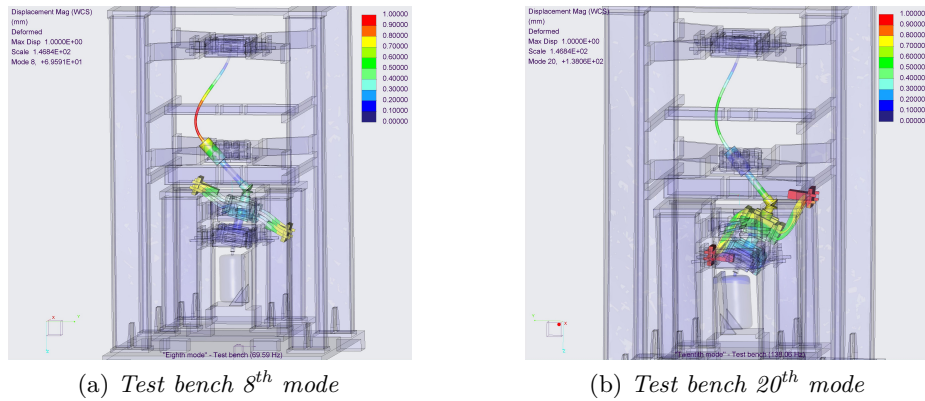


Figure 4.61: Additional shafts assembly modes in test bench model

### Other vibration modes

Both for very low natural frequencies, as well as for very high ones, over  $100\text{Hz}$ , are appreciable modes related to the shafts support structures.

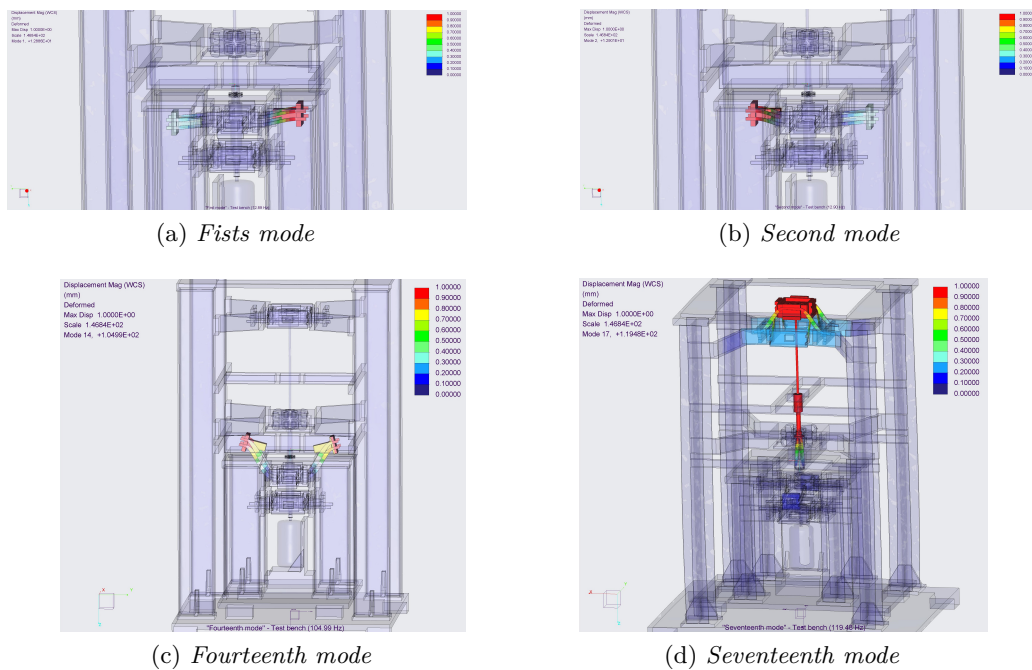


Figure 4.62: Shafts supports vibrations modes

Figure 4.62 shows the vibration behaviour not predictable from the previous analyses. Probably the first two modes will not reflect the real test bench vibration modes, because small changes in the geometry were applied in the CAD model.

For what concern the higher frequencies, modes fourteenth and seventeenth, the real

behaviour is not predictable, and the results cannot be considered reliable before experimental tests. Anyway, anomalous displacement can be avoided with a well controlled shaft rotational speed.

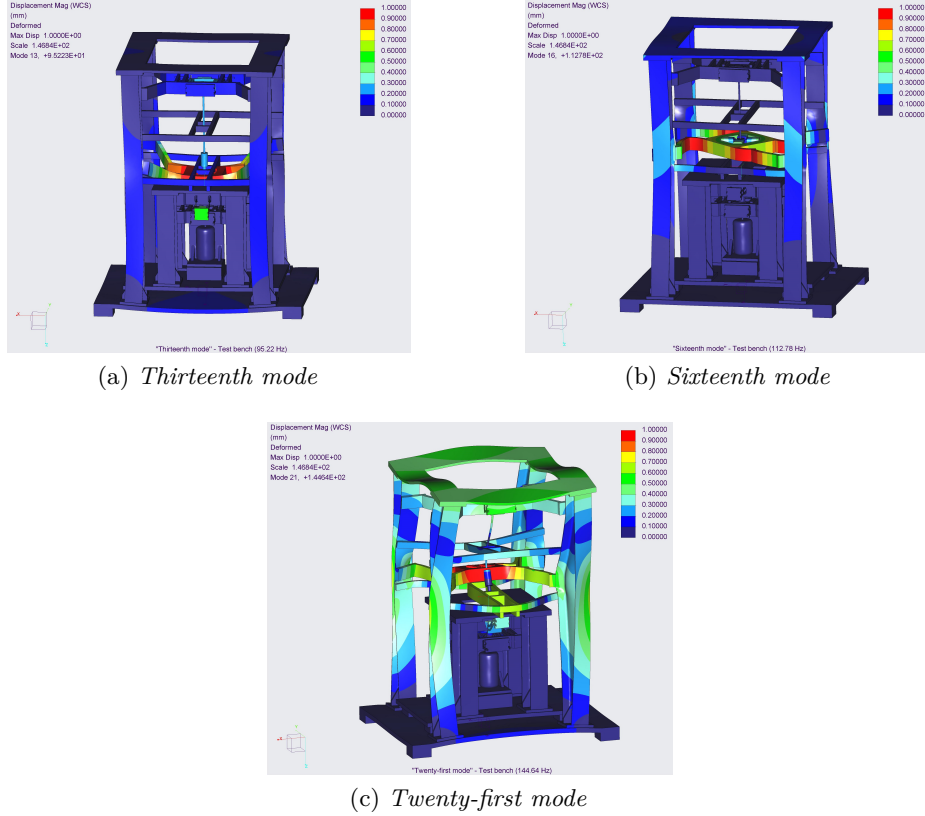


Figure 4.63: Magnetic exciter support vibration modes

Figure 4.63 shows the last three vibration modes. Those imply the displacement and the vibration of the magnetic exciter structure, and therefore, for what concern the mode twenty-first, the external structure in general.

Again, those vibration modes are not predictable, for this reason are not considered in the operation range of the shaft and it is required to validate their existence on the test bench prototype.

### 4.8.5 Conclusion

In the test bench model the majority of known natural frequencies and modes, coming from the previous analyses are presented. Not relevant difference between natural frequencies values are appreciable, with discrepancies lower than  $5Hz$  between the different models mesh.

Interesting is the fact that, the low external structure modes, in particular the first six modes, are present also in the global model. It requires particular attention in working condition in order to avoid extreme displacement caused by the shafts rotation speed.

Also shafts assembly vibration modes are repeated in the test bench analyses, also with consistent displacements. More than before, it is fundamental a correct calibration for the working velocity.

It is expected from the experimental analyses a discrepancy between the analytic results and the experimental ones. The main reasons behind this assumption are: neglecting geometrical features or modification, therefore consisting difference in masses distribution; manual definition of material, like the Al 7075 and FE60, and generic attribution also for complex component, like the electric motor and the magnetic exciter; neglecting the damping material properties, which are difficult to evaluate in an analytic modal analyses.

## Chapter 5

# Experimental analysis

### 5.1 Introduction

The experimental modal analysis, and relative results are presented in this chapter. The topic discussed regards the problem setup, therefore the DAQ system used, the data acquisition process and the following signal post processing.

The analysis have been executed exciting the test bench (5.1) with an impact hummer, in eleven driving points, corresponding to the principal acquisition point. Five accelerometers have been used for the whole DAQ system.



Figure 5.1: Test bench structure

A LabView DAQ program is used for acquiring hummer impact force ad accelerometers outputs. The program displays the impact force and the accelerations outputs, which are

the data stored for the signals post processing, and computed a first FRF, useful for noise detection.

The data acquired are post processed with the Matlab Signal Analysis Toolbox; in particular the functions *modalfrf* and *modalfit* [12] have been used, so that the FRFs, natural frequencies, damping coefficient and modal shapes are estimated.

## 5.2 DAQ system

The DAQ system consists of an impact hammer for the test bench excitation (5.2a), a triaxial accelerometer (5.2b), and four monoaxial accelerometers (5.2c). All these equipment are connected to each canal of two DAQ boards (5.2d).



(a) *Impact hammer*



(b) *Triaxial accelerometer*



(c) *Monoaxial accelerometer*



(d) *DAQ board*

Figure 5.2: DAQ system hardware

The board is made of four channel, therefore two boards are required in order to host the eight channels required.

Table in Appendix A shows the hardware properties.

The software DAQ system was implemented in LabView program language. The acquisition program store the input and output signals already converted in newton, for the impact force, and in gravitational acceleration, for the outputs signals. The data are acquired with a sampling frequency of  $50000 \frac{points}{s}$ , and the records have a period of  $3s$ ,

therefore a total number of 150000 *point* is stored for each channel. The program records also the time at which each point is recorded, according with an internal timer. If the acquisition is considered sufficiently accurate, the data of time, impact force, triaxial accelerometer and the four monoaxial accelerometers, are saved and stored in a document file.

This type of analysis does not use any type of analogue or digital filter during the acquisition process. The data are sampled with the maximum sampling frequency, therefore a successive data decimation is required in order to remove eventual signal noise.

### 5.3 DAQ process

Several DAQs repetition have been performed for each driving point. Usually ten reiteration have been done for each excitation point of interest. The reason behind this choice is overestimating the data acquired in order to compute the mean repetition value for each output signal, so that the bias errors can be minimised.

Eleven driving points are chosen, in a test bench quarter, based on the modal shape obtained from the analytical simulations. In particular, the accelerometers location is decided considering the structure elements in which higher displacement exists, therefore, the driving point was the one in the accelerometer opposite direction.

Being few the disposable accelerometers, the data acquisitions, for the different structure components, were done in different moments: all the driving points are excited with the accelerometers in a specified position, afterwards the accelerometers are moved and again all the driving points excited.

The points of interest are: the external support beam, the internal one, the external superior frame, the internal one, the external base and the internal one, shown with a red dot in Figure 5.3.

The presence of re-peaks in the impulse excitation, single decay acceleration amplitude and acceptable noises levels were investigated after each DAQ. If those three conditions were considered sufficiently consistent with the expected system response, the data would be saved, and a new excitation applied for the following acquisition.

#### 5.3.1 Possible error source

The three principal errors that can be present in acquired data are: human errors, in that specific case related with interference with the equipment or error in the excitation (re-peak in the impulse excitation); external noises, which can come from electromagnetic field in the acquisition area, ground vibration, 60Hz net noise<sup>1</sup>; random errors commonly known as bias.

For what concern human errors, those errors were easily identified analysing the LabView amplitudes plots. Also external noises, as well as human errors, were detected with the same method, in particular, 60Hz net noise was not perceptible from the FRFs plotted in LabView, no picks in that frequency range were present. For what concern bias errors, those are not directly detectable, for this reason post processing data is required.

---

<sup>1</sup>the analyses have been run in Brazil, where the domestic net is provided at 110 or 220V and 60Hz

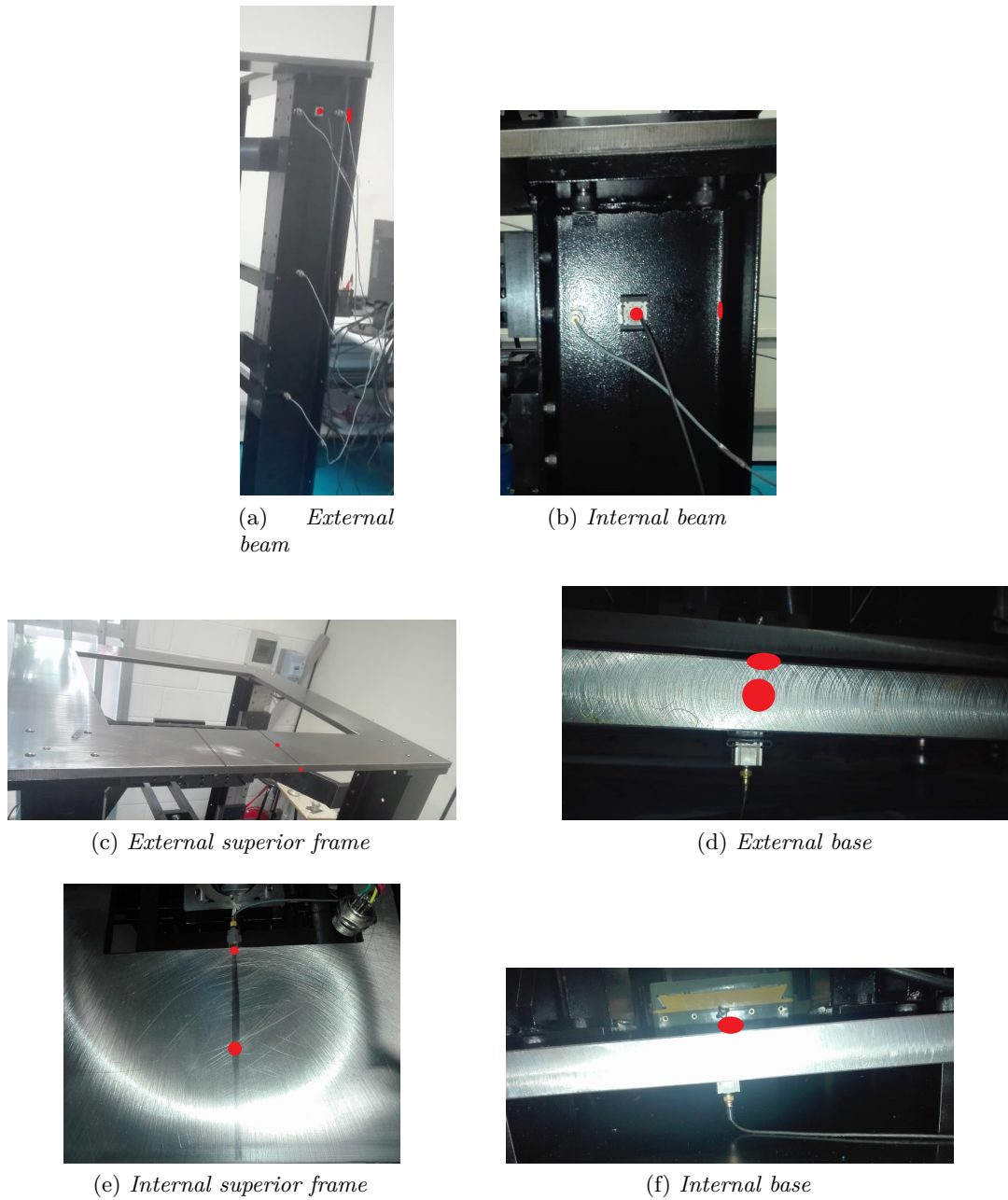
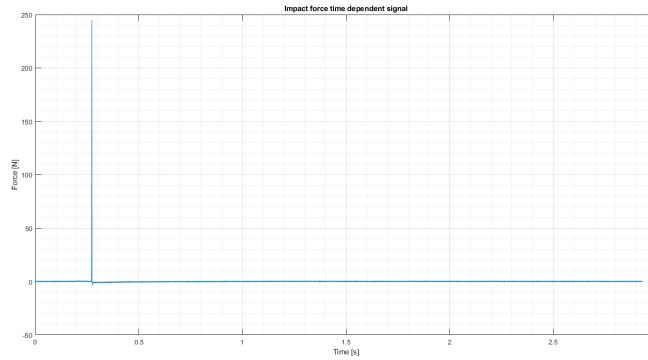


Figure 5.3: DAQ system hardware

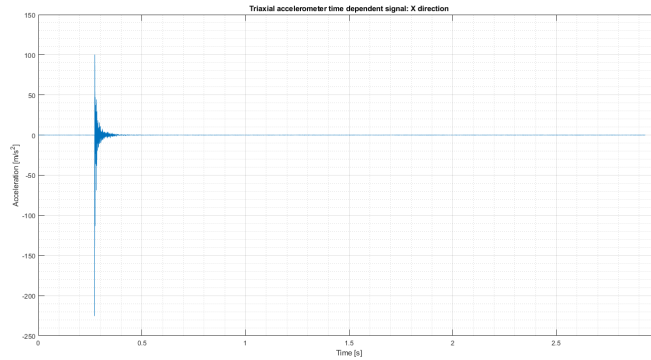
## 5.4 Data analyses procedure

The data acquired with LabView were elaborated with a Matlab code(Appendix B), making use of some functions from Signal Analyses Toolbox. A post processing signal according with SISO theory is done; it is studied the FRF of each output signal relative to its impulse excitation.

First of all the data stored in each file, for each repetition, are read and imported in Matlab arrays, so that time dependent impulse excitation and accelerations can be plotted; an example of signals in time domain is shown in Figure 5.4. The imported files are composed of nine columns in which are stored respectively in columns vectors: time vector information, impulse excitation magnitude, triaxial acceleration magnitude in the  $x$  coordinate, triaxial acceleration magnitude in the  $y$  coordinate, triaxial acceleration magnitude in the  $z$  coordinate, monoaxial acceleration magnitude from channel 5, monoaxial acceleration magnitude from channel 6, monoaxial magnitude from channel 7 and monoaxial acceleration magnitude for channel 8. Remembering that the accelerations values are gravitational acceleration function, the following step is to convert those values in  $\frac{m}{s^2}$ .



(a) *Impulse force in the time domain*



(b) *Acceleration in the time domain*

Figure 5.4: Time domain signals

The modal FRF of each output signal is computed throughout the function *modalfrf*. The FRF are evaluated windowing the input and output signal with an *Hanning* window, whose spectrum in time and frequency domains is shown in Figure 5.5, with a number of points equal to half of the data population (75001points).

Even not being the Hanning window the best windowing technique for a impact hammer analysis, from literature the exponential window is the best choice, it was chosen because it is the most general windowing technique with the best resolution between signal amplitude

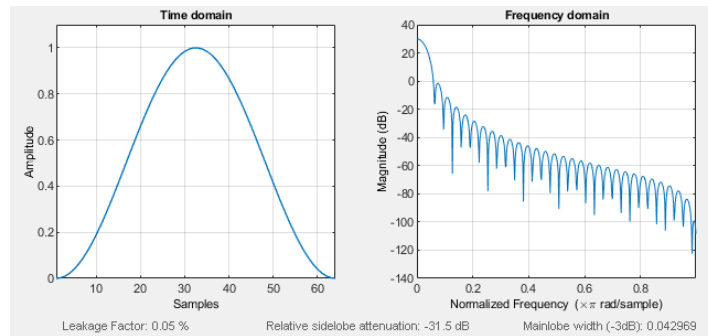


Figure 5.5: Hanning window spectrum in time and frequency domains

attenuation and frequency content shift. Moreover, the exponential window is not directly included in Matlab release.

The windowing technique adopted gives a FRF signal with a lower level of noise, compared with the results coming out the LabView FRFs; an example of filterer FRF for a single repetition DAQ is shown in Figure 5.6.

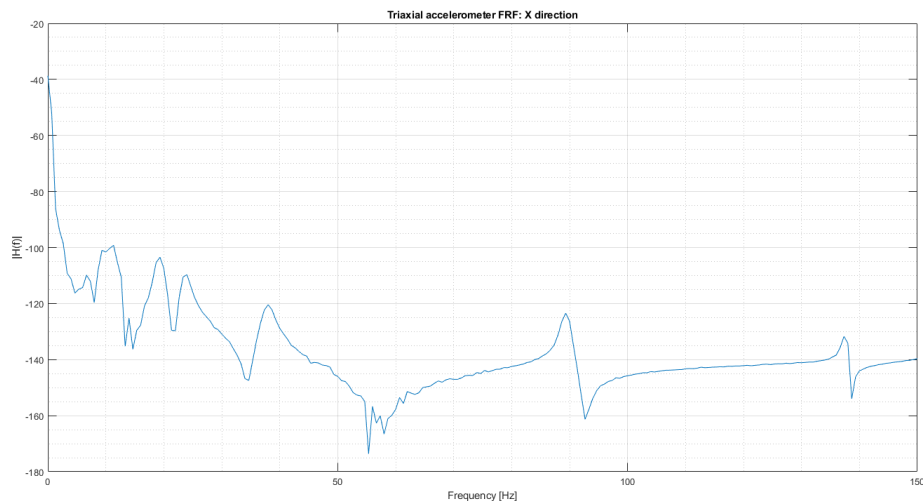


Figure 5.6: FRF for a single signal

Once all the file, containing each repetition data, are acquired and stored in arrays variables referred to the relative channel, the algebraic average value of all FRF of each signal is computed. An example of averaged signal is shown in 5.7.

Comparing Figure 5.6 with Figure 5.7, it is possible to notice how the noise level is well reduced, in particular in the frequency band between  $60 \div 75 Hz$ , which is the most noisy signal zone. It is interesting to notice how averaging overestimated signal can strongly reduce random noises which affect the signals. The main difficulties of applying this technique is the time consumed for repeating the acquisition.

In the end, to the averaged signal is applied the Least Squared Complex Estimation

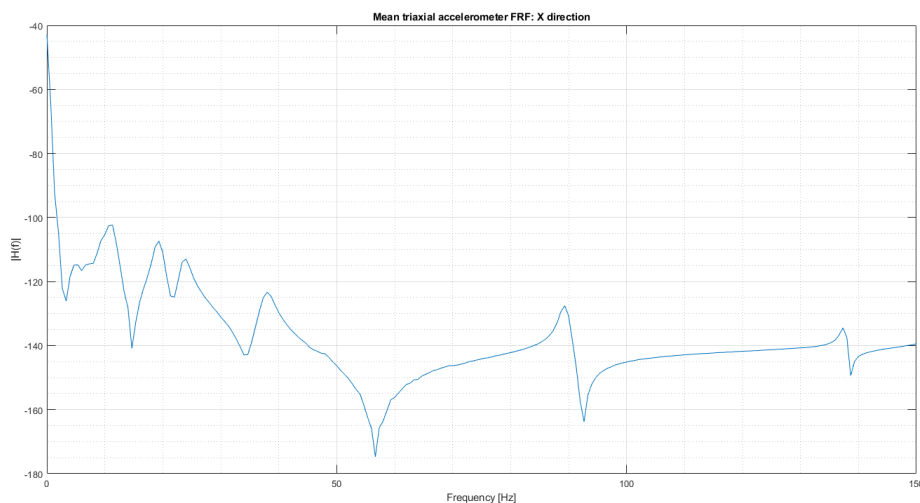


Figure 5.7: Averaged FRF signal

fitting, implemented by the Matlab function *modalfit*, which extract the required natural frequencies, damping coefficients and modes in a specified frequency range. According with the hypothesis followed in the analytic study, the range of frequencies in which the LSCE fitting technique can be applied is between  $0 \div 150Hz$ .

## 5.5 Results

The results here exposed regards the acquisition made on the external and internal beams excited in all the driving points. A general view of all the results will be expose, mainly considering the results obtained from the triaxial accelerometer.

These assumption in the result exposition comes from the fact that the natural frequencies found out are mostly present in all the acquisition, and the results from the monoaxial accelerometers are quite the same of ones from the triaxial  $x$  coordinate.

### 5.5.1 External structure

Around twenty natural frequencies have been found out from the data analysed, considering a data reconstruction between the various signals.

The natural frequencies in the ranges between  $10 \div 50Hz$  and between  $85 \div 140Hz$  are of particular interest, being those associated to the internal and external structure.

From a comparison between the modal fitting natural frequencies results and the FRFs plots (shown in Appendix C), it is reasonable to consider reliable the following results:

Mode	Natural frequency $f_n[Hz]$	Damping coefficient $\zeta$
1	10.5	0.05
2	19.3	0.03
3	23.7	0.025
4	38.0	0.03
5	47.5	0.05
6	50.7	0.043
8	89.9	0.01
9	139.0	0.012

### 5.5.2 Internal structure

For the internal structure the results obtained are quite similar to the ones for the external beam acquisition. An additional information can be obtained observing both the FRF plots (Appendix B) and the numerical values: a distinct peak around  $-120dB$  is present at the frequency of  $129Hz$ .

### 5.5.3 Conclusion

Common to all the analyses is the low amplitude level, especially in the frequency range between  $50 \div 80Hz$ , range in which an higher level of noise is present. The level of noise is more evident for that acquisition in which the driving point was far from the accelerometers position. This is an expected result, because a low energy content reached the accelerometer, therefore the uncertainty for such measurement is higher as well as the noise.

# Chapter 6

## Conclusion

### 6.1 Comparison between the analytic and experimental results

The results presented in Chapter 5 do not face completely the expected results for analytical simulations.

In particular the wild range of frequencies between  $60 \div 80Hz$  are highly uncertain in the experimental data, having a low amplitude value and a high noise content, which was not at all avoided with the post processing process for those data which from the starting point had a weak acceleration amplitude.

Anyway, it is possible to recognise the first and third natural frequencies of the external structure in the complete test bench (the respective second and third in the simplified model). Even if the frequency level is slightly reduced in comparison with the complete model, probably those natural frequencies,  $23.7Hz$  and  $38.0Hz$  matched the analytic study. In the specific the first of the two frequencies is exactly equal to the one reported in Table 4.26.

Analogously, consideration can be done for the clear  $129Hz$  frequency enhanced in the acquisition on the internal beam. This natural frequency match the torsional vibration mode of the internal structure, as reported in Table 4.36.

The possible reason behind the discrepancy between the two studies can be attributed firstly at the shafts absence in the experimental DAQ. The shaft assembly, even if it presents natural frequencies near the uncertainty band, when studied alone, the contributions due to the shafts assembly in various global structure natural frequencies is not negligible.

Not at all expected was also the strong presence of the last natural frequency about  $139Hz$ . This frequency practically always appear in all FRFs with a non negligible amplitude in comparison with other results.

Also the data acquisition system could be improved, applying a filter for reducing the noise in the middle band frequency and cutting off frequencies higher than  $200Hz$ .

A more accurate signal analysis criterion can be used so that modal shape can be investigated from the experimental analysis.

## 6.2 Prospective for future works

Several modification and/or improvements can be done in a future in order to have a higher matching between the experimental and analytical studies.

For what concerns the analytical study, simplification regarding the geometry symmetry, therefore study half or a quarter structure, or using different discretization technique for the structure components, such as beam element and beam theory as well as tiny shell, can be implemented in the CAD model analysis.

Regarding the experimental analysis, the permanent structure response under a periodic excitation is an interesting development for obtaining more accurate results, considering the low reliability of the hammer impact test compared with the shaker one.

In order to match the results, it could be also possible to apply the updating model theory to the analytic study, modifying the possible uncertainty in the model zone, creating a more confident mesh elements.

All the latter result could also be used for further analyses, such as stress in the structure in particular for the rotating and structural parts.



# Appendix A

## DAQ hardware properties

Table continue in the next page.

Component	Model	Properties	Channel
Impact hammer	B&K: type 8207	Sensitivity: $0.2390 \frac{mV}{N}$ (@ 159.2Hz, 24.4°C) Max. measuring range: 22200N ( 5V) Linear error: < ±2%	1
Triaxial accelerometer	B&K: type 4506-B	Sensitivity: $100.6 \frac{mV}{g}$ ( 159.2Hz, 4mA, 23°C) Freq. range (amplitude): 1 – 6kHz Freq. range (phase): 3 – 3kHz Resonance frequency: 19kHz Transverse sensitivity: < 5% Measuring range: ±70g Sensitivity: $10.4 \frac{mV}{g}$ ( 159.2Hz, 4mA, 24°C)	x y z x-y-z
Monoaxial accelerometer	B&K: type 4534-B	Freq. range (amplitude): 0.2 – 12.8kHz Freq. range (phase): 1 – 10kHz Resonance frequency: > 38kHz Transverse sensitivity: < 5% Measuring range: ±70g	1 – 3.5kHz 2-3-4
DAQ board	Ni9234	-	-

# Appendix B

## Matlab codes

```
1 %%%%%%%%%%%%%%%%%%%%%%%%%%%%%%%%%%%%%%%%%%%%%%%%%%%%%%%%%%%%%%%%%%%%%%%%%%
2 %%Michele G. Massafra, last update: 22/11/2018
3 %%%%%%%%%%%%%%%%%%%%%%%%%%%%%%%%%%%%%%%%%%%%%%%%%%%%%%%%%%%%%%%%%%%%%%%%%%
4 %%mean.m
5 %%Inserting as a string char the files names, those arr pass to
6 %%the built function 'file2varFRF.m, which turns out the forces
7 %%time dependent vectors ans the FRFs of each channel.
8 %%The 'FRFmeans.m' function compute the averaged value for the
9 %%whole FRFs computed in 'file2varFRF.m
10 %%%%%%%%%%%%%%%%%%%%%%%%%%%%%%%%%%%%%%%%%%%%%%%%%%%%%%%%%%%%%%%%%%%%%%%%%%
11 %%NOTE: this code can be run only if the Signal Processing
12 %%Toolbox is installed, and with the two buinded functions
13 %%'file2varFRF.m' and 'FRFmeans.m'
14 %%%%%%%%%%%%%%%%%%%%%%%%%%%%%%%%%%%%%%%%%%%%%%%%%%%%%%%%%%%%%%%%%%%%%%%%%%
15
16 fs = 50000;      %Sampling frequency [Hz]
17
18 %%First acquisition
19 filename = 'ColExtXch1ColExt_001.txt';
20 [ch1 , ch2 ,ch3 ,ch4 ,ch5 ,ch6 ,ch7 ,ch8 , f] = file2varFRF (filename);
21
22 %%Second acquiisition
23 filename = 'ColExtXch1ColExt_002.txt';
24 [ch1 (:,2) , ch2 (:,2) ,ch3 (:,2) ,ch4 (:,2) ,ch5 (:,2) ,ch6 (:,2) ,...
25     ch7 (:,2) ,ch8 (:,2) ] = file2varFRF (filename);
26
27 %%Third acquisition
28 filename = 'ColExtXch1ColExt_003.txt';
29 [ch1 (:,3) , ch2 (:,3) ,ch3 (:,3) ,ch4 (:,3) ,ch5 (:,3) ,ch6 (:,3) ,...
30     ch7 (:,3) ,ch8 (:,3) ] = file2varFRF (filename);
31
32 %%Fourth acquisition
33 filename = 'ColExtXch1ColExt_004.txt';
34 [ch1 (:,4) , ch2 (:,4) ,ch3 (:,4) ,ch4 (:,4) ,ch5 (:,4) ,ch6 (:,4) ,...
35     ch7 (:,4) ,ch8 (:,4) ] = file2varFRF (filename);
36
37 %%Fifth acquisition
38 filename = 'ColExtXch1ColExt_005.txt';
```

```

39 [ch1(:,5), ch2(:,5), ch3(:,5), ch4(:,5), ch5(:,5), ch6(:,5), ...
40     ch7(:,5), ch8(:,5)] = file2varFRF(filename);
41
42 %%Sixth acquisition
43 filename = 'ColExtXch1ColExt_006.txt';
44 [ch1(:,6), ch2(:,6), ch3(:,6), ch4(:,6), ch5(:,6), ch6(:,6), ...
45     ch7(:,6), ch8(:,6)] = file2varFRF(filename);
46
47 %%Seventh acquisition
48 filename = 'ColExtXch1ColExt_007.txt';
49 [ch1(:,7), ch2(:,7), ch3(:,7), ch4(:,7), ch5(:,7), ch6(:,7), ...
50     ch7(:,7), ch8(:,7)] = file2varFRF(filename);
51
52 %%Eighth acquisition
53 filename = 'ColExtXch1ColExt_008.txt';
54 [ch1(:,8), ch2(:,8), ch3(:,8), ch4(:,8), ch5(:,8), ch6(:,8), ...
55     ch7(:,8), ch8(:,8)] = file2varFRF(filename);
56
57 %%Ninth acquisition
58 filename = 'ColExtXch1ColExt_009.txt';
59 [ch1(:,9), ch2(:,9), ch3(:,9), ch4(:,9), ch5(:,9), ch6(:,9), ...
60     ch7(:,9), ch8(:,9)] = file2varFRF(filename);
61
62 %%Tenth acquisition
63 filename = 'ColExtXch1ColExt_010.txt';
64 [ch1(:,10), ch2(:,10), ch3(:,10), ch4(:,10), ch5(:,10), ch6(:,10) ...
65     , ch7(:,10), ch8(:,10)] = file2varFRF(filename);
66
67 %%Computing FRFs averaged value – noise reduction
68 sigsFRF_ColExtXColExt = FRFmeans(ch2, ch3, ch4, ch5, ch6, ch7, ...
69     ch8, f);
70
71 %%Apply the modal fitting with LSCE method
72 for i = 1 : length(sigsFRF_ColExtXColExt(1,:)) ...
73     [fn.ColExtXColExt(:,i), dr.ColExtXColExt(:,i), ...
74         ms.ColExtXColExt(:,i)] = ...
75         modalfit(sigsFRF_ColExtXColExt(:,i), ...
76             f, fs, 24, 'FitMethod', 'lsce', 'FreqRange', [0,150]);
77 end

1  %%%%%%%%%%%%%%%%%%%%%%%%%%%%%%%%%%%%%%%%%%%%%%%%%%%%%%%%%%%%%%%%%%%%%%%%%
2  %%Michele G. Massafra, , last update: 22/11/2018
3  %%%%%%%%%%%%%%%%%%%%%%%%%%%%%%%%%%%%%%%%%%%%%%%%%%%%%%%%%%%%%%%%%%%%%%%%%
4  %%Reading acquisition data
5  %%FILE TYPE
6  %%Temp | Force [N] | Tri X | Tri Y | Tri Z | MonCh5 | MonCh6 |
7  %%MonCh7 | MonCh8
8  %%%%%%%%%%%%%%%%%%%%%%%%%%%%%%%%%%%%%%%%%%%%%%%%%%%%%%%%%%%%%%%%%%%%%%%%%
9  %%SFRF
10 %%$Windowing: Hanning(N of points)
11 %%$Number of points: 150000 points/s
12 %%$Total acquisition time: 3s
13 %%$Sampling frequency: 50000 kHz
14 %%%%%%%%%%%%%%%%%%%%%%%%%%%%%%%%%%%%%%%%%%%%%%%%%%%%%%%%%%%%%%%%%%%%%%%%%
15

```

---

```

16 function [ch1, ch2FRF, ch3FRF, ch4FRF, ch5FRF, ch6FRF, ch7FRF, ...
17          ch8FRF, f] = file2varFRF(FileName)
18
19 if nargin ~= 1
20     error('Not enough input')
21 end
22
23 disp('_____')
24 msg = ['Starting inport ', FileName, '.'];
25 disp(msg)
26 disp('')
27
28 vett = importdata(FileName, '\t');
29
30 PointN = length(vett(:,1)); %Number of points
31 Ttot = 3; %Total acquisition period [s]
32 fs = PointN / Ttot; %Sampling frequency [Hz]
33 dt = 1/fs; %Period [s]
34
35 g = 9.81; %Gravitational aceleration [m/s2]
36
37 time = vett(:,1); %Time values
38 ch1 = vett(:,2); %Impact hammer values [N]
39 ch2 = vett(:,3) * g; %Triaxial X
40 ch3 = vett(:,4) * g; %Triaxial Y
41 ch4 = vett(:,5) * g; %Triaxial Z
42 ch5 = vett(:,6) * g; %Monoaxial ch5
43 ch6 = vett(:,7) * g; %Monoaxial ch6
44 ch7 = vett(:,8) * g; %Monoaxial ch7
45 ch8 = vett(:,9) * g; %Monoaxial ch8
46
47 %Check if all the values are correctly inserted in the variables
48 if length(ch8) ~= PointN
49     error('File not correctly read');
50 end
51
52 %%Checking time starts from 0s
53 if time(1) ~=0
54     for i = 2 : length(time)
55         time(i) = time(i) - time(1);
56     end
57 end
58
59 msg = [FileName, ' correctly copied.'];
60 disp(msg)
61 disp('_____')
62 disp('')
63
64 %%%%%%%%%%%%%%%%%%%%%%%%%%%%%%%%%%%%%%%%%%%%%%%%%%%%%%%%%%%%%%%%%%%%%%%%%%
65 %Apply FRF
66 %%%%%%%%%%%%%%%%%%%%%%%%%%%%%%%%%%%%%%%%%%%%%%%%%%%%%%%%%%%%%%%%%%%%%%%%%%
67 disp('Starting FRF computation')
68 disp('')
69
70 %%FRF for channel 2 (X Triaxail)

```

```

71 [ch2FRF, f] = modalfrf(ch1, ch2, fs, hann(PointN/2), PointN/3);
72 disp('TriX-FRF ch2: OK')
73
74 %%FRF for channel 3 (Y Triaxail)
75 [ch3FRF, f] = modalfrf(ch1, ch3, fs, hann(PointN/2), PointN/3);
76 disp('TriY-FRF ch3: OK')
77
78 %%FRF for channel 4 (Z Triaxail)
79 [ch4FRF, f] = modalfrf(ch1, ch4, fs, hann(PointN/2), PointN/3);
80 disp('TriZ-FRF ch4: OK')
81
82 %%FRF for channel 5 (Monoaxail)
83 [ch5FRF, f] = modalfrf(ch1, ch5, fs, hann(PointN/2), PointN/3);
84 disp('Monoax-FRF ch5: OK')
85
86 %%FRF for channel 6 (Monoaxail)
87 [ch6FRF, f] = modalfrf(ch1, ch6, fs, hann(PointN/2), PointN/3);
88 disp('Monoax-FRF ch6: OK')
89
90 %%FRF for channel 7 (Monoaxail)
91 [ch7FRF, f] = modalfrf(ch1, ch7, fs, hann(PointN/2), PointN/3);
92 disp('Monoax-FRF ch7: OK')
93
94 %%FRF for channel 8 (Monoaxail)
95 [ch8FRF, f] = modalfrf(ch1, ch8, fs, hann(PointN/2), PointN/3);
96 disp('Monoax-FRF ch8: OK')
97 disp('')
98 disp('End FRF computation')
99
100 disp('_____')
101 msg = ['End manipulating ', FileName, '.'];
102 disp(msg)
103 disp('')

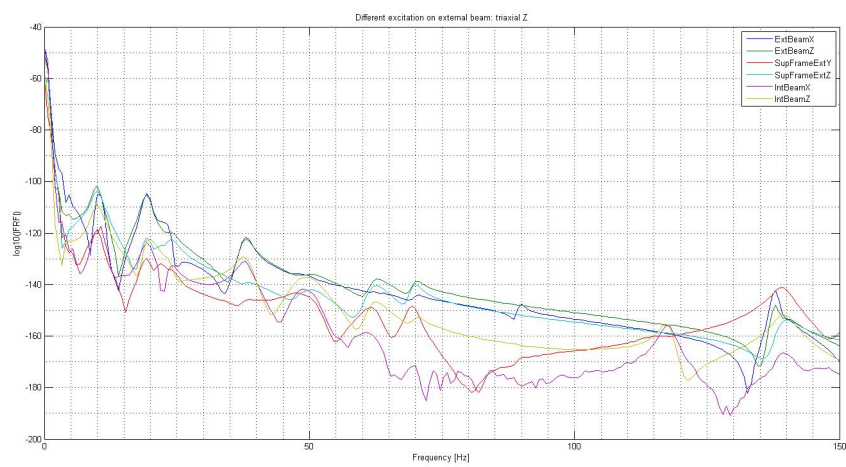
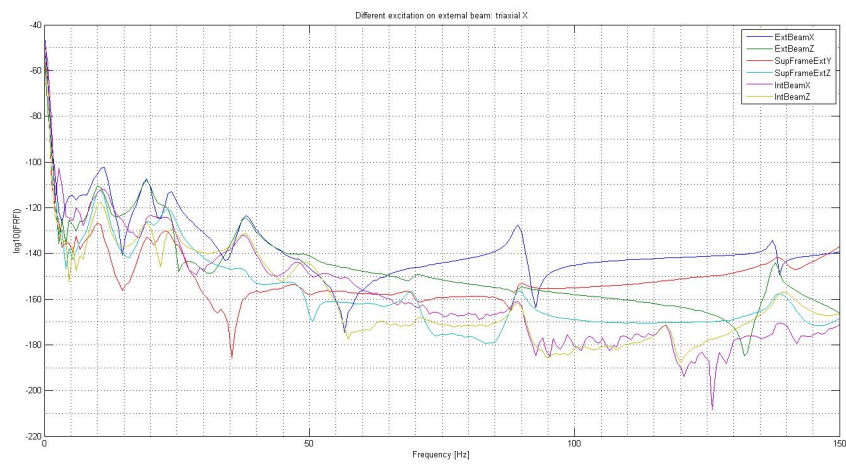
1  %%%%%%%%%%%%%%%%%%%%%%%%%%%%%%%%%%%%%%%%%%%%%%%%%%%%%%%%%%%%%%%%%%%%%%%%%
2  %%Michele G. Massafra, , last update: 22/11/2018
3  %%%%%%%%%%%%%%%%%%%%%%%%%%%%%%%%%%%%%%%%%%%%%%%%%%%%%%%%%%%%%%%%%%%%%%%%%
4  %%Mean computation for the FFT transforms
5  %%VARIABLES TYPES:
6  %%chn (n=2:8) channels for axcelerators
7  %%10 colums for each acquisition
8  %%imaginary numbers from 'file2varFFT.m'
9  %%%%%%%%%%%%%%%%%%%%%%%%%%%%%%%%%%%%%%%%%%%%%%%%%%%%%%%%%%%%%%%%%%%%%%%%%
10
11 function acq = FRFmeans(ch2, ch3, ch4, ch5, ch6, ch7, ch8, f)
12
13 disp('_____')
14 disp('Starting mean values of FRFs')
15 disp('')
16
17 acq(:,1) = mean(ch2,2);
18 disp('Mean TriX ch2: OK')
19
20 acq(:,2) = mean(ch3,2);
21 disp('Mean TriY ch3: OK')

```

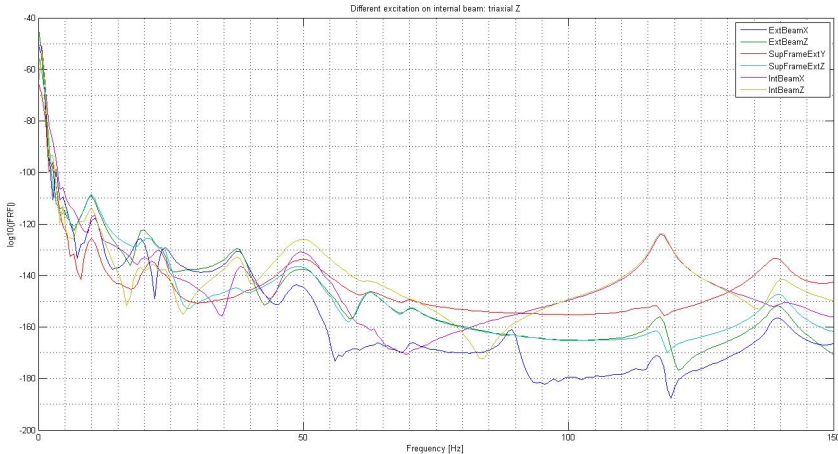
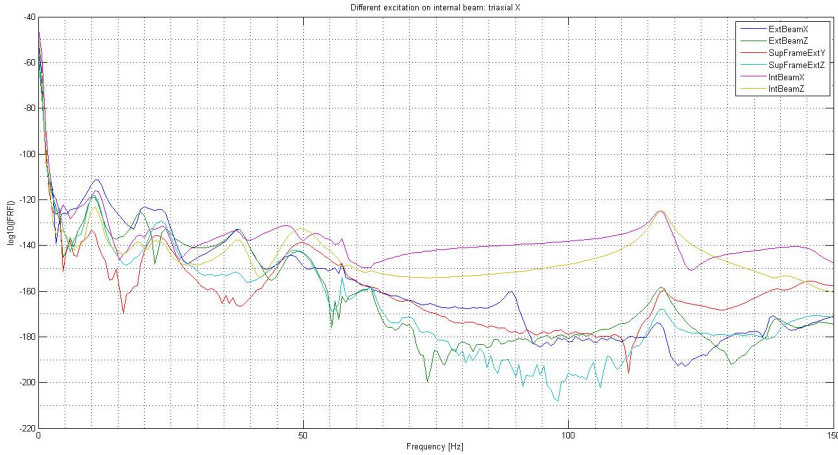
```
22
23 acq(:,3) = mean(ch4,2);
24 disp('Mean TriZ ch4: OK')
25
26 acq(:,4) = mean(ch5,2);
27 disp('Mean Monoax ch5: OK')
28
29 acq(:,5) = mean(ch6,2);
30 disp('Mean Monoax ch6: OK')
31
32 acq(:,6) = mean(ch7,2);
33 disp('Mean Monoax ch7: OK')
34
35 acq(:,7) = mean(ch8,2);
36 disp('Mean Monoax ch8: OK')
37
38 disp(' ')
39 disp('End mean values of FRFs computation.')
40
41 disp('_____')
```

# Appendix C

## FRF for internal and external beams



FRF for internal and external beams



# Bibliography

- [1] Rank E. & Zienkiewicz O. C. (1987) A Simple Error Estimation in the Finite Element Method, *John Wiley & Sons, Ltd.*, 3: 243-249
- [2] Friswell M. I. & Mottershead J. E. (1995) *Finite Element Model Updating in structural Dynamics*, Swansea U.K., Springer
- [3] Inman D. J. (1999) *Theoretical Models for Modal Analysis*. In: Silva J. M. M. & Maia N. M. M. (Eds.) *Modal Analysis and Testing*, pp. 227-240, Lisbon, Springer
- [4] Link M. (1999) *Updating of Analytical Models - Basic procedures and extensions*. In: Silva J. M. M. & Maia N. M. M. (Eds.) *Modal Analysis and Testing*, pp. 281-304, Lisbon, Springer
- [5] Link M & Hanke G.. (1999) *Model Quality Assessment and Model Updating*. In: Silva J. M. M. & Maia N. M. M. (Eds.) *Modal Analysis and Testing*, pp. 305-324, Lisbon, Springer
- [6] He J. (1999) *Damage Detection and Evaluation I*. In: Silva J. M. M. & Maia N. M. M. (Eds.) *Modal Analysis and Testing*, pp. 325-344, Lisbon, Springer
- [7] Farrar C. R. & Doebling S. W. (1999) *Damage Detection and Evaluation II. Field Applications to Large Structure* In: Silva J. M. M. & Maia N. M. M. (Eds.) *Modal Analysis and Testing*, pp. 345-378, Lisbon, Springer
- [8] Sas P. & Augusztinovicz F. (1999) *Acoustic Modal Analysis*. In: Silva J. M. M. & Maia N. M. M. (Eds.) *Modal Analysis and Testing*, pp. 487-506, Lisbon, Springer
- [9] Ewins D. J. (1999) *Modal Analysis for Rotating Machinery*. In: Silva J. M. M. & Maia N. M. M. (Eds.) *Modal Analysis and Testing*, pp. 549-568, Lisbon, Springer
- [10] Rugrali P. (2005) *Analisi Modale Ragionata. Teoria e pratica. Metodi, problemi, procedure di modellazione e calcolo con elementi di analisi sismica*. Rome, Ed. II, EPC Editore
- [11] ©PTC support, *PTC Help Center*, [https://support.ptc.com/apps/help\\_center/help/](https://support.ptc.com/apps/help_center/help/), [Access: May, 14<sup>th</sup> 2018]
- [12] ©MathWorks Documentation, *MathWorks*, modalfrf R2018b, <https://it.mathworks.com/help/signal/ref/modalfit.html>, [Access: November, 14<sup>th</sup> 2018]